

Predictive Site Detection and Reconstruction

**A Data-driven Approach to the Detection, Analysis, Reconstruction
and Excavation of Ancient Near Eastern Monumental Architecture**

Inauguraldissertation der Philosophisch-historischen Fakultät der Universität Bern zur Erlangung der
Doktorwürde vorgelegt von

Manuel Gerber

von Bern und Langnau.i.E.

Selbstverlag, Bern 2003

Von der Philosophisch-historischen Fakultät auf Antrag von Prof. Dr. Markus Wäfler (Bern), Prof. Dr. Johann Georg Schmid (Berlin) und Prof. Dr. Hanspeter Bieri (Bern) angenommen.

Bern, den 4. April 2003

Der Dekan: Prof. Dr. Oskar Bätschmann

Abstract

This text explores new ways of remotely detecting, analysing and reconstructing ancient Near Eastern monumental mudbrick buildings subsumed under the acronym PSDR (Predictive Site Detection and Reconstruction). The ultimate aim were reliable predictive reconstructions that may be used as a basis of highly targeted small-scale excavations. Where parts of a building are too heavily damaged to allow conclusive testing - which is often the case - no room was to be left for subjective speculation and a reconstruction was required to be able to stand convincingly on its own. Its level of detail, therefore, was to be dictated entirely by the data. It must be replicable, logically transparent and resistant to bias in favour of specific outcomes due to personal preconceptions.

The main focus was on the development of simple methods for processing topographic data because this type of data is widely available or can be generated at resolutions ranging from kilometres (space-borne remote sensors) to millimetres (3D-laser scanners). At the level of landscapes, fractality signatures defined by spatial crossover scales typical of eroded urban settlements are proposed as a tool for the detection of potential target sites for excavation in automated large-area scans of remotely sensed imagery [a]. At progressively smaller scales, methods were developed for extracting topographic indicators of eroded architectural features from Digital Elevation Models (DEM) of the chosen settlement mounds [b] and for transforming them into algorithmic complexity signatures that capture every geometric regularity present in potential architectural remains. Based on these signatures hypothetical ground-plans of the original monumental buildings are reconstructed using a mathematical model termed CPSR (Complexity-based Predictive Site Reconstruction) [c]. At this level, key predictions about the layout of buildings are to be tested by small-scale excavation and the results to be fed back into the reconstruction process. Preliminary field tests so far support the theoretical expectation that predictions are thereby forced to rapidly converge towards the original ground-plan at progressively higher levels of detail until the threshold of testability is reached. This iterative approach is demonstrated to be much more effective, both scientifically and economically, than traditional excavation strategies based on surface survey and large-scale excavation.

The methods were developed with VHR (Very High Resolution)-data in mind but were applied only to existing data from Tall al-Hamidiya, Syria. As a consequence, their degree of universality may be modest. [c] was successfully tested under controlled circumstances in the field in 2000, and the excavation strategy in 2001 was largely based on preliminary results from [b]. All relevant aspects of the basic structure of the northern, eastern and western parts of the Central Maitanian Palace that are known today were predicted in advance with high and sufficient accuracy respectively by [b] and [c] independently. The methods proposed at the scale of landscapes [a] are as yet purely theoretical and untested. I am nevertheless confident as to their potential because their implementation in collaboration with other researchers is progressing well (cf. Acknowledgements).

Acknowledgements

Most of the research presented here was undertaken during my time as a research associate and assistant lecturer at the Institute of Ancient Near Eastern Archaeology and Languages, University of Berne. I wish to express my gratitude to my degree supervisor M. Wäfler for granting me complete academic freedom, for access to unpublished data and for the opportunity to test CPSR/PSDR in the field at Tall al-Hamidiya in 2000 and 2001.

I extend my thanks to:

my collaborators in various spin-off projects initiated in the course of this research for their enthusiasm and competence: H. Bieri, R. Blattner, N. Bonfils, S. Tetik (Institute of Computer Science and Applied Mathematics, U Berne), S. Wunderle (Remote Sensing Research Group, Dept. of Geography, U Berne) and J. Donatowicz (Dept. of Computing, TU Vienna, and Institute of Astronomy, U Vienna). This text would have gained substantially if their work could have been included. This was not possible because the archaic 'Dissertationsreglement der Phil.hist.-Fakultät der Universität Bern' forbids multi-author submissions.

D. Stuedler (Dept. of Geomatics, U Melbourne) for access to toposurvey data and inspiring discussions, and my brother Vincent Gerber (Equine Pulmonary Lab, Dept. of Large Animal Clinical Sciences, Michigan State U) for encouragement, discussing statistics, comments, proof-reading and general brothering.

D. Dall'Agnolo, G. Grasshoff, G. Higginbottom, Th. Hofmeier, F. Prendergast, H.J. Schmid, C. Spadavecchia, and many other friends and colleagues who contributed by criticism, scepticism and disbelief in one combination or another.

I thank Estelle for being lovely when all else stinks, and for bearing with my bad mood during the past few weeks when I could no longer postpone writing this stuff down.

My warmest thanks - for everything - go to my parents, to whom this work is dedicated.

For my parents

Heinz (†) and Andrée Jeanne Gerber

Contents

Abstract

Acknowledgements

Contents

0. INTRODUCTION

0.1. Scientific Backwaters

- 0.1.1. Destructiveness and Lack of Intersubjectivity
- 0.1.2. Redundancy and Costs

0.2. Predictive Site Detection and Reconstruction Strategies

- 0.2.1. Aims and Conceptual Outline
- 0.2.2. Why Topographic Data?
- 0.2.3. Project History and Rationale of this Text
- 0.2.4. Chronology and Types of Reconstructions 1998-2002

1. THEORETICAL FRAMEWORK

1.1. Monumentality, Local Stochasticity and Topography

- 1.1.1. Settlement Dynamics
- 1.1.2. Modelling the Dynamics of Ancient Urban Settlement Structure

1.2. Topographic Indicators of Buried Monumental Buildings and Individual Architectural Features

2. DATA

2.1. The DEM based on the 1984 Topo-survey

- 2.1.1. Survey Data
- 2.1.2. Local Measurement Density

2.2. Plans and Sections 1984-1999

2.3. Satellite Imagery and 3D Laser Scanner Data

3. METHODOLOGY, METHODS, PRELIMINARY RESULTS

3.1. Predictions based on Fractality Analysis at Large Scales (Level 4)

- 3.1.1. Aims
- 3.1.2. Fractality
- 3.1.3. Scale vs. Resolution
- 3.1.4. Detection of Sites Potentially Harboursing Monumental Architecture

3.2. Scale-insensitive Alternatives to Fractality Analysis at Small Scales (Level 3)

- 3.2.1. Fractality at the Scale of Individual Buildings
- 3.2.2. Scale-independent Proxis
- 3.2.3. Implementation and Results

3.3. Predictions based on Site-scale Topographic Analysis (Level 2)

- 3.3.1. Topographic Effects of Erosion
- 3.3.2. Slope Development
 - 3.3.2.1. Collapse of Mudbrick Walls
 - 3.3.2.2. Post-Collapse Slope Development
 - 3.3.2.3. Gullies and Wadis

3.3.3. Implementation and Results

- 3.3.3.1. Extracting Slope Information
- 3.3.3.2. Extracting Wall Orientations

3.3.4. Symmetries

3.3.4.1. Quantifying Symmetries and Symmetric Regularities

3.3.4.2. Implementation and Results

3.4. Complexity-based Predictive Reconstruction of Buildings (Level 1)

3.4.1. Rationale and Outline of the Concept

3.4.2. Definitions and Propositions

3.4.3. Other Forms of Encoding y

3.5. Extracting Additional Information from Excavated Structures

3.5.1. Construction Grids, Error Estimates

3.5.2. Reference Systems and Measurement Techniques

3.5.3. Estimation of the Modern Component in Angular Errors

3.5.4. Architectural Units

4. EXPERIMENTAL RECONSTRUCTIONS OF THE CENTRAL PALACE AT TALL AL-HAMIDIYA

4.1. The CPSR-Reconstruction of 1999

4.1.1. Problems of Implementation

4.1.2. Data

4.1.3. The Hypothetical Reconstruction x'

4.1.4. Field Test 2000: Excavation Results

4.1.5. Assessment

4.2. The PSDR-Reconstruction 2002

4.2.1. Predictions 2000-2002

4.2.2. Results

4.2.2.1. Synopsis of Predicted Architectural Features

4.2.2.2. The Reconstruction 2002: Synthesis of Predictions based on Topography

4.2.3. Comparison with Excavations -2002

4.2.4. Assessment

5. DISCUSSION

5.1. Hits and Misses

5.2. Conclusion

6. REFERENCES

6.1. Abbreviations

6.2. Literature

APPENDICES

1. Figures

2. Tables

0. INTRODUCTION

0.1. Scientific Backwaters

0.1.1. Destructiveness and Lack of Intersubjectivity

Archaeology is often jokingly referred to as a science based on unrepeatable experiments. While one may counter that this applies to some of the more esoteric branches of physics as well, the basic truth of the statement is uncontested. Archaeological artefacts are largely defined by their context, and by physically recovering them from the soil the context is inevitably destroyed. Much relevant information survives only in the form of documentation - which is necessarily selective and all too often of poor quality - and therefore cannot be controlled intersubjectively by renewed observation.

Under certain conditions, the dilemma of destroying contexts by studying them may be by-passed by geophysical prospection or other non-intrusive approaches, foremost among them predictive mathematical modelling. Unlike more traditional methods that distort even the raw data by interpretation, results obtained by either are intersubjective: a geophysical survey can be repeated and a mathematical model tested against new data whenever necessary.

The potential of geophysical prospection is immense (Nishimura 2001), but limited geographically to areas with predominantly shallow sites: the maximum penetration depth achieved by current sensors is ~3m in dry, clay-rich soils (GPR at medium frequencies around 300MHz; Conyers and Cameron 1998), which, on a medium sized Near Eastern settlement mound (Arab. *tall*), barely amounts to scratching the surface: fig.1A illustrates the relationship between slope at a given elevation and the area covered by GPR under perfect conditions in the corresponding horizontal section. In fig. 1B the poor percentage of total mound volume that can be reached using GPR in a lentil shaped tall is plotted against the tall's base radius for various heights. The limitations imposed by low penetration depths are the same for air-borne sensors targeting sub-surface features. For large tall, therefore, the potential of sub-surface prospection is low, regardless of sensor type.

Predictive mathematical methods have no such a priori limitations. Appropriate models may conceivably be used to minimize the destructive impact of excavations by restricting digs to very small target areas around probable locations of predefined objects. Applications of predictive modelling at the level of individual sites, however, are as yet few and far between. Archaeological research has so far focused on predictive models acting at the scale of landscapes. On this level, predictive GIS (Geographic Information Systems) have proven much more efficient than traditional non-mathematical methods of discovery. The latter are destructive in an indirect sense insofar as uncontrollable bias resulting from arbitrary search criteria and/or ineffective survey methods lead to artificial patterns in the archaeological record, blanking out potentially relevant sites from cultural resource management and protection schemes (Bettis and Mandel 2002).

Near Eastern archaeology: Firmly rooted in the humanities and, thence, harbouring a deep distrust in all things scientific, Near Eastern archaeology as a discipline has cast a blind eye on the potential of mathematical modelling, even though the situation in the semi-arid plains of the Near East is especially grave on both the site and the landscape levels: sun-dried mudbrick, the only locally relevant building material in antiquity, rapidly becomes unstable when not properly maintained, and architectural remains recovered by excavation start disintegrating almost immediately after being exposed. They collapse within a very short time, often within months. Under normal circumstances the preservation of architectural structures is impossible. Large-scale excavations, still the norm in the archaeology of tall, further aggravate the problem, because - in contrast to other geographical areas - not only context but also the artefact itself is thus lost in its entirety to any form of re-examination.

At the landscape level, a tall is usually chosen for surface surveying and later, provided that datable sherds point to an occupation during the target period, for excavation on the basis of its size and location - criteria that in practice translate into 'prestige' and 'proximity to restaurants' respectively.

Better search and selection criteria have so far found little foothold because tells are by far the most obvious landmarks and also the most frequent. Consequently, the question of where a specific type of settlement is most likely to be found is generally deemed futile and has - in contrast e.g. to North American archaeology with its strong research focus on predictive GIS (Wescott and Brandon 1999) - only rarely been systematically addressed (e.g. Braidwood et al. 1983, Wäfler 2001).

0.1.2. Redundancy and Costs

Redundancy at the scale of individual sites: Excavations of large connected areas are expensive and result in a flood of mostly redundant information: while in the course of such an excavation the costs per excavated unit remain constant, the probability of learning something new about the local situation decreases - after an initial jump - with every new unit opened. In information theory this is known as the learning phenomenon. A certain, low degree of redundancy is necessary statistically to compensate for random variation in any kind of observed data (Pierce 1980). Above this threshold redundancy has no significant informational value, but rather leads to a plateauing of the learning curve (Kearns and Vazirani 1994). Economically speaking, the high costs resulting from a low ratio of knowledge gain vs. investment in large-scale excavations therefore have no scientific justification.

This is most apparent in very big tells containing urban architecture: Covering an area of ca. 30ha the Tell al-Hamidiya, for instance, rises steeply some 40m above the plain in its northern parts. Walls hypothesized to belong to a single Maitanian building, the so-called Central Palace, on the basis of their uniform orientation and regular floor elevations are distributed over much of the area (fig. 2). The expenses in time, labour and money necessary for excavating large connected areas of a building of this size cannot possibly lead to an increase in knowledge proportional to the investment: The argument is simple, and valid for any site with architectural remains: a single straight wall ($n=1$) can be represented in a 2-dimensional space as a graph by its two endpoints. 3 Points are needed for two walls forming a corner ($n=2$), namely the node (i.e. the intersection) and an endpoint each. Since buildings are - in general - closed shapes, the number of points needed to represent their groundplan equals the number of nodes, which, in turn equals the number of wall segments n . In practice this means that once the orientations of two walls are known, so is the position of the related node. The additional effort of prospecting or excavating the corner will therefore result in no new topological or positional information (cf. fig.27).

There is, of course, more to architecture than geometric or topological regularities, and this reasoning is invalid where singular phenomena are concerned, such as the decoration of a specific orthostat or the position of yet another nicely carved cylinder seal. However, these are chance finds by their very nature, and it is a matter of taste whether one considers the low probability of finding a type of artefact that is not already known by the hundreds enough to justify expensive, labour-intensive excavations of large, connected areas. To the scientifically minded archaeologist it is a probabilistic nightmare - and a sign of bad taste.

If, therefore, an increase in new information is to be achieved that is at least proportional to the overall effort invested, methods must be developed that allow highly targeted digging on very small scales thereby minimizing the risk of recovering redundant information.

Redundancy at the scale of landscapes: Similar arguments hold for any kind of information on structures that exhibit some degree of regularity, such as facade decorations, the positioning of doors, even spatial settlement organisation at the scale of whole sites and, ultimately, at the scale of entire landscapes. At this latter scale uncontrollable biases introduced by inappropriate site selection criteria (§ 0.1.1) necessarily lead to an overrepresentation of certain types of sites, while others remain underrepresented. New sites selected by traditional criteria are therefore likely to no more than add to the redundancy of what is already known about the first group. Therefore, at the scale of landscapes as well, the development of targeted, predictive methods is imperative if the gaps in the archaeological record of the ancient Near East are eventually to be filled.

0.2. Predictive Site Detection and Reconstruction Strategies

0.2.1. Aims and Conceptual Outline

Predictive Site Detection and Reconstruction: In all probability there is no single, methodically homogenous solution to the problems outlined above. Rather, potential solutions may be presumed to be methodically diverse, i.e. to consist of different combinations of predictive, ultimately mathematical methods depending on the type of target site. Such sets are in the following collectively termed Predictive Site Detection and Reconstruction (PSDR)-strategies.

Aims: The aim of this work is to validate the general idea of PSDR by presenting one such strategy in some detail. It is limited in scope to sites with monumental architecture and exemplified using data from Tall al-Hamidiya. On both the theoretical and practical levels, the focus was on the development of new predictive methods for processing topographic data based on simple models - newness was not emphasised for the sake of originality but in the hope of widening the meagre spectrum of existing techniques adapted to the conditions in the Near East. On all levels, the predictions were to be replicable, logically transparent and resistant to bias in favour of specific outcomes due to personal preconceptions; their level of detail, hence, was to be dictated by data alone.

Conceptual outline: The PSDR strategy envisioned here encompasses all stages from finding to analysing and excavating ancient monumental mudbrick architecture. It relies on techniques for architectural feature extraction, predictive reconstruction of ground-plans and on iterative feedback: from a given set of topographic data, information about the probable nature of buried architectural remains and about the position of specific architectural elements is to be extracted. Based on geometric regularities within individual elements as well as between elements, the basic structure of original buildings is to be reconstructed in a controlled, consistent and replicable manner. Predicted positions of near-surface architectural key features are hypotheses that are to be tested by excavation or, if feasible, geophysical prospection. The test results, finally, are to be fed back into the reconstruction and prediction process. In such a system, positive and negative test results have the same value insofar as both constitute new, non-redundant information. This is expected to guarantee an increase in knowledge at least proportional to the excavation effort and, hence, to force the reconstructions at later iterations to progressively converge towards reality. Where parts of a building are too heavily damaged to allow conclusive testing - which, of course, is often the case - no room is to be left for subjective speculation and a reconstruction is required to be able to stand convincingly on its own. Its level of detail, therefore, is to be dictated entirely by the data.

Ideally, every step from the detection of potential targets to the prediction of promising sample areas should be automated, or, at least, formalized with automation in mind. In logical order, these steps correspond to four procedural stages at different spatial scales.

Level 4: Landscapes	Detection of sites potentially harbouring monumental buildings.	(§ 3.1)
Level 3: Individual sites	Prediction of probable locations of monumental buildings.	(§§ 3.1, 3.2)
Level 2: Individual buildings	Prediction of key features with high information content.	(§§ 3.3, 3.4)
Level 1: Individual features	Testing of predictions by excavation or, where feasible, geophysical prospection.	(§ 3.4)

Methodological limitations: The choice of site type may seem ironic since monumental architecture is usually associated with large, urban settlements - a heavily over-represented group of sites in the Near East (§ 0.1.2). It was pragmatic insofar as of all Near Eastern settlement mounds, I am most intimately acquainted with Tall al-Hamidiya, a site dominated by Maittianian monumental architecture. In this particular case the risk of redundancy was considered negligible because the dimensions as well as the topology of the Maittianian remains were known in advance to be singular (Wäfler TH1, Wäfler TH2). The singularity of the site, however, is problematic itself because the exclusive use of data from Tall

al-Hamidiya potentially limits the degree of universality of the proposed methods. Field experiments at Tall al-Hamidiya during which key predictions about unknown architectural features were tested by excavation have so far been the only means of assessment. While this effectively controls for prior knowledge as a potential source of bias in favour of a specific outcome obtained by a given method, it cannot guarantee its applicability under different conditions.

Practical limitations: Obviously, a study of this scope is heavily interdisciplinary. In the present case the disciplines touched upon range from two rather exotic forms of mathematics - algorithmic complexity theory and fractal geometry - to landscape ecology and quantitative geomorphology. My competence in these fields is limited to the interested layman's superficial understanding. Evidently, PSDR may only reach a satisfactory level of sophistication in collaboration with other researchers (see *Acknowledgements*). The present text contains the basic work done by myself, i.e. the simple concepts, ideas and crudely implemented methods that served as a starting point for the serious collaborative research.

0.2.2. Why Topographic Data?

Interdependence of Data and Methods: On the most basic level any choice of method - existing or to be developed - depends on the type of data that is available or can conceivably be generated.

The limitations of subsurface prospection with air-borne as well as geophysical sensors (§ 0.1) do not apply to surface scans: satellites are unimpaired in their functionality by difficult topographic conditions, and the commercial availability of very high resolution (VHR) data - multispectral as well as photographic - at competitive prices will soon allow the generation of inexpensive Digital Elevation Models (DEM) at sub-meter resolution (Wheatley and Gillings 2002), i.e. far exceeding in measurement density any elevation map of a Near Eastern tall published to date. In combination with extremely high-resolution photogrammetry (McFarlane et al. 2002) or 3D medium to long-range Laser scanning (Langer *et al.* 2000, Gerber 2002, Sawyer 2002), decimetre and sub-centimetre resolutions respectively are feasible.

Thus, active and passive sensors for remote surface prospection and reflectorless position and range finders, especially the latest generation of 3D long-range Laser scanners, hold the greatest potential for generating relevant new data. Dense topo-survey data and remotely sensed surface data are ideal in terms of both availability and generateability. Their potential for the detection of sub-surface archaeological remains has to date only been made use of unsystematically in aerial photography in such rather trivial cases as e.g. the mapping of earthworks or large stone-walled buildings. For remains made of unbaked mudbrick it has never been examined. Research on the detection of artificial features in 2D remote sensing data, on the other hand, is an active field. However, here as well, buried or eroded structures have so far largely been left out of the picture, except - by analogy - in military applications targeting camouflaged artificial objects (§ 3.1.).

The methods proposed here were developed with this kind of remotely sensed surface imagery and 3D topographic data at very high resolutions in mind. However, for reasons discussed in § 0.2.3. they were applied exclusively to the data available to me in 1999 (§ 2.1.-2.2.). This restricted database consists of the 1984 toposurvey data (TH1, Steudler 1986, § 2.1.) as well as plans and sections drawn and digitised from 1984 -1999 (§ 2.2.). No plans drawn after 1999 were employed, and the potential of the new VHR-data is only theoretically discussed where its use would conceivably make a relevant difference. Implementations of the proposed methods designed for processing VHR-data are currently being explored in two PSDR spin-off projects in collaboration with other researchers and will be published elsewhere (§ 0.2.1.). The focus of these sub-projects is on a series of Corona satellite photographs and Ikonos multispectral imagery at 1-m resolution centred on Tall al-Hamidiya acquired in 2001 and on experimental VHR 3D-Laser scanner data from archaeological and historical sites in Switzerland, France and Turkey collected since 2002 (Gerber 2002; § 2.3.).

0.2.3. Project History and Rationale of this Text

PSDR was devised as a means to tackle the logistic problems of excavating very large buildings and to reconstruct such buildings in the absence of obvious typological parallels. At first, in 1999, the aim was to find ways to go beyond the determination of minimal floor level extensions on the basis of linear extrapolation from the known parts of a building (Wäfler TH4: Rekonstruktion 1998). By extracting a complete set of building-specific geometric regularities from the known remains by maximally compressing their algorithmic description I intended to define characteristic construction rules ('complexity signatures'; § 3.4.) on the basis of which a complete three-dimensional shape could be reconstructed that would preserve the characteristics extant in the excavated remains. This approach, provisionally termed CPSR (Complexity-based Predictive Site Reconstruction), is conceptually related to reverse engineering (§ 3.4.1.). The resulting shape was to be used as an entirely data-driven prediction on the basic shape of the original building, resistant to biases due to preconceptions and subjective interpretation.

In 2000 a primitive preliminary CPSR model was tested at Tall al-Hamidiya in the eastern and western parts of the Central Palace. Since all tested predictions were confirmed to a higher degree than initially expected (§ 4.1.), a post-hoc reconstruction was produced by Wäfler that incorporated the tested and untested predictions as well as the excavation results (Wäfler TH4: Rekonstruktion 2000).

The post-hoc reconstruction was problematic because, although CPSR is data-driven, this first attempt at an implementation was heavily influenced by interpretation on two levels: a) the data were extracted directly from the detailed but heavily schematised plans of the previously excavated squares. The schematisation represents an interpretation of the original excavation data, and in order to control its influence on the predictions, the positional and angular errors in the plans would have had to be assessed. Because the plans, i.e. what is supposed to be 'raw data', are updated and significantly changed according to the current ideas on the structure of the palace after each campaign, this was not possible post-hoc. b) Due to the primitive mechanism of the first model, it was necessary to assign a functional interpretation to individual architectural elements (§ 4.1.3.). This interpretation may or may not have been reasonable but it does, in any case, not follow with any logical necessity from the data.

In 2000 and 2001 I concentrated on prediction methods based exclusively on topographic data that were by their very nature uninfluenced by interpretation (§§ 3.2. and 3.3.). Predictions based on these methods closely matched those obtained in the year before, and were used for planning further excavations in the western and eastern parts of the palace in 2001. After the campaign the post-hoc reconstruction of 2000 was updated with the new results, and both tested and untested predictions were again incorporated and elaborated on. The functional interpretation of individual elements as stairs was thus propagated and projected on predictions that were themselves free of a subjective component (Wäfler TH4: Rekonstruktion 2001, Plan 2).

By mixing various types of results and interpretations indiscriminately the post-hoc reconstructions of 2000 and 2001 (last updated in 2003) have become hybrids that are methodically oblique. They may not count as hypotheses but merely as subjective interpretations because where they deviate from the CPSR/PSDR-predictions (figs. 36, 38) they are arbitrary and cannot be tested:

The level of detail in the predictions obtained by CPSR/PSDR is - at least theoretically - dictated entirely by the data. In general it is very low. Wäfler's post-hoc reconstructions, on the other hand, have become extremely elaborate. Their high level of detail is not positively supported by the data - cf. e.g. the representation of the western and eastern protrusions as stairs of a specific length down to the level of individual steps - but rather only negatively insofar as the details do not *seem* (sic!) to contradict the data. An objective assessment is impossible because sets of 'raw data' shown in the plans published in TH4 in support of specific elements of the post-hoc reconstructions exhibit considerable angular, positional and structural deviations from the same sets in earlier plans. With the exception of a scanned plan from 1999 published in Gerber 2000b (fig. 28) that may be compared to TH4: plan 4 (§§ 2.2. and 3.4.), these changes fall in-between TH2 and TH4 and are therefore undocumented and uncontrollable.

In order to assure data integrity within the present text I have refrained from processing any data extracted from plans generated after 1999. The CPSR-reconstruction of 1999 (§ 4.1.) was not - as originally planned - repeated under more controlled circumstances because the original data set can no longer be replicated, i.e. the new results would not be comparable to the older. Furthermore, in order to clearly separate the PSDR results after 1999 from both the CPSR results in 1999 and from the two published post-hoc reconstructions, I have here limited the application of the methods set forth in §§ 3.2. and 3.3. to topographic survey data generated in 1984, i.e. before the inception of excavations at Tall al-Hamidiya. A synthetic reconstruction based exclusively on these results is presented in § 4.2. (fig. 38). This latter reconstruction would be exactly the same if it had been done in 1984. In this way the risk of an uncontrolled interplay between different methods is eliminated and the predictive potential of the proposed methods of topographic analysis can be assessed objectively by comparison with later excavation results regardless of their reliability.

0.2.4. Chronology and Types of Reconstructions 1998-2002

Various types and stages of reconstructions are repeatedly referred to in this text. The following chart is intended as a guideline through the jungle.

	PSDR (Gerber) Type (Content) Level of detail (<i>LD</i>)	Refs.	Post-hoc (Wäfler) Type (Content) Level of detail (<i>LD</i>)	Refs.
1998	--	--	Post-hoc Autonomous (Full) (like 1997 but with terraced monumental stair in the South) <i>LD</i> : North: low, dictated by data South: higher than supported by data	TH4: Rek. 1998
1999	CPSR (Full) (Predictions on the structure and extension of the eastern, northern and western parts of the Palace) <i>LD</i> : low, dictated by data extracted from the post-hoc reconstruction of 1998	Gerber 2000b, 2001 § 4.1.; fig. 36	Post-hoc Autonomous (Full) (stair straightened, minimal length determined) <i>LD</i> : North: low, dictated by data South: higher than supported by data	TH4: Rek. 1999 fig. 36 (inset)
2000	PSDR (Partial) (Analysis of topography, Order Symmetries) <i>LD</i> : low, dictated by data	§§ 3.2., 3.3., 3.5.	Post-hoc Hybrid (Full) (incorporates CPSR-predictions of 1999 [east: 2 nd monumental stair, west: beak shaped, odd-angled extrusion], and Order Symmetry predictions 2000 [west: 3 rd monumental stair]) <i>LD</i> : much higher than supported by data	TH4: Rek. 2000
2001	PSDR (Partial) (Analysis of topography) <i>LD</i> : low, dictated by data	§§ 3.2, 3.3.	Post-hoc Hybrid (Full) (incorporates PSDR-predictions 2000, 2001 [west: connection of southern parts of stair with main body of palace], Order Symmetry predictions 2000 [East: connection of northern parts of stair to main body of palace]) <i>LD</i> : much higher than supported by data	TH4: Rek. 2001, Plan 2
2002	PSDR (Full) (Synthesis of PSDR-predictions 2000, 2001, 2002) <i>LD</i> : low, dictated by data CPSR (Partial) (Construction principles, architectural units, error estimates) <i>LD</i> : high, dictated by data	§ 4.2.; figs. 38, 39 § 3.5		

1. THEORETICAL FRAMEWORK

1.1. Monumentality, Local Stochasticity and Topography

1.1.1 Settlement Dynamics

Relevant characteristics of urban settlements: Monumental architecture is, as a rule, associated with urban settlements in the ancient Near East. Such settlements are complex, hybrid entities consisting of artificial structures but also sharing characteristics with their natural surroundings. Understanding this fundamental dichotomy is essential for the development of methods for detecting the remains of monumental buildings.

The problems encountered in the analysis of probabilistic surveys in settlement contexts may serve to illustrate this point: probabilistic sampling requires that the elements recovered from a totality of interest be distributed stochastically, thus allowing statistical estimates of this totality based on samples (Shannon 1997). This is usually the case where human impact on the examined area is low, which makes probabilistic sampling an ideal tool for planning regional-scale surveys, e.g. of artefact scatter. At smaller scales and higher resolutions sampling designs have to be used that minimize distortions to expected distributions caused by the clustering of settlement sites (Nance 1983) or violations of the stochasticity criterion by the periodic behaviour of sample elements, often caused by a buried building's grid-structure (Wilkinson 2001). The progressively lower degree of stochasticity at smaller scales - groups of settlements and buildings respectively - is a direct reflection of the artificial component that gets more pronounced at higher resolutions; this component cannot be satisfactorily dealt with in a purely statistical framework.

Furthermore, on a more practical level, the uneven vertical stratification of many settlement sites poses a serious problem to sampling approaches in general: information obtained from one sample area may not be stratigraphically relatable to information from another. The heterogeneity thus introduced in the data frequently renders the interpretation of results obtained by sampling uncontrollable (Barker 1993).

The ineffectiveness of probabilistic sampling strategies as tools for the investigation of a settlement's internal structure is due to an underlying model of reality that is thoroughly stochastic. Though trivial, this nevertheless shows that a method is only as good as the assumptions it is based on. The effectiveness of detection methods for monumental buildings will therefore depend critically on a thorough understanding of potential topographical manifestations of the hybrid character of ancient urban settlements.

Settlement dynamics: Quantitative models for the internal dynamics of settlement structure have become increasingly sophisticated in recent years (Schweitzer 1997); their time horizon, however, is usually in the range of decades or, at best, a few centuries, and the model parameters are chosen so as to be measurable in a modern, living environment. For this reason, they cannot be adapted *telquel* to archaeological contexts. In order to check their validity for ancient Near Eastern settlements, archaeological proxies for the relevant parameters have to be found.

The structure of a settlement at a specific point in time can be viewed as the result of a multitude of differential processes of guided - i.e. deterministic - and chaotic growth, local collapse and continuous reorganisation of parts (Makse et al. 1995, Weidlich 1997). In large urban settlements, one or many relatively stable and ordered cores surrounded by more dynamic and less organized areas are the rule. The distribution of elements within a settlement, be it lane segments, buildings, elements of buildings or small artefacts, can therefore be expected to have a stochastic component that gets more pronounced towards the periphery of the relatively more stable cores (O'Neill et al. 1988, Shiner 1997). It seems intuitively reasonable to assume that after a settlement is abandoned, these differences

in local stochasticity will be reflected - and hence remain detectable - in the topographic structure of the site that results from subsequent collapse and erosion. If this assumption is correct, it should be derivable from an appropriate model of ancient settlement dynamics.

Looking at the extremes and disregarding the complexities in between, modern buildings in very stable zones tend to be large, to have regular shapes and a complex interior organisation whereas in the highly dynamic border zones they tend to be small, less regularly shaped and to have a simple interior organisation. The financial districts of large cities and the slums bordering them provide visual examples of this contrast. For modern settlements an arbitrary model for local stochasticity s might consist of the following parameters:

$$s(a): f(P, L, S, R, T, \dots) \quad (\text{Eq. 1})$$

where P is the mean change in position of the outer walls of buildings in area a relative to the buildings preceding them, and L is the mean lifetime of buildings in a . (P/L), then, is a measure for structural instability. For central areas L is in the range of decades or even centuries, and both L and P are usually well-documented; for slums the rate of change is so fast that it can be determined within years or even months by comparing satellite images or ground survey data. Size (S) is directly measured by volume if multi-storied buildings like skyscrapers are present, otherwise by area. R denotes the regularity of shapes; this can, for example, be expressed statistically as the goodness of fit of the actual outline of buildings to sets of geometrical primitives (Roth and Levine 1993), by the degree to which buildings exhibit mathematical symmetry (Weyl 1989, Zabrodsky et al. 1995), or by their algorithmic complexity C (§ 3.4.). T is the topological complexity of the interior organisation, quantifiable, for instance, by the minimum number of loops (West 2001) containing other loops in a path through all its doors. This number equals the number of embedded room systems, i.e. room systems accessible through a single door.

The expected correlations between the discussed parameters are summarized in the matrix

R	(+)			
T	(+)	(+)		
P/L	(-)	(-)	(-)	
	S	R	T	

1.1.2 Modelling the Dynamics of Ancient Urban Settlement Structure

With the exception of R , quantification is less straightforward in ancient settlements: lifetimes cannot usually be determined even where wood is present in sufficient quantities for dendrochronological dating, and size as well as topology are just as problematic because buildings are frequently not preserved in their entirety. Also, where they are tightly clustered, the boundaries between individual houses are often a matter of speculation.

Definition of archaeological proxy parameters: Possible archaeological proxies (') for P , L , S and R were found by analogy and are explained in the following by reference to data from Tall Asmar and Khafajah. T was excluded for lack of sufficient data. The resulting model was applied to sections through the area between the Temple Oval and the Sin temple in Khafajah as an example. A statistical determination of its near or non-equivalence respectively with the original model based on a representative sample of ancient urban settlements was not attempted. Near Eastern archaeology has always had a penchant towards neglecting private quarters in favour of official parts of settlements, and far too little material has been published to date.

L' : Lifetimes can be assigned to archaeological structures by reference to some measurable quantity A with a clear relative chronological component instead of years. In a reliable stratigraphic framework, mean lifetime might, for instance, be expressed as the number of sequential building phases B of structures in area x relative to the number of sequential building phases A of structures in area y in the

overlapping parts of the sequences in x and y, where y is the sequence with the highest number of building phases, i.e. the best temporal resolution. For Khafajah, A denotes the house levels while B denotes building phases of the Temple Oval, the Small Temple and the Sin Temple respectively (table 1:A-A, adapted from Delougaz et al. 1967: "table at end").

P': Mean positional change per building level is the sum of horizontal differences of the mass centres of walls from successive building periods (table 1: A-B) divided by the number of building levels of the sequence (table 1:B-B). The rate of change, i.e. a measure of instability, determined from sections is therefore (P'/L') (table 1:C-B). The section 8-8' (Delougaz 1940: Plate 8) and the cross section through houses, Temple Oval, and Sin temple (Delougaz 1940: Plate 12) were taken as examples; the coding used in table 1:A-B is explained in fig.3.

S': Wall thickness (table 1:D-B) is a proxy for building size. In large official buildings, such as palaces and large temples, walls usually make up a quarter to a third of the covered area (H.-J. Schmied, *personal communication*; and Wäfler TH4); smaller buildings like private dwellings and small temples generally have thinner walls in relation to their size. Wall thickness, then, is correlated with building size via room size. Since this cannot be shown in vertical sections, a brief demonstration using plans from Tall Asmar shall be given here: for those buildings of which the spatial extension is known (Delougaz et al. 1967: plate 23), the correlation (Spearman rank-order) is strong at $c=0.833$, the only outlier being the overly thick-walled Gimilsin temple:

Size (rank)

8. Southern building							7
7. Northern Palace						6	
6. Palace of the Rulers				5			
5. Gimilsin Temple							8
4. Azuzum Building			3				
3. Audience Hall of Naramsin				4			
2. Snake Shrine			2				
1. Private Houses	1						

Wall thickness (rank)

R': Regularity of shape cannot be determined from sections either. For Tall Asmar (Delougaz et al. 1967: plate 23) visual grading of the linearity and orthogonality of a building demonstrates a strong correlation of geometric regularity and wall thickness, i.e. one of the parameters measurable in vertical sections (a better definition of geometric regularity based on algorithmic complexity is given in §3.4.). The correlation (Spearman rank-order) is nearly functional at $c=0.929$:

Geometric regularity (rank)

8. Gimilsin Temple							8
7. Southern building						7	
6. Palace of the Rulers				5			
5. Audience Hall of Naramsin				4			
4. Northern Palace						6	
3. Azuzum Building			3				
2. Snake Shrine			2				
1. Private Houses	1						

Wall thickness (rank)

Khafajah: Calculation of the correlations (continuous values: Pearson, graded values: *Spearman*) between the proxy parameters (P',L', S',R') when applied to the data from Khafajah (Table 1) yields:

L'	0.259			
S'	0.401	0.937		
R'	-0.090	0.782	0.745	
P'/L'			-0.043	-0.354
	P'	L'	S'	R'

Where comparable (bold print) this is in accordance with the original model. The extremely weak size (S')-instability (P'/L') correlation may be due to the short distance covered by the sections and the stabilizing influence of the two important and long-lived official buildings framing the area, the Temple Oval and the Sin temple. Within this small area, however, a clear dependence of instability on the distance D (table 1: H-B) to the nearest official building is apparent (bold print):

D	0.242	-0.488	-0.501	-0.837	0.548
	P'	L'	S'	R'	P'/L'

Thus, the correlation of local stochasticity $s(a)$ and distance to stable cores observed in modern urban settlements can be demonstrated in Khafajah as well. The replicability, coherence and robustness of this specific data structure were not tested on a representative number of additional sites for lack of data. The proposed proxy model will *faute de mieux* serve as a theoretical basis for further discussion.

1.2. Topographic Indicators of Buried Monumental Buildings and Individual Architectural Features

Definition of Monumentality: Monumentality is an often discussed but rather ill-defined concept that has seldom received other than philosophical treatment emphasizing its symbolic and metaphoric aspects (Ockman 1993). Trigger (1990), as the probably most often cited recent voice, sees as the principal defining feature of monumental architecture that its scale and elaboration exceed the requirements of any practical functions that a building is intended to perform. Superficially more formal are definitions focussing on the combination of scale, order, repetition and unity (e.g. Safdie 1984). Intentions, functions, unity etc., however, are themselves rather flimsy terms that are hard to translate into an archaeological context. If automated detection is the ultimate aim, an intuitively fitting definition - however provisional - based on measurable observables is needed.

Judging by the way the word and its derivatives are used in Near Eastern archaeology, "monumentality" may be attributed to buildings as diverse as the palaces of Mari (Heinrich 1984), the Anu Ziqurrat (Heinrich 1982), the Gimilsin temple at Tall Asmar (Delougaz et al. 1967), the "Monumental Palace" at Tall Brak (Oates et al. 1998), possibly even the early temples at Eridu (Safar 1981). Size alone, therefore, does not make a building monumental. The context of a building would seem to play an important role: the small Eridu temples might be considered monumental because of a pronounced contrast to their proto-urban surroundings. In the setting of Eana, these temples would not be counted as monumental. The closest thing to a common denominator may be an impression of weight and static detachedness from a contrastingly lighter, more dynamic urban environment (e.g. a stone building surrounded by wooden huts, or the heavy-walled house of a rich merchant vis-à-vis of houses in a poor quarter).

In the framework of the proposed model, monumentality may be defined by high S' and R' relative to the average in a given area. Great wall thickness and high geometric regularity, then, are the hallmarks of monumentality, while size counts only by implication via its strong correlation with wall thickness. Large buildings, then, are not necessarily monumental, but monumental buildings tend to be large.

Stability and topographic signatures of buried monumental buildings: S' and R' are both negatively correlated with D , which in turn is positively correlated with instability (P'/L'). On the scale of entire settlements, high S' and R' are therefore to be expected in areas of relative stability. The vertical structure of such areas is characterized by sequences of successive walls (table 1: G-B) that stay in place through a comparatively high number of strata, as implied by the strong negative correlation (Spearman rank-order: $c = -0.783$) between $L(\text{seq})$ and D . In the plane, the outline of monumental buildings is therefore less prone to change over time than the outline of less regular or less thick-walled buildings.

Intact parts of walls and the debris-filled spaces between walls have different physical properties, and can be expected to be subject to erosion at different rates. Because of the greater average depth of homogenous material over several strata, the probability that a buried monumental mudbrick building will manifest itself by a distinct topographic signature is higher than in the case of a non-monumental building of the same size.

Thus, the empirically well-corroborated observation of variations in local stochasticity in regard to both modern settlement structure (O'Neill et al. 1988) and artefact distribution in ancient settlements (Wilkinson 2001), may be assumed to manifest itself in the topography of highly stratified settlement mounds. The higher the tall, the better.

2. DATA

2.1. The DEM based on the 1984 Topo-survey

2.1.1. Survey Data

The 1984 topo-survey was conducted by D. Steudler using a DKM-2AE theodolite and a DM 501 range finder with reflectors. A total of 720 reflector positions was measured within an area of ca. 700x600m. A summary of the measurements relevant for establishing the basic survey grid as well as a list of control measurements was published in TH1:77-86, and a more narrative account of the survey and the post-processing of the data was given in Steudler (1985). The complete, so far unpublished, set of measurements used for generating the contour map published in TH1 as "Plan 1" may be found in table 2 (available in electronic form [ASCII-coordinates] on request). In the present text, a new DEM based on the QuickGrid-Algorithm (QUICKGRID 2001) was used as a basis for all calculations. A comparison with the original DEM showed the differences to be negligible.

In fig.5B, the xy-point layer is projected onto the original contour map. The very uneven spacing of measurements is typical of traditional surveys using reflectors: areas that appear featureless to the surveyor are loosely sampled and inaccessible parts of the terrain that cannot be reached with reflectors necessarily remain unsampled. Within the area defined by the 355msl elevation line the average measurement density is 0.25points/100sqm (100 sqm=1 square), which corresponds to a mean resolution of 20m. Local variation, however, is very high, and while in some areas the density exceeds 4points/100sqm, in large parts of the DEM it may not reach the density thresholds required for computing a DEM with appropriate grid size, potentially leading to misrepresentations of topography (Zang and Montgomery 1994). In order to at least roughly assess the applicability of a method to specific parts of the DEM, an easily interpretable mode of representing local resolutions was needed.

2.1.2 Local Measurement Density

Kernel density: Local resolution, i.e. measurement density, can be determined in various ways. From the xy-point layer a simple density grid can be created, for example: a circular search area is defined around each point. The total number of points is calculated within the search radius, and is then divided by the search area size, resulting in a density value for each grid cell. A density map generated in this way is basically a trivariate histogram with discontinuous values between grid intervals and holes in loosely sampled areas. A much better, continuous representation of local densities can be achieved by estimating kernel densities (Silverman 1986, Beardah and Baxter 1996, Baxter et al. 1997, Bowmann and Azalini 1997): a kernel is a known probability density function. Averaged across the observed data points it creates a continuous density curve (univariate) or surface (bivariate); kernels in higher dimensions can be calculated as well. Except for a uniform distribution, points lying near the centre of the search are weighted more heavily according to the type of kernel (gaussian, triangular, etc.). The smoothness of the resulting curve or surface, however, depends mainly on the kernel bandwidth and not so much on the chosen distribution (Beardah and Baxter 1996). Whereas well-established methods for determining appropriate bandwidths exist for univariate kernel density estimates, the multivariate case is a matter of little theoretical consensus and, until recently, complete computational intractability in practice. Only at the time of writing have transparent, universally applicable algorithms for this task been published (Gray and Moore 2002, 2003); too late for being incorporated here.

Measurement density map: fig.5A is a colour-coded xy-kernel density map of the original survey data. The kernel is a bivariate gaussian (normal) distribution with a bandwidth $t=0.25$ of the data range in x and in y. The bandwidth was chosen interactively so as to conform to my subjective visual impression of measurement density in fig.5B.

2.2. Plans and Sections

The methods set forth in §§ 3.4.-3.5. were applied only to data extracted from plans and sections completed until 1999. These plans represent an unpublished stage in between TH2 and TH4; they no longer exist and cannot be reconstructed from the plans published in TH4 (§ 0.2.3.).

The drafts for the plans and sections published since 1984 (TH1, TH2, TH4) were drawn by hand in the field on the basis of measurements taken by different people using various types of theodolites and levels, but also, within squares, measurement tape and plummet. This conforms to the standard procedure in most excavation projects. It is problematic insofar as measurement errors vary locally and are difficult or impossible to determine post-hoc.

From 1990 onwards, 2D-CAD post-processing was done by D. Dallagnolo and, between 1997 and 2001, myself. The level of schematisation is high in large brick layers. Only bricks close to wall faces or layer boundaries were drawn individually; the same applies to areas with irregular brick packing. Where packing was regular within a layer, dividing the total area of the layer by the number of bricks averaged the dimensions of bricks as well as joints. In vertical sections, small deviations of individual layers from the horizontal within large compact wall sections were ignored. For individual bricks this results in centre-point deviations from measured horizontal position of probably not more than a decimetre in the centre of large layers. In the vicinity of layer boundaries, where the plans are ziegelgerecht, positional and angular accuracy may in most cases be assumed to be in the range of the - unknown - measurement errors.

Plans 3, 4 and 5 (TH4) were generated in 2002-2003 by merging and updating the original CAD drawings of individual squares. *These new plans do no longer accurately represent excavation data.* They were repeatedly adjusted according to the changing ideas on the structure of the Palace derived from my hypothetical predictions. As a consequence, they exhibit considerable positional as well as angular deviations from the plans used in the present text. In at least one case, a relevant architectural element appearing in the plans of 1999 was removed entirely (§ 0.2.3., 3.4). Results based on excavation data up to and including 1999 can therefore not be replicated using data from these later plans.

2.3. Satellite Imagery and 3D Laser Scanner Data

VHR-remote sensing data (Wheatley and Gillings 2002) and ultra-dense 3D point clouds acquired by Laser scanning (Langer *et al.* 2000, Sawyer 2002) are occasionally referred to in the theoretical sections of this text (§ 0.2.2). These two kinds of data are the potentially richest, as yet almost untapped sources of topographic data for PSDR.

Corona and Ikonos data: In 2001 various Corona b/w-images of the surroundings of Tall al-Hamidiya were acquired (CORONA 2002) as well as Ikonos multispectral VHR-imagery (1m and 4m-resolutions) of a 11x11km square centred on the tall (IKONOS 2002; cf. fig. 2). Classification, analysis and feature extraction from 2D remote sensing data is being conducted in collaboration with other researchers (Gerber and Wunderle).

3D Laser scanners: In 2001 the Institute of Ancient Near Eastern Archaeology and Languages, University of Berne, together with three partner institutes, acquired a Cyrax 2500 Laser Scanner (Cyrax/Cyclone 2002). This device determines the position of ca. 1000 points per second within a field of view of 40x40deg (max.) over a distance of up to 100m. It uses a pulsed laser beam and records the time-of-flight from emission to return of the pulse to remotely capture 3D surfaces. Resolutions in the sub-centimetre range are possible ($\geq 2\text{mm}$ point-to-point spacing @ 50m), and the accuracy is 6mm (1σ @ 50m) for individual points and 2mm for modelled surfaces (data courtesy of Leica Geosystems, Switzerland). Comparable devices based on continuous wave emission emit a

beam with constantly changing amplitude. Each reflection from a point has a specific amplitude signature that also reveals the time of flight. Such continuous wave scanners are much faster and usually have a wider field of view than pulsed Laser scanners. The current model of the Quantapoint scanner, for instance, scans at 150'000pts/sec in a window of 360x320deg (QUANTAPOINT 2002, Sawyer 2002), exceeded only by the iQsun system, which reaches 200'000pts/sec (IQSUN 2002).

In both types, the finished scan results in a point cloud consisting of millions of xyz-coordinates requiring specialized CAD software able to handle such vast amounts of data (e.g. LASERGEN 2002), additionally a reflection intensity value for each coordinate is usually noted, and, if the scanner has an appropriate passive channel, a true colour value (RIEGL 2002, Z+F 2002). Objects are scanned from various positions and the individual scans registered by fixed or natural targets, i.e. well-defined points common to more than one scan (CYRAX/CYCLONE 2002) or by statistically finding the best fit between modelled surfaces (e.g. PARAFORM 2002) in order to compensate for wholes and shadows due to invisibility from a specific scanner position (Besl 1998, Lapointe and Mercier 2000).

At Tall al-Hamidiya a Laser scanner will be used for the first time in 2004 for both topo-surveying and documentation of excavation results. In 2002, various tests were conducted in France and Switzerland in collaboration with other researchers (Gerber 2002, Hoffmann 2002, Theocharis *unpublished data*) and in Turkey (Hoffmann and Theocharis, *in preparation*). A database of archaeological VHR-scans is being planned as a research tool.

3. METHODOLOGY, METHODS, RESULTS

3.1. Predictions based on Fractality Analysis at Large Scales

3.1.1 Aims

A multitude of different feature extraction techniques may be used to detect linearity, parallelity and other traces of artificiality in remote imagery (Chen 1999). Appropriate combinations of such image processing methods are ever more frequently employed in archaeology (e.g. Campano 2002, Pavlidis et al. 2002) the targets, however, normally being relatively easily recognizable structures, usually made of stone or other imperishable materials. Although they might conceivably be used to detect indicators of heavily eroded monumental mudbrick architecture within a natural environment if appropriately calibrated, a more direct approach based on fractality analysis that I believe to be better adapted to detect deviations from 'naturalness' is explored theoretically in this section.

Fractality is a geometric, scale-invariant property of most natural structures. Artificial objects are usually non-fractal and obey the simpler laws of Euclidian geometry. Since the collapse and subsequent erosion of buildings leads to progressively more natural shapes and, hence, an increase in fractality, a tall's specific fractality signature is assumed to be an indicator of its potential for harbouring monumental architecture.

3.1.2 Fractality

To the human eye a house in front of a mountain scenery stands out clearly even when viewed from a considerable distance or depicted in greyscales. The contrast between the relatively smooth surfaces and clear boundaries of the house and the heterogeneous surface structure and broken boundary lines of natural rock is apparently great enough for the brain to distinguish between the man-made object and its natural background. Much of the information one might intuitively consider important - details like windows or the shape of a roof as well as colour information - have comparatively little distinctive value. On a conceptual level, this contrast in perception corresponds to two fundamentally different geometries. Man-made objects are generally best represented within the framework of Euclidian geometry, and can often be modelled by combining geometrical primitives like cubes or cylinders. Most natural structures, on the other hand, are more adequately represented by fractal geometry.

Fractals, in the words of Mandelbrot (1977) who coined the term, are geometric shapes that are equally complex in their details as in their overall form. A "perfect" fractal can be thought of as a shape that can be subdivided in parts, each of which is an exact copy of the whole. Such a fractal is self-similar and scale-invariant in the sense that its - impossible - physical realisation would appear the same if seen from a great distance or viewed under a microscope. Mathematical structures like the von Koch curve (von Koch 1906) are perfect in this sense. The von Koch curve is generated by splitting a line segment into three equal parts and replacing the middle one by two joined segments of the same length (fig.6). Iterating this procedure indefinitely results in a truly self-similar and scale-invariant pattern.

The rough and fragmented shapes of most natural objects, such as branches of trees, edges of clouds, turbulence phenomena, but also mountains, coastlines and other landscape features (Goodchild and Mark 1987), are fractal or partly fractal in a different sense. Their fractal elements belong to a class of fractals called fractional Brownian (Mandelbrot and van Ness 1968). The degree of their self-similarity is limited by stochastic irregularities in the mapping of the whole onto the parts, and they are self-similar only within a certain range of scales. Algorithms adequately replicating such structures, so called Iterated Function Systems (Barnsley and Demko 1985, Barnsley 1988), therefore have a deterministic and a stochastic component: for instance, iteratively moving the middle of a line segment perpendicularly by a fixed distance with a normally distributed error results in a natural looking shape

with a strict, though not immediately obvious, underlying regularity. This procedure, the stochastic interpolation of a line, may be extended to two dimensions to model terrain surfaces (Clarke 1987, Laurini and Thompson 1992: 158). Note, however, that while the elevation coordinate relates statistically to the two horizontal coordinates, it has an order of magnitude which is less than the other two. Thus, horizontal sections of the terrain exhibit isotropic scaling, while longitudinal sections exhibit anisotropy. As a result, coastlines and contours are statistically self-similar while vertical terrain profiles are self-affine (Bindlish and Barros 1996, Turcotte 1997).

No conclusive explanation of the physical universality of fractality has yet been found. Based on the observation that channel and hillslope adjustment by sediment transport can often be modelled by the diffusion equation with a diffusivity dependent on discharge, the fractal nature of topographic transects is believed to be due to a non-linear term introduced in the partial differential equation for landscape elevation by an empirically well-corroborated dependency of diffusivity on discharge (Pelletier 2002).

Fractal Dimension: Fractal geometry thus lends itself to the algorithmic description of natural objects by generating adequate replications of them. The inverse problem of determining if an object is fractal, and to what degree, is linked to the definition of an appropriate measurement unit. Subjectively, the rugged outlines of natural shapes would seem to fit the space they occupy more densely than those of their artificial counterparts. This subjective feeling can be quantified by various numbers associated with fractals and referred to as fractal dimensions (Barnsley 1988: 173-182). They have in common that all are calculated by taking the limit of the quotient of the log change in object size and the log change in measurement scale as it approaches zero; in other words: fractals scale according to a power law. For open-curve non-stochastic fractals a special case applies insofar as this quotient is constant and the fractal dimension d can be obtained by the equation

$$d = \log N / \log (1/r) \quad (\text{Eq. 1})$$

where N is the number of linear elements in the repeated pattern (the repetitor), and r the self-similarity ratio (the inverse of the scaling factor s). For stochastic fractals or structures comprising of a combination of fractals d is determined by regressing the quotient elements against each other to compensate for random scatter.

Having established fractal dimension as a measurement unit, a mathematical definition of fractality can be given: a shape is considered a fractal if its fractal dimension is larger than its topological ("normal") dimension. Hence, if, in the simplest case, a shape made up from line segments (topological dimension 1) has a fractal dimension >1 it is a fractal. This is true for the von Koch curve in fig.6, for example, which is formed by repeatedly replacing the 3 segments of the initial line with 4 new segments (repetitor), where each of the 4 new lines is $1/3$ the length of the initial line (self-similarity ratio): its topological dimension is 1, because scaling the line segments it consists of by a factor of 2 results in new segments twice as long as their originals, hence: $\log 2 / \log 2 = 1$. Linearly scaling the whole curve by a factor of 3, however, will result in a curve 4 times as large, and its fractal dimension is therefore $\log 4 / \log 3 = 1.261$. The coastline of Britain, a famous example of a typically fractional Brownian real-world structure, has roughly the same fractal dimension (Mandelbrot 1967).

3.1.3. Scale vs. Resolution

Problems of Scale and Resolution: Fractal dimensions are experimental observables, and under ideal conditions their estimation poses no problems. However, in practice, an object or a structure of interest can frequently not be measured directly but only via some sort of abstracted representation - in the case of Tall al-Hamidiya a remotely sensed 2D raster image with fixed resolution and a vector DEM with interpolated surfaces based on unevenly distributed measurements. In both cases, the range of scales available for analysis is limited by resolution (raster) or local measurement density (vector). If an object or a structure of interest is very big relative to the level of detail of its representation, a sufficiently large part of the range of scales within which it exhibits fractality remains available for

analysis. For smaller objects or structures the measurement errors (raster) or interpolation errors (vector) become relatively larger and the range of accessible scales may be too limited to allow any confident estimate of fractality. In other words, if the ratio of object size/pixel size (raster) or object size/[1/local measurement density] (vector) is below a certain threshold T , the object's self-similarity, if present, is not preserved through the imaging process and cannot be determined.

Eq. 2 is a somewhat rubbery approximation of T for the fractal outline of an independently known object. It is presented only for the sake of a thought experiment intended to give an idea of the object sizes necessary for assessing fractality.

$$T \approx \{K(1/r)\}^n \quad (\text{Eq. 2})$$

where r is the self-similarity ratio of the object's outline, and n the minimum number of sample scales considered sufficient for regression. K is the minimum number of pixels in an orthogonal grid necessary to reproduce the repetitor pattern in sufficient detail to be recognizable under a given definition of d . Kube and Pentland (1988, cf. McGunnigle and Chantler 2001) analysed the properties of images of fractal surfaces and showed that the image of a fractal Brownian surface is fractal Brownian - i.e. self-similar - only under certain conditions, some of which are unrelated to the problem discussed here. T as defined above does not explicitly take account of these conditions. Nevertheless, with some goodwill K can be thought of as a proxy for their combined effect on T .

If, in a raster image, $r=0.5$ and $n=3$ for a given object and regression method, and $K=(3^*4)$, then the object has to be represented by ≥ 13824 pixels in the image. In the case of an Ikonos VHR-image with a pixel size of $1*1\text{m}$ this corresponds to a boundary line $\geq 470\text{m}$ assuming a roughly square outline, and side lengths $\geq 117.5\text{m}$. Under these conditions, i.e. with only 3 scales for assessing scale-invariance and working with the best satellite data available commercially at the time of writing, the fractality of a smaller object can therefore be estimated only at scales $\ll 0.10\text{km}$. Employing mixed-pixel methods or other approaches to extract sub-pixel information would probably not lead to a significant reduction of this limiting scale (Blaschke et al. 2000). This illustrates that the fractality of structures in the size-range of most architectural objects relevant to the archaeologist cannot at present be assessed: VHR remote imagery is sufficient only where exceptionally large buildings are targeted, and elevation maps of Talls not generated by laser scanning are useless for this task.

3.1.4. Detection of Sites Potentially Harboursing Monumental Architecture

Theoretical basis of detection algorithms: Talls harbouring monumental architecture are expected to exhibit a fractality-signature with two crossover scales within a range that is slightly lower but equivalent in width to the size range of its monumental buildings (§1.4.1.). Typically, then, this range would be somewhere around 0.01-0.10km (fig. 4). Using state of the art VHR-satellite imagery or traditional topo-survey data, the lower crossover scale will therefore remain undetectable. However, these are purely practical limitations that may be overcome in the nearest future. Theoretically, this signature, if corroborated empirically, would be clearly distinguishable from the signature of non-urban talls (1 crossover scale $< \text{ca. } 0.05\text{km}$) as well as from those of the surrounding landscape: the majority of topographic data sets cannot be adequately characterized by a single fractal dimension either. Rather, the behaviour of natural topography tends to be divided into scale ranges with fairly distinct crossovers (Brown 2000). Over scales $< 0.6\text{km}$ many of the surfaces can be modelled as fractional Brownian surfaces with d around 2.2 - 2.3. Over larger scales, higher dimensions around 2.75 are noted while at still larger scales many terrestrial surfaces exhibit periodicities (Mark and Aronson 1984, Clarke 1987). The surroundings of talls will often show signatures that differ systematically from those of natural landscapes due to more or less intensive agriculture. Field patterns and plough marks may lead to a region-specific signatures with a fairly low average fractality - in all probability lower than that of most talls, and with different crossover scales.

Once the price for VHR imagery at appropriate resolutions drops to an affordable level, large-area searches for such differences could be conducted using techniques borrowed from landscape ecology

to determine local fractality (Milne 1988), or by adapting existing military image processing algorithms for detecting man-made structures in aerial photographs like the one initially developed by Stein 1987, where the deviation from fractal behaviour over a range of scales is measured using a least squares model

$$\epsilon = \sum_r (\log M(r) - (a \log(r) + b))^2 \quad (\text{Eq. 3})$$

where $M(r)$ is some metric property of the image such as its power spectral density or surface area, r is the scale of measurement, a and b are constants that minimize the residual error ϵ . For fractals $M(r) \sim r^{f(D)}$ where $f(D)$ is some function of the fractal dimension D . As discussed *sub* Eq.1, log-log regressing r vs. $M(r)$ yields a straight line with slope a for fractal geometries. If applied to a running window, ϵ therefore tends to be small over those portions of an image containing natural terrain features and large where there are artificial structures.

In areas and periods from which written sources are known, the combination of such fractality-based detection algorithms with predictive GIS (Wescott and Brandon 1999) or localisation techniques as those set forth by Wäfler (TH3) would allow targeted searches for specific sites or even buildings with an unprecedented degree of precision, control and replicability. Despite having been employed in military reconnaissance for more than two decades, these methods are not in widespread academic or civil use - with the notable exception of the SETI community that has adopted them eagerly in the search for extraterrestrial artefacts (Carlotto 1988, 1993, Carlotto and Stein 1990, Crater 2002).

3.2. Scale-insensitive Alternatives to Fractality Analysis at Small Scales

3.2.1. Fractality at the Scale of Individual Buildings

Over scales much smaller than the size of an eroded building, the fractal dimension of its contours may be assumed to be in the range expected for natural structures (§2.1.4.), and to depend only on the time of exposure to erosion and on the specific erosion behaviour of the building material, usually mudbrick. The shape and size of the original structure are irrelevant, and information on either may therefore not be deduced from the fractality of the building at such small scales.

At scales approaching a building's size, fractality - if measurable, i.e. under the condition that s is small enough (cf. fig. 4) - will assume values typical for artificial structures, i.e. very close to its topological dimension. The most common estimate of the fractal dimension of natural shapes derivable from Eq. 1 (Brown 2000) is

$$d = 2 * s \quad (\text{Eq. 4.1})$$

where s is the slope of the regression of the log of patch perimeter versus the log of patch area (Lovejoy 1982, Krummel et al. 1987, O'Neill et al. 1988, Sugihara 1990). At the single scale equal to the building's size, finally, it cannot be measured because scale-invariance can only be assessed over a range of scales. In this special case,

$$d' = \log(\text{area})/\log(\text{perimeter}) \quad (\text{Eq. 4.2})$$

which is a pure shape index and, as such, building specific. d' , in contrast to d , is not a dimension estimate. Because contours resulting from building collapse and subsequent erosion preserve parallelity (§3.3.2.), a significant change in the shape index from one contour (n) to the next ($n-1$) may be assumed to point to a change in shape at elevation $n-1$.

3.2.2. Scale-independent Proxis

Proxies for Fractal Dimension: Over the past two decades, quantitative landscape ecology as a discipline concerned with finding correlations between changes in landscape patterns and ecological processes has developed a wealth of spatial metrics appropriate for automated analysis of remote sensing imagery. Under the empirically well-founded assumption that the overall fractality of a landscape is negatively correlated with human impact, various of these indices quantify the average fractality of the patches (clusters of pixels with identical or similar attributes) of a specific area in order to allow comparisons between different regions (Turner and Gardner 1991). There is much debate as to the techniques of estimating fractal dimensions where no direct measurements are possible (Russ 1994); judging by the methods implemented in two widely used software packages, APACK (2001) and FRAGSTATS (McGarigal and Marks 1995) the most common estimates are by log-log regressing box size in a specific area versus the number of boxes required to cover the area (Loehle 1990) or by applying Eq. 4.1. The latter estimate is commonly known as the Shape Complexity Index (SCI).

The consistency of the SCI between sets of images of different resolution has been scrutinized repeatedly. The results, however, are inconclusive: in some cases the index was consistent over various scales (Rami 1997) in others not (Gasper and Menz 2002). Since the assumptions underlying the SCI are well grounded theoretically and empirically, a low object size/pixel size ratio (§3.1.3.) in some of the images used for testing may account for much of the inconsistency: the sensors noted by Gasper and Menz (2002) are CORINE (30m), REKLIP (30m) and, without further specifications, NOAA (1000-1100m). In the same study, a variant index (Durchschnittliche Normierte Fläche = DNF) is proposed as a scale-insensitive alternative. The correlation between the two indices applied to the same data was not very high at $c=0.5$.

Shape indices: Because DNF as an alternative metric is scale-insensitive, it might also be used at lower scales as a pure shape index. As such, it contains no information on the actual shape of a building but only on the degree of elongatedness and, thus, ruggedness of its outline. While possibly appropriate to detect boundaries between buildings, it cannot be used to determine the type of a building. For the latter task, more shape-sensitive methods are currently being investigated, such as shape indexing using histograms of cumulative distances from points within the shape to points on the shape boundary (Tetik and Wymann 1997, Ankerst et al. 1999) or using exact distributions of the average of the two distances from a point a running along the shape boundary to the points b and c on the boundary line defined by its intersection with a straight line starting from a at 90deg and 45deg to the local tangent respectively (Gerber and Tetik, *in preparation*).

3.2.3. Implementation and Results

Detecting changes in shape between contours at Tall al-Hamidiya: The following simple variant of DNF was used to detect changes in shape of buried structures between contours of different elevation at Tall al-Hamidiya:

$$B = \text{SQR}(\text{area}) / \text{perimeter} \quad (\text{Eq. 5})$$

Obviously, B is also a shape index, not a measure of fractal dimension. Its sensitivity to changes in shape between objects built of identical elements and, thus, with identical surface areas, but different outlines is illustrated in fig.7: The index is highest for the compact shapes 1 and 3 and much lower for shape 2 which is the most rugged and, therefore, has the highest degree of elongatedness. B can only be determined for closed shapes, in this case whole contours. This is problematic because a) a contour may represent the merged shapes of more than one eroded architectural structure, and b) a contour may include areas with insufficient measurement densities. For Tall al-Hamidiya, calculation of B therefore only makes sense within blocks that can reasonably be assumed to represent a constant number of structures, and an assessment is possible only through comparison with results obtained by other methods. Fig.8A is a hierarchical tree of such blocks at Tall al-Hamidiya: the nodes are defined by mergers of two contours at 1m-intervals and correspond topographically to saddle-shaped watersheds (fig.8B). The lower in the hierarchy a block is located, the more likely it is to be a conglomerate of various structures, and the smaller the likely influence of individual buildings on a contour.

In fig. 9 the B -values of the contours from a single branch of the hierarchical tree (blocks 2-8-9-11-14-15) are plotted against elevation. Between blocks, large but meaningless differences in B -values are apparent. Within individual blocks the relative differences between the values of B may be meaningful insofar as B gets smaller the more elongated a shape. For the generally rounded shapes exhibited by the tall contours, B increases over decreasing elevations if the buried shape exhibits broad protrusions, i.e. one or many convex corners below this specific elevation, and decreases in the case of one or many concave corners. However, within very slim blocks, the potentially relevant differences in B may well be within the range of stochastic noise or - in areas with insufficient measurement densities - interpolation errors.

Basic shapes: Only blocks 8 and 15 extend over a relevant number of contours. Block 8 (387-367msl) shows a fairly continuous series of values with two platforms at 386-379msl and 373-370msl respectively (red caps). It overlaps to a fair extent with the area having the greatest measurement density (bold line in fig. 5A), and since B decreases from the higher platform to the lower, one or many concave corners not present in the shape represented by the higher platform are to be expected in the larger shape represented by the lower platform, obviously located in one or both of the areas defined by the wadis cutting into block 8 from NE and SW (black arrows in fig. 8). At 370-367msl, the steep increase towards values of B comparable to those at 386-379msl may suggest a shape hidden in the northern part of block 9 that is similar to the one represented by the higher platform.

Block 15 (360-355msl) exhibits a very stable increase in B and no platforms. The increase is caused by two large wadis (blue arrows in fig. 8) getting shallower towards the plain, which results in more rounded contours at lower elevations.

Assessment: the shape index (Eq. 5) is unspecific in all aspects of shape except general elongatedness or ruggedness. By itself it is therefore only useful for comparing shapes and determining changes in shape within blocks. It has to be supplemented by visual interpretation when the influence on B of localized attributes of shape is to be assessed. For automation the histogram methods mentioned in §3.2.2 would have to be implemented.

Vertically, the B-values in block 8 would seem to point to a sandwich structure with two sets of contours of similar shape separated by a set of contours of different shape exhibiting two broad incisions, i.e. concave corners. The upper and middle sets are well-defined by constant B-values whereas the lowest can only be guessed on the basis of the direction of change in B in the transitional zone before blocks 8 and 4 merge into 9, and of the specific value of B at the block boundary.

The small variation in B values within the two platforms excludes the presence of multiple structures at the relevant elevations. Otherwise, one would expect B to scatter more widely around a constant running mean. The contours defining these platforms, therefore, correspond most probably to the debris cone of a single terraced structure extending over the whole area of block 8.

3.3. Predictions based on Topographic Analysis

3.3.1. Topographic Effects of Erosion

Early models of natural hillslope development were mostly qualitative-dispositional and based on philosophical inference rather than representative empirical data (Parsons 1988, Kienholz 1993). In the 1970s more mathematical approaches were nourished with ever more abundant quantitative data, and rapidly developed into sophisticated process-response models employing numerical simulation techniques (e.g. Kirkby 1971, 1976, 1990, Armstrong 1976). The exponential increase in computing power during the past two decades soon allowed numerical modelling on the particle level and has led to a rapid generalization of models and a deeper understanding of the interacting physical processes underlying hillslope evolution (Jaeger and Nagel 1992, Ritter et al. 1995, Tucker et al. 1997, Favis-Mortlok et al. 1998, Tucker et al. 2000, Harmon and Doe 2001, *et multa alia*).

Artificial and semi-artificial slopes: Far less thoroughly researched are artificial and semi-artificial slopes. Only occasionally have erosional changes in slope form of recent artificial mounds been monitored and modelled (Haigh 1979, Goodman and Haigh 1981, Evans et al. 1992). For semi-arid archaeological sites the situation is even worse. Although various aspects of erosion have been investigated in depth (e.g. Bell and Boardman 1992, Wainwright 1994, Christopherson and Guertin 1995, Peterson et al. 2002), only very few studies employed quantitative models to simulate the morphological/topographic evolution of individual sites (Kirkby and Kirkby 1976, Haita 2001).

Determination of initial states: Most erosion processes exhibit non-linear behaviour to a certain degree (Favis-Mortlok et al. 1998, Martin 2000, Tucker et al. 2000, Istanbuloglu et al. 2002) and are on the whole unidirectional in the sense that from a specific outcome - e.g. the modern shape of a tall - a specific initial state - its shape in 2000 BCE - cannot be determined by simply running a process model backwards. Sophisticated models like CHILD (2002) or the concept-stage Geobot-model (Haff 2002) might, in an appropriate probabilistic framework, allow a narrowing down of the range of likely initial states by retro-calculation below the threshold of the obvious, but to my knowledge, this has never been attempted.

The approach advocated here is much less ambitious: using very simple models the preservation of shape attributes of specific types of initial states was investigated. These attributes were viewed as signals in the form of topographic markers containing mainly relative positional and orientational information. They deteriorate in strength and specificity over time and, at some point, are irretrievably lost in the increasing noise of progressive fractalisation caused by non-linearities in the erosion process. Of interest are only a signal's detectability and systematic changes in specificity. An attribute A initially representing the precise position of an architectural element (x,y) , for example, may at the time of detection only contain information on the upslope or downslope direction in which the element was originally located resulting in statements of the form $A(x',y' | x',y')$. The total of such signals retrieved from the modern topography of a tall only illustrates what must minimally have been present originally, and in which areas the elements associated with detected signals were most likely located.

Assumptions concerning shape development in Near Eastern talls: In order to compensate for the lack of empirical data on the erosion behaviour of different materials potentially present in talls, it was assumed throughout the following sections that talls are relatively homogenous in respect to material, specifically, that they consist exclusively of sun-dried mudbrick or mudbrick debris. The influence of wind-borne sediments, the occasional stone etc. was consciously ignored in order to exclude material-dependent differential impacts of erosion processes from the models, as e.g. the differential sedimentation of particles according to size or changing friction coefficients between soil layers of different material composition. Additionally, the following simplifying assumptions were made:

a) If not intentionally levelled, unused mudbrick structures on the surface of a settlement mound collapse within a very short time after their abandonment. The tallus-like debris slopes that result from

this initial collapse have a predictable angle of repose that is slightly lower than the stability threshold gradient for material of this kind.

b) The post-collapse changes in form of the debris slope are continuous and may be modelled using diffusion equations. Creep, i.e. gravity-driven particle transport without significant mass loss, is considered the only relevant physical process at this level. Mass loss by sheet flow, wind erosion, rainstorm events etc. is only implicitly present in the models in the form of unrealistically high creep rates .

c) Incisions and cuts formed by running water are viewed as effects of a separate process that acts independently on the eroding slope. The local loss of mass effected by channelled water is assumed to be dependent on the density of the near-surface material.

The relevant attributes of a,b and c are summarized in the following chart:

Time	a	→	b	→	→
				→	c
Process type	catastrophic		continuous		continuous
	rapid		slow		slow
Effects	permanent		permanent		impermanent

The actual processes involved are not only much more complicated but also highly interdependent (Ritter et al. 1995). However, even though inaccurate as a physical description, the relative temporal succession and mutual independence of a, b and c agrees reasonably well with the succession of most of the relevant, topographically visible effects of erosion over time.

Measurement density: It was argued in § 1.2. that the shape of monumental buildings is likely to be preserved to some degree through collapse and subsequent erosion, but also that both processes necessarily lead to progressively more natural, i.e. fractal, shapes (§ 3.1.). Characteristic elements of a building are signals of its artificiality insofar as they can usually be described using Euclidian geometry. The progressive fractalisation resulting from erosion, then, necessarily leads to an increase in noise hiding that signal.

Noise is the limiting factor for the information content of a signal. It manifests itself in the form of random variation around the local signal mean and can often be reduced by simple averaging if sufficiently dense measurements are available (Pierce 1980). Because, in this particular case, the degree of noise is a function of time, a generally valid statement on limiting measurement densities for detecting eroded elements of mudbrick buildings cannot be given at present. Even if the relevant material properties of mudbrick were known, the increase of noise over time could only be quantified on the basis of fractality measurements on a large number of dated Near Eastern sites. The resolution required for such measurements on the scale of buildings can only be achieved by using 3D laser scanners (§ 3.1.3.); such a device will not be in use at Tall al-Hamidiya before 2004, however. For lack of objective criteria, the topographic analyses in this section are largely restricted to areas of medium to high local (Kernel) density (denoted by broken lines in fig.5B).

3.3.2. Slope and Gully Formation

3.3.2.1. Collapse of Mudbrick Walls

If particulate or granular matter is poured from a point (x,y,z) on a flat surface in the (x,y) -plane at $z=0$, it accumulates in the form of a cone spreading from its centre at $(x,y,0)$ with a fixed slope α , the so-called angle of repose. Tilting the plane will not affect the settled cone until a specific angle $\beta > \alpha$ – the threshold gradient of stability - is reached at its underside. At this point the straight cone surface collapses causing an avalanche to cascade downslope in a thin moving layer until it is again stopped by an obstacle and the angle of repose is restored (Jaeger and Nagel 1992, Möller et al. 2002). Unconsolidated heterogeneous material of any kind acts in the same way as long as the mean particle or lump size is relatively small as in the case of thoroughly weathered mudbrick. In abandoned mudbrick buildings, weathering sets in immediately on exposed wall surfaces. Rapidly progressing inward it causes the walls to become unstable and, eventually, to collapse. On flat ground, the unconsolidated debris then forms a talus-shaped cone at the wall base, which protects the lower parts of the original wall (fig. 10). This process stops when the debris cone reaches the height h_2 of the remaining wall.

Debris cones resulting from building collapse are traditionally said to have an angle of repose $\alpha \approx 30\text{deg}$ (Kirkby and Kirkby 1976, Schmid, personal communication). Field studies as well as experiments under standardized conditions have, however, shown this angle to vary considerably between 20-40deg for loose, unconsolidated soils as well as different types of debris (Young 1961, Brethoud 2001, Möller et al. 2002). Because it falls well within the uncertainty of the accepted traditional estimate of α , the slight systematic difference between α and the consistently steeper threshold angle of stability β has, to my knowledge, so far been neglected in archaeology.

Fig. 11A demonstrates the effect of ignoring the threshold gradient β in favour of a simplistic angle of repose model assuming $\alpha = 30\text{deg}$: In complex situations, where multiple buildings located close to each other collapse at different elevations, all slopes tend towards the stable angle of repose. Steps with a ratio of $\text{base}_n / (h_{n+1} + h_n) < 1$ are therefore covered completely by a featureless slope surface.

In a more realistic setting as shown in fig. 11B, the stability threshold gradient - arbitrarily set at $\beta = 35\text{deg}$ - is observable at the boundary between the remains of a wall and its associated debris cone (red arrows). Where the latter extends below the wall base it may itself be stabilized by a plateau formed by the difference of α and β in the debris of a lower wall. After collapse, i.e. when stability is reached, slight bumps in the otherwise even slope surface will therefore coincide positionally with original walls - even where $\text{base}_n / (h_{n+1} + h_n) < 1$.

3.3.2.2. Post-Collapse Slope Development

Mudbrick buildings usually start collapsing within a few months after abandonment. Compared to the erosion processes changing the shape of the debris mound after it has reached stability, collapse is extremely rapid, and the two types of processes may therefore be modelled as acting in sequence and independently from each other.

Simple shapes: Under lab conditions a settled cone of particulate or granular matter with a constant slope α will be subject to very slow acting processes roughly corresponding in their effect on the cone's shape to the combined effects of non-catastrophic mass wasting by soil creep, rain splash etc. in a natural environment. On the cone surface the random Brownian motion of particles is uninhibited in all directions away from the cone, resulting in individual particles tumbling downslope and accumulating at the base. The linear longitudinal profile (red line in fig. 12A) of the original cone is thereby transformed into an S-shaped slope that flattens progressively over time (blue curves in fig. 12A).

Due to the pull of gravity the average direction of these particle movements is perpendicular to the local orientation of the cone contour, i.e. the parallelity of original contour segments is preserved in the corresponding segments of the new shape.

This process can be modelled in one dimension (Fig. 12A) as a diffusion process by invoking a transport rule

$$S = -D(\Delta E/\Delta x) \quad (\text{Eq. 6.1})$$

and a rule of mass continuity

$$\Delta S/\Delta x + \Delta E/\Delta t = 0 \quad (\text{Eq. 6.2})$$

where x is the horizontal distance from the cone centre, E is the elevation above the plain and t is the time elapsed since the process onset (initial shape). S is the average rate of mass transport, which is proportional to the tangent of the local slope angle ($\Delta E/\Delta x$), and D (diffusivity) is the constant of proportionality.

Elevation (E) can then be expressed as a function of distance (x) at a given time (t) by

$$E = \{A/\text{SQRT}(4\pi Dt)\} \text{EXP}[-x^2/aDt] \quad (\text{Eq. 7})$$

where A is the cross-sectional area of the shape.

Obviously, Eq.7 is a variant of a normal density function, and the resulting shapes therefore are normal (Gaussian) curves (blue in fig. 12A). Such diffusion equations accurately represent changes in shape under lab conditions and may be used in isolation to describe a 'general case' of natural slope development if the influence of channelled water and non-continuous, catastrophic events like storms and landslides is ignored (Martin and Church 1997). They are thoroughly deterministic and can therefore not be used to accurately model the behaviour through time of a specific mound. However, as stated in § 3.3.1. the interest here was in determining generally applicable topographic markers for specific types of eroded artificial structures; for this task these simple, economic models are ideally suited.

Complex, composite shapes: Targeting large, urban tall, the expected slopes are more likely to have resulted from the erosion of complex, composite structures than from single walls collapsing on a horizontal plane. Fig. 12B illustrates the use of a slightly modified equation in such a complex setting. The slope (blue curve) tends towards developing convex and concave segments; only where the space between the two initial peaks is filled up does a fairly straight segment appear as a transitional shape before concavity is re-established by mass flowing unhindered into the plain at the base. The slope therefore may be described by a series of segments that are either convex (A), straight (B) or concave (C). At iteration 9 a second run was initiated by adding a small square block to the mound profile (red curves) in order to simulate occasional changes in mound form by re-settlement.

From this encoding of local attributes alone the boundary conditions at the base of a mound may be inferred directly from a DEM (fig. 13A):

- 1) If mass flow into the plain is unhindered, the series will necessarily terminate in a C-segment.
- 2) B-segments at the end imply the constant removal of mass by water running along a tangent to the base, i.e. a river that does not cut into the mound.

3) If the slope is convex at the base (A) more mass is removed by running water than is supplied by downslope transport. In latter case a river necessarily cuts into the mound. Parts above a straight line at β from the intersection of the slope with the water level are bound to collapse.

Segmentation Analysis: Mass loss by slope collapse causes the profile curve to move backwards. In case 3, therefore, attributes of the initial mound shape are a priori unlikely to be preserved. In cases 1 and 2 initial attributes may be preserved. Their detection depends on the vertical resolution of the DEM. In Fig. 13B the detectability of the turning points in the original shape to the left is illustrated. If the slope is represented at a relatively high resolution (red) both turning points are detected and their positioning is fairly accurate. At half this resolution (blue) the sensitivity is too low: the first turning point can no longer be detected and the double-convex upper part of the mound shows as a single A-segment with a turning point positioned too low in the slope. Obviously, the vertical resolution R_v required for a sufficiently detailed and accurate representation is $<$ the height h_m of the markers of interest, which, themselves, are necessarily $<$ than the height of the artificial elements they have evolved from. Concave as well as convex curve segments and the position of turning points in the transition zone are defined unequivocally by 5 points; as a rule of thumb, I therefore suggest using $R_v=0.2h_m$ as the minimum vertical resolution; turning points detected at this resolution are off-target by $0.1 h_m$ max.

Decimation: The opposite problem, oversensitivity, is encountered where the vertical resolution of a DEM is $R_v \ll h_m$. In this case small random bumps caused by the vagaries of weather, by trampling, temporary surface rilling etc. will by their presence in the encoded description hide the relevant shape attributes at the scale of h_m . I propose a robust, flexible decimation scheme that allows to filter unwanted noise at scales below h_m of the expected attributes (fig. 13C): assume a very high-resolution slope profile (smooth black line). Encoding yields 15 segments, each of which is evidently much smaller than h_m . By decimating all points except the turning points (red) the number of segments is lowered to 5, and, by repeating this procedure, to 3 (green), effectively cancelling out noise. At both levels of decimation the general form of the slope is preserved. At level 2 the segment height roughly equals h_m . B-segments resulting from decimation usually have no real world pendant; they have to be classified as A or C depending on the position above or below the new slope line of the majority of original turning points.

It goes without saying that this decimation scheme is robust only within a range of vertical resolutions (in a contour map = equidistance) limited by the local density of the topo-survey data underlying the DEM (Zhang and Montgomery 1994). The threshold is reached where local interpolation errors exceed $0.5R_v$, because below this value of R_v turning points may be purely artefactual.

Horizontal and vertical movements of slope attributes: Fig. 14 shows the development over time of the composite shape from fig. 11B. After the first iteration ($I=1$) the elevation of the encoded attributes at 5m-resolution corresponds well with the vertical position of the floor levels in the non-eroded post-collapse shape (initial state, $I=0$). The progressive levelling at later iterations causes the turning points defining the C-segments to move distinctly in the horizontal. Turning points at higher elevations become less distinct over time and eventually become undetectable. Their horizontal movement is slight. Upslope segments merged in this way preserve the original elevations of their upper and lower boundaries to a satisfactory degree. In the middle parts of the slope a slight downward movement is apparent whereas in its lower parts the accumulating debris moves the upper boundary of the terminal C-segment upwards. These vertical movements of the turning points are shown in fig. 15.

Automation: The proposed segmentation analysis can easily be automated because it relies exclusively on turning points directly extractable from profiles. Even though not quantifiable precisely due to a lack of empirical values for the necessary parameters (including time!), the known directions of both horizontal and vertical movements may be taken account of in the automatic classification of the results:

In a given longitudinal profile, markers M_n detected at (x_n, E_n)

a) indicate that the relative original horizontal position $x_{n \text{ original}}$ lies slightly upslope from $x_{n \text{ observed}}$ in A-segments and downslope in C-segments at the base of the slope.

b) indicate relative original vertical positions $E_{n \text{ original}} \geq E_{n \text{ observed}}$ if the turning points defining the relevant M belong exclusively to A-segments. If an A and a C-segment are included then $E_{n \text{ original}} \leq E_{n \text{ observed}}$.

c) do not exclude the presence of additional markers in the intervals $[E_{m-1}, E_m (m < n)]$ at earlier states.

3.3.2.3. Gullies and Wadis

Gully formation criteria: The formation of rills and gullies is still imperfectly understood in its details. Early models and their contemporary successors were deterministic and focused on quantifying average soil loss (e.g. RUSLE 2002). Today the formation processes themselves are more often dealt with in probabilistic models using 3D topographic data and including non-linear, non-deterministic components (Favis-Mortlok et al. 1998, Tucker et al. 2000, Brethour 2001, Haff 2001, Istanbuloglu et al. 2002). The processes of rill and gully formation are largely unidirectional, i.e. it is possible to some degree to predict how channels evolve if the initial topographic situation for the relevant area is known, but not the reverse. For the purpose of extracting indicators of eroded artificial structures from the topography of hills, four points are especially relevant:

a) Water follows the path of least resistance and its flow is more turbulent if channelled. In other words, less material is removed by sheet flow than by concentrated flow. If mass removal and sedimentation are not in equilibrium, for example in the steep parts of a hillslope, a small initial incision may become trapped in a positive feedback loop in which the increased mass removal leads to a progressive deepening of the incision, thereby further concentrating water flow and turbulence. In this manner a small rill may become a gully or even a large wadi.

b) Rills may form temporarily on any surface if the underlying soil is saturated. Most are rapidly destroyed by wind-borne sediment, raindrop impacts, soil creep and other predominantly stochastic processes. Only on relatively steep slopes with a flat or concave surface can some rills grow into gullies. On convex surfaces gully formation is very unlikely.

c) Gullies trapped in a growth cycle not only deepen but also expand in width because particle movement on both faces of the V-shaped incision is oriented towards the locally steepest slope angle, i.e. towards the gully axis.

d) Sediment transport rates are positively correlated with slope gradient and catchment area.

Extracting original wall orientations and positions of corners: From a and b it follows that in the early stages of tall erosion gullies are likely to form on steep slopes preserving original linearity or resulting from the erosion of concave corners. Because of their much larger contributing area, the latter will generally be deeper and wider from the beginning and are likely to grow into large wadis.

From c and d it follows, that the general flattening of a slope over time will reduce the impact of secondary formations in local concavities resulting from progressing random fractalisation of the mound surface. Primary gullies are less strongly affected by flattening because once trapped in a feedback-loop the gully gradient constantly remains steeper than the surrounding mound surface until a threshold is reached below which the flow velocity is too low to maintain a rate of sediment transport exceeding sedimentation. At this point both primary and secondary gullies will start to fill up from the base.

Therefore, regardless of changes in the mound contours large gullies may be assumed to have been caused by the last major change in local mound shape due to building collapse, and to have preserved their original orientation.

Fig. 16A is a schematic representation of these processes. In (1) the outline of a massive mudbrick structure before its collapse is shown. The arrows along the border point in the direction of least resistance towards the border of the structure, their length correlates with the extension of the contributing area of the point where the border intersects with the arrow. The relative size of the contributing area is taken as a proxy for the likelihood of a specific zone to cause gullying after collapse. Its is small for convex corners and largest for concave corners. In (2) gullies and a wadi are forming on the post-collapse surface, and (3) shows the deepening of the initial channels and the formation of secondary gullies in small concavities caused by random small-scale changes in shape.

The proposition that primary channels retain their original orientation implies that the direction of flow in gullies is approximately perpendicular to the original orientation of linear building elements, whereas in the larger wadis caused by concave corners the latter is likely to be located on or close to the line defined by the channel. In both cases, however, the channels may at a certain depth cut into older material below the collapsed walls. Differences in material composition or shallow buried wall remains might potentially alter the course of the channel bed while leaving the upper borders of the incision unaffected for some time.

In fig. 16B a simple way to determine the channel type (primary or secondary; caused by a corner or by a linear wall segment) and orientation is presented that by-passes the problem of deviating channel beds: In horizontal sections, the progressive flattening of a mound will lead to rounded forms in the vicinity of original corners. Since the number of convex corners along the outer hull of a building necessarily exceeds the number of concave corners, the shape of a contour becomes more convex as a whole.

Therefore, in originally straight parts of the mound surface there should always be a tangent to the contour that touches both borders of a channel incision (first order tangents; red lines). In primary gullies several approximately parallel tangents will be found in neighbouring contours; their mean orientation is an estimate for the orientation of the eroded wall (dotted red lines). Secondary gullies may be expected to consistently produce smaller numbers of parallel tangents.

No tangent to a contour touching both borders of the incision caused by large gullies or wadis representing concave corners will normally exist because the original concavity is preserved in the contour. In such cases any tangent touching a point on the contour to each side of the incision (blue) will define an area (light grey) that includes the smaller gully incisions in the linear parts of the contour (dark grey). These second order tangents do not coincide systematically with any original wall orientations; they may, however, be used to objectively distinguish wadis from gullies.

Automation: The distinction between first and second order tangents is relevant in view of automation because only first order tangents may be used as indicators of original local wall orientations: An algorithm GT ('Gully-Terminator') smoothing the contours of a DEM by replacing local concavities coinciding with drainage channels regardless of incision width by their first order tangent where such a tangent exists but leaving those concavities in place that can only be bridged by second order tangents, will create a new shape that is on the whole more linear than the mother contour and approximates the pre-collapse shape of the eroded structure in those contour segments whose first order tangents exhibit a near-uniform orientation over several (n) vertically adjacent contours (dotted red lines in fig. 16B). The relative likelihood of a good orientation fit for individual segments may be assessed by n -ranking. Local concavities that only have a second order tangent remain in the contour, thereby acting as rough indicators of original concave corners

Eliminating all local concavities by running existing smoothers, like e.g. a Pivoting-Ball (PB) algorithm (Bernardini 1999), along the contours of the same DEM is much less efficient: while PB will restore approximate parallelity relative to the original wall orientations in highly linear parts of

the contour - provided the ball perimeter $d \gg$ average gully width - it will also eliminate indiscriminately those concavities representing original corners. The number of eliminated concavities depends on the value of d . If d is too small there will be no significant smoothing effect, i.e. no information on original orientations, and if it is too large the number of 'false' eliminations, i.e. incisions representing original concavities, increases. In order to work well in the present setting, PB and comparable smoothing methods known to me would require a lot of interactivity. Because they cannot automatically discriminate between different types of local concavities the parameter representing sensitivity - d in the case of PB - would have to be changed according to subjective judgements for each contour segment. Results obtained in this way would not be replicable.

GT, on the other hand, discriminates automatically between incisions caused by concave corners and primary concavities by the order of existing tangents, and in the latter group discriminates between primary and secondary incisions by n -ranking. For the artificial situation shown in fig. 16B applying GT yields

n-Rank	Case	n	Orientation
<u>2</u>	1	4	~ <u>90</u> deg
<u>2</u>	4	4	~ <u>0</u> deg
<u>2</u>	7	4	~ <u>90</u> deg
5	2	2	~100deg
5	3	2	~175deg
5	5	2	~25deg
6.5	6	1	~50deg
6.5	8	1	~105deg

for first order tangents.

The ranking correctly mirrors the succession of primary gullies preserving original wall orientations (90, 0 deg) and secondary gullies at random angles. The original concave corner is correctly characterized - and, thus, located - by its second order tangents.

Expected exceptions: A special case (Fig. 17) occurs where secondary gullies develop on the lateral slopes of primary gully walls or of wadis cutting into originally straight contour segments in areas below saddle watersheds, i.e. at the boundaries of individual blocks (§ 3.2.). In the first case such secondary incisions may at some point become large enough to be detected (dark grey in fig. 17), thereby changing the tangent of the primary channel from first to second order. To provide for this possibility the GT algorithm must be extended by the following rule: If in a sequence of connected first order tangents a second order tangent shows up that shares their common orientation and fits the sequence in incision width, then it is to be included in the sequence. In the second case, it cannot be decided whether or not the concavity was present in the original state or not.

Another situation to be accounted for separately is case 3 in fig. 13A, where a river cuts into the mound base. In the area of highest impact at the base, a local concavity extending over all contours of the lowest A-segment of the slope in this part of the tall may develop (Fig. 18). Due to constant slope instability and local small-scale collapse the slower processes of channel incision cannot lead to the formation of detectable secondary gullies in this area. If the impact of the river is restricted to the edges of an originally straight wall segment (fig. 18B), first order tangents touching both sides of the resulting incision do not correspond to the original wall orientation. They do, however, if the impact zone is located near the middle of the original walls (fig. 18C). In order to take advantage of the second case, GT should not only be run in the areas defined by the drainage network but also in the vicinity of A-slope segments devoid of gullies at the base of the mound.

3.3.3. Implementation and Results

3.3.3.1. Extracting Slope Information

Sample profiles: Figs. 19A and B show four sample profiles extracted from the DEM in order to illustrate the points made in § 3.3.2.2. For each profile, level 1 and 2 decimations are shown. Assuming an original wall height of $h_m=3-5\text{m}$, level 1 is sufficient in all four cases to filter out the noise caused by random bumps at a resolution of 1m.

a-a': in this profile first order tangents to the contour incisions of the only large gully on the northern flank of the mound were measured. The decimated segment sequence is A-A-A indicating the recent action of a river cutting lightly into the base and affecting only the lower parts of the slope; its bed is still visible in the Ikonos image in fig.2. The instability of the terminal A-segment precludes secondary gully formation in this area after the river course started colliding with the tall. The gully, therefore, may be assumed to be more ancient, and the average orientation of its first order tangents to be representative of original wall orientations in this area. For block 8 (§ 3.2.3.; fig. 8) the average is -4.2deg from horizontal in the survey grid.

Plateaus/floor levels indicated by level 1 turning points in a-a' (§ 3.3.2.2.): $\geq 381\text{msl}$; $\geq 372\text{msl}$.

d-d': The decimated segment sequence here is A-A-C indicating the unhindered flow of material onto the plateau formed by block 11 between blocks 9 and 10 (fig. 8). The terminal C-segment extends from 364-376msl; in this area, therefore, potential indicators of eroded architectural elements are covered by debris in this range of elevations and cannot be detected.

Plateaus/floor levels indicated by level 1 turning points in d-d': $\geq 381\text{msl}$; $< 376\text{msl}$.

b-b': this profile consists of a single A-segment at level 1, pointing to severe recent loss of mass due to a river cutting into the base. Here as well the meandering riverbed is clearly visible in fig.2. Because the instable A-segment extends over the whole profile, no information on original plateaus may be extracted.

Plateaus/floor levels indicated by level 1 turning points in b-b': none.

c-c': the information lost in b-b' may be retrieved on the north-western flank of the mound by measuring the first order tangents bridging the incision cut by river. The situation is comparable to the one shown in fig. 18C, where the main impact zone is located near the centre of a flank. The segment sequence is A-A-C, and the average orientation of first order tangents belonging to block 8 is 61.8deg .

Plateaus/floor levels indicated by level 1 turning points in c-c': $\geq 381\text{msl}$; $< 376\text{msl}$.

Assessment of indicators extracted from sample profiles: the sample profiles extracted from the northern, western and eastern sides of the main mound at Tall al-Hamidiya independently point to two major plateaus located at $E_1 \geq 381\text{msl}$ and $376\text{msl} > E_2 \geq 372\text{msl}$, respectively. Though the sample size is too small to be statistically relevant, this is accordance with Wäfler's (TH1) hypothesis of a single vast building extending over much of the mound area published already in 1985. Profiles b-b' and d-d' correspond to areas of low measurement densities in the DEM (fig. 5), and may therefore be of minor quality. In order to increase the amount of profiles from high measurement density areas, a series of profiles oriented S-N were examined along the northern flank at 10m-intervals.

Profiles from the northern flank: Fig 20A shows the positions of the 16 additional profiles extracted from the northern flank of the mound (black lines, bold print). The distribution of turning points (blue Kernel curves) is shown in fig. 20B for the undecimated profiles and for the level 1 decimation. The difference is most apparent at elevations between 370-380 where the undecimated curve is very noisy and indistinct while the decimated curve exhibits pronounced peaks. There are five clearly distinguishable clusters of level 1 turning points; the upper four are vertically spaced at 5m-intervals

and consist of points joining A-segments whereas the lowest consists of points at A-C intersections; thus:

Plateaus/floor levels indicated by profiles 360-510: $\geq 382\text{msl}$; $\geq 377\text{msl}$; $\geq 372\text{msl}$; $\geq 367\text{msl}$; $< 359\text{msl}$.

The turning points of all clusters are distributed evenly over those profiles that include the relevant elevations, i.e. the detected plateaus extend over the whole length of the examined part of the northern flank. The contour segments corresponding to the found plateau elevation minima and maxima are coloured blue in fig. 20A.

3.3.3.2. Extracting Wall Orientations and Positions

'*Gully Termination*': in fig. 21 the areas defined by first (red) and second (blue) order tangents to gully and wadi incisions in 5m-contours are shown. The first order tangents to the western flank of the main mound - discussed in § 3.3.3.1. - are indicated by red lines. The numbers are referred to below as '*N upslope*', i.e. including all upslope contributors of the numbered channel, or as '*N downslope*', meaning only the numbered flow. '*N+M*' refers to the point of confluence.

The extraction of the drainage network as well as the exclusion of irrelevant secondary channels (≤ 5 1m-contours in sequence) were done manually in the 1m-contour map (not shown) according to the rules proposed in § 3.3.2.3. and controlled through visual comparison with the Ikonos image (cf. fig. 2).; in an automated survey of satellite imagery, algorithms for automatic drainage network extraction would have to be implemented (e.g. Mark 1984).

N	up/downslope	1st order tangents	2nd order tangents
1	up	oo , <i>sequence of 7 (5m-contours)</i>	none
2	down	oo , <i>sequence of 3</i>	oo , <i>fits 1st order sequence</i>
3	down	none	corner , <i>no defined restrictions apply</i>
4	down	oo , <i>sequence of 3</i>	none
2+3+4	down	none	oo , <i>sequence of 2</i>
5	down	oo , <i>sequence of 5</i>	none
6	down	?? , <i>variation too large?</i>	none
7	down	oo ; <i>sequence of 2</i>	none
8	up	excl. , <i>contributors channelled by watersheds (blocks 4+8; 11+13)</i>	
9	up	excl. , <i>watersheds (blocks 11+13; 10+9)</i>	
10	down	oo , <i>sequence of 2</i>	none
11	up	excl. , <i>watersheds (blocks 9+10; 11+12)</i>	
12	down	oo , <i>sequence of 3</i>	corner , <i>no defined restrictions apply</i>

oo: small variation in orientations; average of sequence \approx original wall orientation

??: large variation in orientations; no defined interpretation

corner: 2nd order tangent bridges original concave corner

excl.: excluded; no defined interpretation

italics: reason

Applying the GT-method, two original concave corners in the areas marked by black arrows in fig. 8 have been detected as well as a series of averaged orientations that may be assumed to correspond to the original orientation of walls in the respective parts of the mound. (6) was excluded because, subjectively, the angular and positional variation respectively between tangents on consecutive contours seemed too large. In a fully automated implementation such cases would require a clear

definition of the maximum angular and positional spread considered acceptable in a sequence of tangents to be counted as an indicator.

Testing the validity of 1st order tangents as indicators of original wall orientations: If - as argued here - first order tangents to primary gullies are valid indicators of original wall orientations, one would expect the orientations extracted from an eroded ancient settlement to reflect the basic orthogonality of the individual buildings or building elements by clustering in groups of paired angles separated by 90deg. If the underlying theory is wrong and first order tangents found by GT are not representative of original wall orientations, the distribution of angles should be uniform over the whole 180deg-range in large samples whereas in small samples clusters should be spaced randomly.

In fig.22A the kernel density distribution ($t=0.15$) of the unaveraged orientations normalized to 180deg is plotted; orientations extracted from block 8 are shown separately from those found in the rest of the mound. The four most obvious peaks form two pairs of orientations at right angles ($\Delta=90\text{deg}$) with local maxima at 61/151deg (group 1) and 85/176deg (group 2) respectively. This distinctly non-random spacing of clusters in a pattern clearly mirroring basic orthogonality corroborates the validity of first order tangents as indicators of original wall orientations.

Completing the circle: While the overall distribution of angles points to an interconnection of individually orthogonal building elements with at least two major orientations, the unequal densities of the paired orientations within groups indicate that not all walls were detected by GT. In order to fill the gaps between areas of known original orientation along the DEM contours, i.e. areas uninfluenced by the drainage network of a tall, areas of high linearity need to be identified. Such areas are by definition less fractal than those exhibiting rugged outlines (§ 3.1.) and original signals of artificiality like linearity and parallelity may therefore be assumed to have deteriorated less severely relative to the local increase in fractal noise. Original orientations are therefore likely to be better preserved, and, in cases where the average orientation of the contour segments within an area of high linearity closely fits one of the averaged angles extracted by GT, the latter is likely to approximate the original orientation best because, judging by Occam's razor, the number of elements - here: assumed original angles - is thus kept at the minimum.

Defining areas of high linearity: In order to define areas of high linearity within block 8, relative directional change between points spaced 10m apart on 1m-contours was measured. In Fig 23 these changes are plotted vs. the clockwise percentage of the contour perimeter measured from the starting point indicated in the map for the 375msl elevation. The threshold for high linearity was arbitrarily set at 1sd (dashed line in the lower plot). For an area to count as highly linear (shaded blue) at least six steps in a row with changes <1sd were required in order to bridge the known gullies and wadis. The map indicates those areas of block 8 meeting the requirements of high linearity by blue shading (data for other elevations not shown individually). Within these areas, segments corresponding in orientation to one of the main groups found by GT were coloured accordingly in fig. 22B. The grey area in the south-eastern part of block 8 could not be assigned to a defined group.

Original wall orientations: Fig. 24 shows all original wall orientations extractable directly from the DEM in block 8 at 3m intervals. For the grey area of high linearity wall orientations were assumed to conform to the mean orientation of its contour segments (46.5deg). Blue and red denote groups 1 and 2 respectively. The lines correspond only to the orientation of walls at a given elevation; their position is defined independently by the relevant turning points extracted in § 3.3.3.1.

A basic change in the overall shape is apparent on the eastern and western sides of the mound between 376-373, which independently confirms the predictions concerning block 8 in § 3.2.3. The rugged lower part of the southern flank of block 8 cannot be assigned any original orientations. The mean orientation of the contour segments in this area changes continuously in clockwise direction from roughly horizontal (~group 2) at higher elevations to orientations clearly belonging to group 1 at 365msl. Subjectively, one should think that this change is largely due to the wide incision separating blocks 8 and 4 (8 upslope in fig.21), and that, therefore, the whole area originally corresponded to group 2.

3.3.4. Symmetries

3.3.4.1. Quantification of Symmetries and Symmetric Regularities

Symmetry: Symmetry is encountered in many forms in natural as well as artificial objects (Washburn and Crowe 1988, Weyl 1989). Perfect geometric symmetry - as achieved, for instance, by flipping or rotating an object - is often associated with artificial shapes, while natural shapes are more likely to exhibit degrees of symmetry: Fractals scale according to a power law (§ 3.1.), and are therefore symmetric in an elementary sense in regard to scale; for stochastic fractals this symmetry - analogous to its fractality - is approximate, a property that artificial objects generally lack. Approximations to perfect geometric symmetries are frequently used in reverse engineering for the reconstruction of complex shapes (Mitsumoto et al. 1992, Mills et al. 2001). CPSR (§§ 3.4.) implicitly encompasses the detection and quantification of such geometric symmetries because they are highly regular in terms of algorithmic complexity: in a maximally compressed algorithm symmetries are reproduced from a subset of the data by symmetric transformation. In this section, therefore, the focus is on non-geometric or only partly-geometric symmetries that might potentially be present in the overall ordering of architectural elements detected by the techniques set forth in the preceding sections. For lack of a better term, I refer to such symmetries as 'order symmetries'.

Isometric symmetries: Perfect geometric symmetries are isometric, i.e. they may be represented by contortions or movements of a space or an object that preserve distances between its points. The result of an isometric transformation is a congruent space or object. Mirror symmetry occurs when an axis passes through a given shape such that the two sides thus defined are mirror images of each other. The degree of mirror symmetry of a given object can be measured as the normalized difference between the image of an object and its reflection about a hypothetical axis of symmetry (Marola 1989). Values may range from zero (no symmetry) to one (perfect symmetry). If $a(i,j)$ is an image, the Marola symmetry in the horizontal and vertical directions is

$$\beta_h(m) = 1 - 1/2 \sum_{i,j} [a(i,j) - a(m-i,j)]^2 / \sum_{i,j} a^2(i,j) \quad (\text{Eq. 8.1})$$

$$\beta_v(n) = 1 - 1/2 \sum_{i,j} [a(i,j) - a(i,n-j)]^2 / \sum_{i,j} a^2(i,j) \quad (\text{Eq. 8.2})$$

where $0 \leq \beta \leq 1$. For a given window the axes of symmetry coincide with the maxima of (m, n) ; their absolute value is the degree of isometric mirror symmetry within the examined window. Methods similar to but more generally applicable than Marola's exist for detecting and describing reflexive symmetries both in 2D and 3D shapes (e.g. Kazhdan et al. 2002). For rotational symmetries a very flexible approach implemented in many commercial image analysis software packages was first proposed by Bigün (1988) who modelled symmetry in the Fourier domain, but used convolutions in the spatial domain for detection. All these techniques, however, use a symmetry descriptor that essentially depends on distances between points in space comparable to Eqs. 8.1 and 8.2.

Non-isometric symmetries: If the search space is restricted to isometric or approximately isometric symmetries topographic manifestations of artificial structures that are heavily skewed or distorted or only exhibit order symmetry can neither be detected nor used as a compatible input for CPSR models (§ 3.4.). Obviously, techniques operating in the frequency domain are conceptually closer to the idea of non-geometric order symmetries than distance-based models. In the sense of an unsophisticated general test of their applicability to the problem at hand, the potential of autocorrelation for the detection of traces of order symmetry in two dimensions is in the following examined.

Autocorrelation of 2D-slices: The autocorrelation of a data series of length n - usually but not necessarily a time-series - is the correlation of the series with itself measured at all lags $1, 2, 3, \dots, n$. A high correlation at lag m means that the series resembles itself with a period of length m . Since elevation lines are closed shapes that can be encoded by listing relative directional changes along their border at specific intervals, periodicities detected in this way in a horizontal slice through a tall would point to rotational symmetric behaviour of the shape.

If regular distance intervals were used, isometric rotational symmetry would show up in the autocorrelation plot by a peak at lag $[m \cdot \text{interval}]$ equalling the distance along the contour between segments resembling each other. The same basic regularity in a contour representing an original form that may have been skewed or stretched by its builders to fit specific needs or that was heavily affected by erosion can, however, not be detected in this way, because such distortions differentially affect the length of the contour segments representing the period and thus destroy autocorrelation. This is illustrated in fig. 25A, which shows the autocorrelation plot of the 375msl elevation line of Block 8 (blue) encoded by the sequence of directional changes (deg) between points spaced 10m apart on the contour. As expected there is no interpretable pattern.

One possibility to compensate for both original non-isometry and noise consists in using an encoding scheme in which angular changes measured at fixed distance intervals are substituted by changes in probable original orientations along the contour at intervals defined by the changes themselves. In other words, the sequence to be examined consists of an essentially topological description of a contour where corners are nodes and walls are undirected graphs. If each node is classified according to whether it connects graphs belonging to same group (1) or belonging to different groups (2), the relationships between architectural elements can be described without reference to distances and may be examined as a sequence.

Encoded in this way, the description of a contour preserves the order and type of the segments relevant to the original shape of the mound, but contains no information on the distance between the nodes. It is therefore robust in regard to non-isometric behaviour due to skewing, partial scaling etc. It is robust in regard to erosion only to the degree that the employed techniques for extracting wall orientations compensate its effects.

3.3.4.2. Implementation and Results

It was shown in § 3.3.3.2. that the most likely original wall orientations in block 8 cluster in three groups of angles. In fig. 25B block 8 is divided into zones of known original orientation (blue, red, grey) and zones of unknown original orientation (green) (cf. fig. 22B). Because there is only one detectable change in shape occurring at 376-373msl (§§ 3.2.3. and fig. 24), the contours need not be examined individually but may rather be represented by a composite schematic shape with the same attributes consisting of 7 sectors with an upper and a lower element each (shape 1). Segment sides correspond to nodes; sides adjacent to green segments cannot be classified. They appear as missing values (.) in the encoding. For shape 1 the encoded sequence starting from the upper side of the sector indicated by the arrow in counter-clockwise direction is: [1. 22 21 12 1. 2. 2.]

Because the values for the sector sides are paired, only the even numbered steps (solid blue) correspond to a lag of $n+1$ in the autocorrelation plot. There are two pronounced positive peaks at lags 4 and 7 indicating rotational order symmetry between sector sides spaced four sectors apart in clockwise direction. The incomplete shape therefore is strongly symmetric in terms of order symmetry. By projecting the node attributes of the symmetric parts back onto the segments of unknown orientation the autocorrelation pattern is preserved (shapes 2 and 3).

The resulting wall orientations are shown in fig. 26 (dashed lines). Obviously, the strong order symmetry does not translate into a detectable geometric symmetry. The rotational aspect is visible mainly in the eastern and western protrusions from the otherwise heavily skewed main body.

3.4. CPSR: Complexity-based Predictive Reconstruction of Buildings

3.4.1. Rationale and Outline of CPSR

Traditional approaches to architectural reconstruction: For every set y of known architectural remains of a destroyed building x there exist an infinite number of possible reconstructions x' within a given area S . From among this infinitely large class X' only one realisation $x' \in X'$ is congruent with x . Every attempt at reconstructing x can therefore be seen as a choice of one particular reconstruction out of X' . In order to be intersubjectively verifiable, i.e. to be scientifically valid, the criteria for this choice have to be known completely.

Trivial cases excluded - e.g. where disrupted wall lines are interpolated - traditional, non-mathematical approaches to architectural reconstruction suffer from a non-fundamental deficit insofar as the criteria leading to a specific choice of x' are not usually clearly exposed, and a fundamental deficit insofar as these criteria are ultimately based on typological similarities, i.e. based on prior knowledge or conditioning (Heinrich 1982, 1984). The possibility of innovations or singularity in architecture is ignored in such reconstruction schemes, because regularities in y that have no known precedents cannot be classified, and extrapolation beyond y based on typical features exhibited by its class is not possible. The only way to deal with innovation or singularity in such a conceptual framework is by letting intuition or random, uncontrollable insight guide the reconstruction process. Many attempts at reconstructing the geometric principles and units underlying ground-plans fall into this category (Allinger-Csollich 1997). The arbitrariness of most architectural typologies - where classification criteria are a matter of individual taste rather than the result of exploratory data analysis - is a separate but no less important problem.

Complexity-based Predictive Site Reconstruction (CPSR): CPSR is a mathematical reconstruction technique largely developed in early 1999 as an alternative to traditional approaches to architectural reconstruction in cases where the remains of a building do not conform to any known building type (Gerber 2000b, 2001). In the framework of the envisioned PSDR-strategy it represents stage 4. It differs fundamentally from traditional approaches insofar as the information utilized for reconstructing a building stems entirely from its known remains. Because this information consists of the complete set of geometric regularities (trivial and non-trivial) inherent in any set y of known remains, the number of possible reconstructions is always finite within S and independent of any prior knowledge.

Algorithmic Complexity: The supposed high degree of geometric order in monumental buildings can conceivably be exploited for predictions: by definition, any geometric shape can be described by an algorithm, i.e. a series of instructions that replicates it. Such algorithms can be compressed by substituting regularities in the series, i.e. its redundant parts, with short sets of rules. At some point, every regularity will be encoded by rules and the algorithm cannot be compressed further. The length of this maximally compressed algorithm is independent of the description language up to an additive constant; it can be determined and it is by definition a measure of the algorithmic complexity (C) of the object it represents (Li and Vitani 1999).

Architectural identity and building-specific complexity signatures: the trained eye can often associate the archaeological remains of a building with a certain period or culture or "style" on the basis of its incomplete ground-plan alone. This means that the regularities defining its architectural identity are imprinted to some degree in the parts as well as in the whole. Therefore, because it captures *every* regularity inherent in the elements, a complete, maximally compressed description of the architectural elements y found by extracting topographical indicators from a DEM - or, at stage 4, by excavation - defines a part of the architectural identity of the original building x , both quantitatively by its length and qualitatively by the rules encoding the regularities in the algorithm.

Using these rules to connect the individual elements to a single shape, then, results in a number of new wholes x' with an architectural identity that is necessarily similar to the original x . The degree of similarity depends on the percentage of relevant regularities in x represented by the known elements y , and on the way the complexity C of y relates to different parts of y : information i that can be encoded

in rules is not necessarily evenly distributed over the elements comprising y , and eliminating different elements from y will therefore lead to different values of $C(y)$. However, the observation that the whole is reflected to some degree in its parts suggests a certain scalability of C relative to the amount of relevant information $|I|$ available in y . One would therefore expect $C(y)$ to exhibit a building-specific slope S if regressed against $|I|$ for all possible combinations of elements in y , with actual values scattered more widely for small samples y than for large ones. An experimental corroboration of this is planned using a turtle graphics generator suited for the task (Blattner, Bieri, Gerber, *in preparation*); at present, it is but a reasonable assumption.

S (or some other variable s defined by the relationship between C and the shape area), therefore, is a building-specific complexity signature of x apparent in y . Among all reconstructions x' based on a specific number of elements $|y|$ those preserving s will therefore have the highest degree of similarity to x .

CPSR as a form of reverse engineering: CPSR may be seen as a special form of reverse engineering: the ancient architects or, more generally, the builders of a monument partly retrieved by excavation, at some point converted a concept, i.e. the plan, into an artefact, i.e. the building. In the course of construction random errors occurred and the resulting artefact deviates in an essentially random fashion from the plan. After its abandonment the exposed parts of the building are subject to structural collapse and erosion; in extreme cases also to permanent skewing in the wake of earthquakes or other tectonic processes. The excavated parts of a building therefore never mirror the original design intent one-to-one.

After excavation the accumulation of errors continues when to monument is surveyed and documented. The use of a variety of measurement instruments - from measuring tape to median-seeking theodolites or laser scanners - and, in most cases, insufficient documentation of topo-survey methods prohibits the quantitative determination of these errors. As if this was not enough, further deviations from the original structure are introduced during the drawing and CAD post-processing of plans. In reality, the documentation will be further affected to various degrees by selective interpretation of excavation results.

Reconstructions that do not take these potential errors into account (§ 3.5.1.-3.5.3.) run a high risk of becoming trapped in circularity because they may merely propagate preconceived notions hidden in data compromised by interpretation.

In contrast to traditional approaches to reconstruction, CPSR - at least theoretically - takes account of the various levels of conceptualisation as well as of the sources of random and systematic errors. It converts an artefact back into a concept that has a specific probability of accurately representing the original design intent. Its goal is to reconstruct an ideal model of a physical object with intended geometric regularities in a manner that conforms to the basic scientific standards of intersubjective controllability. The result is neither a simple copy nor a representation of modern ideas.

3.4.2. Definitions and Propositions

An object's Algorithmic (Kolmogorov) Complexity C is defined as the length of the shortest algorithm replicating its complete description. C thus measures the amount of an object's inherent regularity. I propose an analogous measurement unit C_R (Restricted Descriptive Complexity) appropriate for the special case of buildings. From the regularities encoded in the algorithms defining C_R a building-specific set of constants can be derived, namely an algorithmic complexity signature that is expected to effectively capture a building's architectural identity. All possible reconstructions of a partly destroyed building that preserve the algorithmic complexity signature extracted from its known parts are then to be generated by exhaustive searching. In contrast to traditional strategies, excavation in the CPSR framework is limited to testing predictions about architectural key structures close to the present site surface. The newly gained information is to be fed back into the model. Whereas non-predictive methods necessarily yield a less than proportional

information gain relative to the total excavated area (§0.2.), hypotheses generated iteratively by CPSR should theoretically exhibit rapid asymptotic convergence towards the original ground-plan.

Algorithmic complexity (Kolmogorov complexity C): Intuitively, one would say that an object that can be described precisely in a few words is less complex than an object which requires a very long description. In the theory of Algorithmic complexity this intuitive notion is formalized by defining the complexity C of an object as the length $|p|$ of the shortest program p_0 that generates the binary string x representing the object (Li and Vitányi 1997:93-96). More precisely: the Algorithmic (Kolmogorov) complexity $C(\cdot)$ of a binary string x with respect to a partial recursive function $\phi: \Sigma^* \rightarrow \Sigma^*$ is defined as

$$C_\phi(x) = \min\{|p| : \phi(p) = x\} \quad (\text{Eq. 9})$$

where $|p|$ is the length in bits of a string p . $|p|$, and thus C , are negatively correlated with the regularity inherent in the described object, and positively correlated with its inherent randomness. Take, for example, two numerical strings $X: 3.40957715\dots$ and $\pi: 3.14159265\dots$. Both strings are infinite and aperiodic, i.e. they share the same surface properties. However, assuming X is truly random, its description cannot be shorter than $|X|$ because no rule can be utilised to predict its individual digits, thus $p_0(X)=X$. The description of π (i.e. the algorithm generating π), on the other hand, can be compressed almost to the length of its definition: $\pi=c/d$ in any circle. Regularity is extremely high in π and extremely low in X , thus, $C(\pi) \ll C(X)$. In colloquial terms, C measures the amount of regularity, and p_0 captures regularity itself in the form of algorithmic rules. While $C(\cdot)$ is the same for a class of objects of equal complexity, $p_0(\cdot)$ is object-specific because the program it represents replicates exactly one object.

Architectural identity and building-specific complexity signatures: The trained eye can often associate the archaeological remains of a building with a certain period or culture or "style" on the basis of its incomplete ground-plan alone. This means that the regularities defining its architectural identity are imprinted to some degree in the parts as well as in the whole. Therefore, because it captures every regularity inherent in the elements, a complete, maximally compressed description of the architectural elements y found by extracting topographical indicators from a DEM - or, at stage 4, by excavation - defines a part of the architectural identity of the original building x , both quantitatively by its length and qualitatively by the rules encoding the regularities in the algorithm.

Complexity of fragmentary architectural structures: Theoretically, p_0 of a complete building x captures every regularity in x , and thus its 'architectural identity'. In order to reconstruct the original state of x long after its destruction, information about these specific regularities can therefore be gained from the remains y whose $p_0(y)$ partly consists of elements of $p_0(x)$. Using elements of y obtained by topographic feature extraction (§3.3.), this poses no practical problem. If, however, at stage 4, excavation data is used indiscriminately, the regularities encoded in $p_0(y)$ may be drowned beneath large amounts of randomness introduced by fragmentation, erosion and other shape-changing factors, leading to odd situations where $p_0(y) \gg p_0(x)$. In practice, this has to be avoided by using only the geometrically or topologically relevant parts of the remains in the feedback loop, such as wall surfaces and floors that were found intact. At stage 4, it is furthermore imperative that modern measurement errors and, if the excavation data are extracted from plans, the precision of the drawings be estimated statistically (§ 3.5.). The quantified errors have to be included in the model as tolerance terms.

'Restricted Descriptive complexity' C_R : For the purpose of reconstructing a monumental building like the Central Palace, the definition of C given above is too general. It is valid for any type of mathematical object and any language chosen for the description. However, a building is a real-world object which cannot itself be used in complexity calculations; only its description is relevant, and the way the building is described determines the type of regularities that can be found by compressing the original algorithm. Individual elements of $p_0(y)$, then, should not encode arbitrary mathematical regularities, but rather only those that conceivably mirror the architectural identity of x . In order to

clearly differentiate between the general and the special case, C if restricted to types of descriptions appropriate for buildings is, in the following, provisionally termed 'Restricted Descriptonal complexity' C_R .

The architectural identity of x may be viewed as the result of a process of geometrical construction in the plane, aimed at optimally using the available space. The remains y of x can, for example, be represented and described by a series of ruler-and-compass constructions, by square grid constructions or by descriptions that differ depending on their starting point (see § 3.4.3.). The first two types of description are static in the sense that the starting point of the description has no impact on the result, i.e. there is no historical error to be dealt with (§ 3.4.3.).

C_R and building specific complexity signatures for ruler-and-compass constructions: In the first case, the construction process is modelled by a series of ruler-and-compass constructions without measurements: A construction resulting in a wall line is called a step ψ . Each ψ consists of a number of operations ω . Each ω generates exactly one constructor. Starting from an arbitrary point in y (y being the known parts of ground-plan x), two operations ω are possible: a) the drawing of a straight line, or b) the drawing of a circle.

Let the restricted $p_o(y)$ (i.e. the shortest description of y) be a two-part code, its first part describing an appropriate Turing machine and its second part describing the program that interpreted by the Turing machine replicates y ; the second part may contain only ψ -elements, which themselves consist of ω -elements. And let $C_R(y) = |p_o(y)|$, where $|p|$ is the number of operations ω explicit in p (instead of its length in bits). In this form, $p_o(y)$ encodes only the specific information of interest, namely the rules guiding the ruler-and-compass construction of the target building's basic layout. The separate coding of ψ - and ω -elements facilitates the definition of a complexity signature (§ 3.4.1.) appropriate for this specific case. Because of this coding format and the definition of $|p|$, C_R is completely language independent. C is language independent only up to an additive constant (Li and Vitáni 1997:103-104). The different cumulative effect of new vs. redundant information (I) on C and C_R is illustrated in the schematic plot in fig.27: moving from left to right, the 100^g -corner A_1 contains new information; replicating it requires all this information. Corner B_1 is mathematically more difficult to describe ($\neq 100^\text{g}$) and therefore contains more new information than A_1 . B_2 and A_2 are copies of B_1 and A_1 , their information is redundant and replicating them has little (C) or no (C_R) effect on the structure's complexity. This difference between C and C_R arises because the additional information required to generate these redundant parts is located in the Turing machine: C_R is not defined as the length of p_o but by the number of ω explicit in its second part and therefore remains unaffected.

The odd-angled corner in 43/37: The first attempt at applying these concepts in 1999 was the replication of the odd-angled corner in square 43/37 at Tall al-Hamidiya (fig.28). The surface of the wall pointing north-eastwards was well preserved, if only on a very short distance of ca. 1.4m. (The filling shown in the original drawing between the protruding bricks was removed from TH4: Plan 4, generated in 2002). The wall's angle relative to the Central Palace's southern facade ('baseline' in fig.28) was determined by repeated measurements to be $\alpha=62.75^\text{g}$. In the absence of error estimates at that time, an angular error of $\pm 0.25^\text{g}$ was assumed in accordance with manufacturer specifications. In hindsight, this was naïve: the 1σ -precision of wall alignments in this part of the palace was later established to be $\pm 1.45^\text{deg}$, i.e. $\pm 1.61^\text{g}$ (§ 3.5.1.), making the measurement error negligible and completely changing the conditions for replicating α . Because the reconstruction presented in § 4.1 is uninfluenced by the way α is replicated, the original solution is repeated below for its theoretical interest.

The majority of angles cannot be constructed; every angle, however, can be approximated by continuous bisection starting from a constructible angle like 100^g or $66.67/33.33^\text{g}$. Given the baseline, the approximation of α by continuous bisection requiring the least operations ω starts from 100^g (4ω) and reaches a value $\beta=62.5^\text{g}$ in the assumed error range of α after 4 bisections (3ω each). If the corner 43/37 is considered in isolation from the rest of the fragmentary ground-plan y , this solution (A) is the shortest description $p_o(\text{corner})$ with $|\psi|=16$.

If, however, the corner in 43/37 is treated in the context of y , a slightly more complex solution B (documented in fig.29) resulting in an angle $\beta=62.72^\circ$ with $|\psi|=22$ is favoured because many of its constructors coincide with constructors that can be used to generate other parts of y (bold type in fig.29): Scaled to the dimensions measured in the field (fig.30), A, for example, corresponds in width to the main ascent structure a extending southwards from the baseline ($r=81.85\text{m}$, thus $A=r(\omega 17)(1-\sin[90-\beta])=34.49\text{m}$; $a=34.70\text{m}$), the three walls b , c and d are tangents to the circle $\omega 17$, and line $\omega 4$ through the centre of $\omega 17$ corresponds to the axis of structure a . The ψ -elements responsible for the replication of a , b , c and d in the uncompressed $p(y)$ thus contain information already present in solution B. This redundancy in the description of y with solution B results in a decrease of $|p(y)|$ after compression that is greater than the difference of 6ω between solutions A and B. Therefore, solution B is contained in $p_0(y)$, while solution A must be rejected.

Algorithmic complexity signatures: Let x be the palace's ground-plan in its original state, y the known fragments of x after its destruction, and x' the best hypothetical reconstruction of x from y . How can regularities found by compressing the information in y to $p_0(y)$ be used to generate x' ? The special properties of C_R and restricted p_0 allow for the definition of an architectural signature, which transforms the regularities found in y into a site-specific set of constants. Reconstructions with the same signature, i.e. the same 'architectural identity', can then be generated by simulation, ideally by exhaustive searches. Further restrictions like optimal use of terrain or exclusion of certain areas etc. can be introduced at will to narrow down the number of possibilities to the desired level.

Assuming a certain degree of scalability and a general decrease of variance at higher lil , a combination of two proxies (s_1, s_2) for lil was used as a signature in the first experimental implementation using data from Tall al-Hamidiya as discussed in § 4.1. The first part of this signature is defined by

$$s_1 = C_R / |\psi| \approx \text{const.} \quad (\text{Eq. 10.1})$$

Since $C_R = |p_0|$, i.e. the number of explicit ω -elements in p_0 , this number encodes the complexity of a typical construction step ψ . The second part of $s(\cdot)$ is

$$s_2 = |p| / A \approx \text{const.} \quad (\text{Eq. 10.2})$$

where $|p|$ is $|p_0(y)|$ for y and $|p_0(y)'|$ (*sic!*) for x' . It specifies the typical amount of 'construction effort' per area. $A(\text{rea})$ would have to be substituted by $V(\text{olume})$ if complex constructions in the z -axis are expected as would be the case, for instance, in the reconstruction of a Gothic cathedral. This is unnecessary for mudbrick architecture, which does not allow for much 3d-extravagance beyond simple projection along z . The signature used in 1999 has the advantage that both its elements s_1 and s_2 have a straightforward interpretation; because of problems encountered during the first trial implementations, other types of signatures are currently being investigated (§ 3.4.3.).

3.4.3. Other Forms of Encoding y

Historical errors: somewhat ironically, ruler-and-compass constructions as a basis for encoding y were initially chosen despite their obvious historical inaccuracy precisely in order to avoid 'historical' errors. Historical errors are deviations in results obtained by methods whose outcome depends on the starting point of calculations. Such errors are stable up to an additive constant for a specific method and a specific set of data, and Monte Carlo runs with a large number of different starting points or other simulation methods are commonly used to determine them. When CPSR was developed in 1999, devising a sophisticated simulation-dependent model on my own would have been both too time-consuming and error-prone, and work on potential non-static encoding methods was discontinued until 2001 (Blattner, Bieri, Gerber, *in preparation*).

Square grid constructions: A second static (and historically much more likely) method was suggested to me by H. Bieri (*personal communication*), namely square grid constructions. In an infinite grid of identical squares, every angle can theoretically be constructed by connecting grid intersections (fig. 31). In practice, of course, a finite grid with a finite number of constructible angles would have to be used, its minimal number of squares in the x and y-direction depending on the specific angles to be constructed. In a CPSR-model two types of grids might be used:

Type A: a small grid consisting of a sufficient number of squares for constructing all relative angles between actual or extrapolated intersecting wall segments in y. Such a grid may be much smaller than the plan of y, because distances can be bridged using a ruler once an angle has been constructed. The uncompressed description algorithm for a type A grid-based reconstruction would therefore consist of a starting-point invariant series of two commands (pseudo code) *draw* [n_x, n_y, d] and *bridge* [n_x, n_y, d] where positive n is the number of grid intersections to be moved upwards and the right-hand side respectively from an arbitrary starting point or from the point defined by the previous command, and negative n for movements in the inverse directions. d is the distance to be moved.

Type B: a large grid covering the whole plan of the building such that a grid intersection coincides with each known or extrapolated intersection of two linear wall segments in y. In contrast to a type A grid, distances result directly from the construction of angles. The uncompressed description algorithm would therefore consist of two more economic commands: *draw* [n_x, n_y] and *bridge* [n_x, n_y].

When choosing a grid type for implementation its plausibility as a tool used by the architects of the building to be reconstructed should be considered: A small type A grid is useless for calculations. It may, however, be used for drawing relative angles in conjunction with a ruler. In this case, the grid has to be realigned after each constructed angle. Each reorientation necessarily results in a random imprecision leading to a cumulative error that, if an open shape is drawn, increases proportionally to the number of construction steps. In closed shapes the targeted coincidence of starting and endpoints can be used as a corrective for the last construction steps. Since the basic plan of a building is usually a closed shape, the cumulative error may be kept slightly below proportional. If, on the other hand, a large type B grid is used for drawing, there is no cumulative error because it need not be realigned during the construction process. A ground-plan designed in this way may be assumed to be much more precise than one drawn with a type A grid. However, a 'virtual' type B grid may be used as a planning tool in conjunction with a rough sketch. Every angle on the sketch may then be defined by a two-digit code [n_x, n_y] naming the number of squares to be moved in the x and y direction respectively. If the grid includes nodes that coincide with a reference system set up in advance in the building area, then such a sketch would provide a perfectly sufficient basis for triangulating of the building's corner coordinates in the field, as well as during construction.

While large deviations from parallelity or from the mean of recurring angles in the known parts of an excavated building need not be a reflection of imprecise planning - who would blame the architect for the mistakes of a drunk mason? -, very small deviations in the actual building would seem to imply careful planning and a good translation mechanism between a plan containing ideal, intended distances and the positioning of discrete points in the field. Although a clear threshold error cannot be determined, the possible use of a type B grid should be considered in buildings with a low degree of measurable imprecision.

In cases where the number of elements in y is high, the side length of a grid square is likely to coincide with the main architectural unit used by the original builders. Such a unit could be used as an empirical restriction in the turtle graphics generator presented in Blattner, Bieri, Gerber (*in preparation*) to narrow down the number of possible reconstructions to be examined. In § 3.5.1. the grid type, grid unit and grid size necessary for encoding y in the case of the Central Palace is determined and the plausibility of the resulting square length as an architectural unit discussed.

3.5. Extracting Additional Information from Excavated Structures

3.5.1. Construction Grids, Error Estimates

Determination of grid type: In § 3.4.3. square grid constructions were introduced as a potentially interesting basis for encoding y in a CPSR-model and - assuming that such grids were actually used - as a means of determining the main architectural unit used by the builders of a given architectural structure. The type of grid most likely to have been used by the original builders depends on the estimated precision of the original wall orientations. Very high precision tips the balance in favour of a type B grid. Because wall orientations have to be extracted from available modern plans any precision and accuracy estimates can only be approximate (§ 2.2.).

Precision: Fig. 32 shows the distribution (Kernel density, bandwidth=0.4) of wall or brick patch orientations extracted from the plans available in 1999. Orientations are given in degrees relative to the survey grid and were normalized to values $< 90\text{deg}$ in order to make them comparable. In the area defined by 32/23-48/51, then assumed to roughly represent the Palace's main body, only preserved wall faces were included. In the isolated patches 49-51/45 no wall faces were preserved; here the average brick orientation was noted for each square.

The extracted values show two clear clusters centred around ca. 52deg and 83deg respectively. The larger cluster (cluster 1) includes all extracted wall faces of the southern façade and the southern ascent structure (group 1) and those of the Palace's known rooms (group 2). Cluster 2 consists of the odd-angled outer wall segment excavated in 43/37 and the values from the isolated patches in 49-51/45.:

	Cluster 1			Cluster 2
	Group 1	Group 2		Group 3
N of cases	7	21		5
Minimum	82.0	79.0		48.5
Maximum	86.0	87.0		56.0
Median	83.5	82.0		54.0
Mean	83.6	82.9		52.5
sd	1.492	2.330		3.500

Taking into account the long distances between extracted façade angles in group 1 (max. ca. 150m: 34/25-41/37), the precision (sd) of the measured wall orientations is extremely high at $\sim 1.5\text{deg}$. In group 2, consisting exclusively of measurements taken in rooms, precision is lower at comparable distances (max. ca. 140m: 41/38-42/50). Group 3, which includes the interiors of massive walls, exhibits by far the lowest degree of angular precision at the shortest distances (max. ca. 90m: 43/37-51/45).

While not conclusive, the high precision in group 1 points to triangulation as the original means for determining the position of the corners and walls to be built, and thus to the availability of a very detailed plan prior to the start of the construction works. If the reference system had been set up in the field by distance measurements using ropes, one would expect much wider angular spread over such long distances in group 1 as well as in group 2.

In view of this observed precision, the use of a type B grid as a basis for planning and on-site measurements is a distinct possibility: It cannot be decided whether a drawn plan or a sketch supplemented by calculated angles and distances was used. Judging by the rare representations of ground-plans extant in the cuneiform record, the latter appears more plausible. However, the function of these tablets is not known with any certainty. Some may be field notes or school exercises, others

may represent volume and area calculations for construction logistics, conceivably even retrofits. The possibility of precisely drawn plans should therefore not be discarded entirely.

Square grid orientation: In the following it is assumed that a type B grid with squares of minimal side length u (=unit distance) was used. On a scaled plan, the known corner coordinates of the building are supposed to coincide with grid nodes, and the grid itself may then be treated as a 2D Cartesian coordinate system. Determining optimal grid orientations in building remains without any clear preference for specific angles would require computation-intensive numerical models. At Tall al-Hamidiya the matter is more straightforward because a narrower search space is defined by two main wall orientations known in 1999 for outer walls (facades), 83.6deg (mean group 1) and 48.5deg (single façade segment in 43/37), as well as their angular precision, $sd=1.492$ (group 1). Fig. 33 shows the positions of the 5 discrete points defined by the known corners in 1999 and their relative distances at fixed angles corresponding to the two main wall orientations.

Determination of minimal grid size: If a grid G oriented at a given angle α has nodes coinciding with the known corners of an incompletely known building, then, ideally, the distances measured in the direction of α between the corners are integer multiples of the side length u of a grid square. u , therefore, in this ideal case, is the Greatest Common Divisor (GCD) of the measured distances. The minimal grid size expressed in u is the minimal extension of the plan in x and y divided by u , i.e. $G[\lfloor x(\min)/u \rfloor, \lfloor y(\min)/u \rfloor]$. However, in reality these distances represent a combination of ancient measurements - on the basis of which the palace was built - and modern field measurements. The data therefore have an unquantified error (§ 3.4.1.). A distance d measured in y is therefore not a precise scaled equivalent of the "true" distance D in the Maittanian architect's plan. For this reason, the prime factorisation required for determining the GCD cannot be computed.

The solution presented here is a best-fit estimate based on a resampling method: Within an initial search space defined by a preliminary estimate δ of the - unknown - true distance precision Δ of d , the range of scaling factors between the possible values of the unknown true distances $D(1..m..n)$ was determined as the largest value of $d(x) \pm \delta$ divided by the lowest of all $d(m \leq x \leq n) \pm \delta$. Of all integer scaling factors within this range the three lowest intermediate or adjacent integer fractions were then multiplied with the actual measurements $d(1..m..n)$. In this way, the actual - absolute - deviation from the unknown $D(x)$ in each individual measurement $d(x)$ was propagated towards all other d , thereby creating a cloud of artificial equivalents d' of repeated measurements around each d that is representative of the actual, absolute distance errors in the data. The mean of each cloud around $d(x)$ therefore is an estimate of $D(x)$; its sd equals the true distance precision Δ , and - as a nice side effect - the standard error of mean is the distance accuracy ϵ . Together with the known angular precision $sd(\text{group 1})$ these values quantify the overall positional uncertainty to be expected between the Maittanian plan and the built structures observable today as they appear in modern plans

This resampling procedure is iterated with the newly gained estimates $D(n)$, $D'(n)$ etc. instead of $d(n)$ until only one set of consistent integer scaling factors or integer fractions is left, or, until the spread of resampled values falls below the chosen precision threshold (here: first decimal). Dividing all values $D'(n)$ by the remaining scaling factors results in a series of estimates of the grid unit distance u . The mean of these estimates is the best-fit solution for u .

In a last step, multiples of u can be used to calculate the final values of D , i.e. the precise distances intended by the Maittanian architects, and the minimal grid size in x and y respectively can be determined.

Determination of δ : Assume that distance measurements in the field prior to the construction of the palace were obtained by triangulation within a fixed reference system. If a distance $d(A)$ were determined by crossing two sight lines A and B at right angles (fig. 33A), then the angular precision of A and B ($1\sigma=1.6\text{deg}$) results in a spread of possible intersections $A \times B$ in two dimensions (red area). This positional uncertainty has a distance component $\delta(A)$ in the direction of A dependent only on $d(B)$: $\delta(A)$ is the angular precision of B expressed as a percentage of $|B|$ at $d(B)$, thus: $\delta(A) \approx 2.6\%$

(max.) of $d(B)$. δ is a maximum value because cross-checking from other reference points reduces the positional spread even if $d(B) \gg d(A)$; for the same reason, angles $\ll 90\text{deg}$ need not be considered (fig. 33B).

The initial search space: The field variates $d(\text{mlm} \leq n) \pm \delta(\text{max})$, where $\delta(\text{max})=2.6\%$, for the two main wall orientations (fig. 34) are

	$\emptyset: 83.6^\circ$			$\emptyset: 48.5^\circ$		
	$-\delta$	$d(\text{m})$	$+\delta$	$-\delta$	$d(\text{m})$	$+\delta$
$d(\text{m})$ [~% of $D(\text{m})$]	102.6%	100%	97.4%	102.6%	100%	97.4%
$\sim 1\sigma$ -range for D	105.5	108.3	111.1	81.8	84.0	86.2
bold =measured [meters]	39.9	41.0	42.1	32.1	33.0	33.9
	20.7	21.3	21.9	23.2	23.8	24.4
	6.2	6.4	6.6	22.0	22.6	23.2
				16.3	16.7	17.1
				8.6	8.8	9.
				4.8	4.9	5.0
				3.8	3.9	4.0

In the following, intermediate steps are shown only for the smaller group (83.6deg).

Resampling: Dividing the largest and lowest value in $d(\text{m}) \pm \delta(\text{max.})$ with the lowest and largest respectively for all $d(x|x < m \leq n)$ yields

$d \pm \delta$	[lowest- <u>measured</u> -highest]		
108.3 $\pm \delta$	[16.0- <u>16.92</u> -17.9]	[4.8- <u>5.09</u> -5.4]	[2.5- <u>2.64</u> -2.8]
41.0 $\pm \delta$	[6.0- <u>6.64</u> -6.8]	[1.8- <u>1.92</u> -2.0]	-
21.3 $\pm \delta$	[3.1- <u>3.33</u> -3.5]	-	-
6.4 $\pm \delta$	-	-	-
	6.4 $\pm \delta$	21.3 $\pm \delta$	41.0 $\pm \delta$

The integers and/or the lowest intermediate or adjacent integer fractions within the range of possible scaling factors are

d			
108.3	[16, 16.5, 17, 17.5]	[5, 5.34]	[2.66]
41.0	[6, 6.5]	[2, 1.8]	-
21.3	[3.2, 3.25, 3.34, 3.5]	-	-
6.4	-	-	-
	6.4	21.3	41.0

Fig. 35 plots the values for each $d(\text{m})$ obtained by resampling, i.e. by multiplying each $d(x|x < m \leq n)$ or dividing each $d(x|x > m < n)$ respectively by these factors. The relevant statistics for each group are

	108.3	41.0	21.3	6.4
N of 'repeats'	8	5	8	10
Min.	102.40	38.30	20.30	6.09
Max.	113.60	43.30	22.80	6.83
Median	107.65	41.10	21.05	6.47
Mean	107.58	40.80	21.29	6.46
Std. Error (abs.)	1.451	0.860	0.331	0.075
(ϵ = % of mean)	1.35	2.11	1.55	1.16
sd	4.105	2.106	0.937	0.238

The means are statistical estimates $D(x)$ of the true distance intended by the architects. The standard error of mean is a measure for distance accuracy ϵ . Accuracy is relatively high at an average 1.54% and its percentage is uncorrelated with distance at $c(\text{pearson}) > 0.005$, i.e. there are no additive errors. This strengthens the assumption of sophisticated triangulation techniques but also excludes measurement tape as a means of determining large distances, because the latter inevitably leads to additive percentage errors highly correlated with distance (§ 3.5.2.).

Determination of u and minimal grid size: Repeating the resampling procedure with $D(m)$ yields the ranges

D \pm St. Error (not shown)

107.6	[16.07-17.04]	[4.91-5.19]	[2.50-2.63]
40.8	[6.04-6.51]	[1.85-2.0]	-
21.3	[3.18-3.36]	-	-
6.5	-	-	-
	6.5	21.3	40.8

as well as the integer factors and smallest integer fractions

D

107.6	[16.5, 17]	[5]	[2.5]
40.8	[6.5]	[2]	[1]
21.3	[3.25, 3.34]	[1]	
6.5	[1]		
	6.5	21.3	40.8

Further iterations lead to changes in the estimate D below first decimal precision and are therefore meaningless. For all cases except 107.6:6.5 and 21.3:6.5 only one scaling factor remains. For each case at least one fraction can be made integer through multiplication by 6 or 4. Under the condition that square side length is to be maximized (GCD), the latter is more consistent with the rest, meaning that division of D by the quadrupled scaling factors times the scaling factor necessary to reach $D = 6.5$ in the matrix, results in a series of approximations to the grid unit distance u . The mean of these values is a best-fit estimate of u .

107.6m	/	([67, 68]*1) = 1.63,	1.58m	/	([20]*3.25) = 1.66m	/	([10]*6.5) = 1.66m
40.8m	/	([26]*1) = 1.56m		/	([8]*3.25) = 1.60m	/	([4]*6.5) = 1.57m
21.3m	/	([13]*1) = 1.63m		/	([4]*3.25) = 1.63m		
6.5m	/	([4]*1) = 1.63m					

$u = \text{mean}$	1.615m
Std. Error (% of mean)	0.667
sd	0.036

All distances can now be expressed as integer multiples of u . Retranslation to the metric scale yields what may be considered the best-fit estimate of the ideal values D'' for the distances as intended by the Maittanian architects:

$d; \delta=2.6\%$	\rightarrow	$D; \epsilon=1.54\%$	\rightarrow	D'' (supposed ideal; no error)
108.3m		107.6m		108.2m (67u)
41.0m		40.8m		42.0m (26u)
21.3m		21.3m		21.0m (13u)
6.4m		6.5m		6.45m (4u)

Thus, at the scale of the building, the grid unit u has an ideal length of 1.615m (Salve Fibonacci!). At this scale, the current reconstructions of the palace cover a square area of 320x320m. The minimal size of grids to be used in future implementations of CPSR for encoding the geometry of the known building remains, is 200x200 u .

For the 48.5deg group, there is no solution for $u > 0.5m$. Therefore, if a grid was used, it was oriented in the direction of the southern façade, i.e. the most prominent view of the palace.

3.5.2. Reference Systems and Measurement Techniques

The low angular and distance errors apparent in the outer walls of the Central Palace (§ 3.5.1.) are not only evidence for a very precise triangulation of the positions of the palace's outer corners preceding the actual construction works, but also, in a somewhat wider context, for separate reference systems used at each floor level, and for the exclusive use of optical alignment devices over long distances:

Marking the position of rooms on the ground prior to the start of the construction works makes no sense in a terraced building with massive substructions; rather, room positions had to be determined after the substruction was built and their position marked on a platform at the height of the planned floor level. The necessary measurements must therefore have been taken from new reference points. At a mean difference between floor levels of ca. 6m only the outermost of these new points on each platform can be controlled by triangulation from the original reference points on the ground. The majority of new points, however, is necessarily below the line of sight and therefore had to be triangulated on the basis of independent reference systems. This is in accordance with the difference of 1.5deg in the medians of groups 1 and 2.

The precision of a triangulation depends inter alia on the number of reference points that can be used to cross-check measurements and on the distance between the reference points. The first criterion is independent of the type of measuring device, but not the second: if an optical device is used, positional accuracy (ϵ [%]) is uninfluenced by distance, and positional errors furthermore translate into smaller angular deviations from mean the longer the distance. If tape or rope is used the opposite is true because the material is stretched and bended by its own weight leading to a cumulative error increasing with distance.

The observed decrease in angular precision from group 1 to group 2, then, points to the use optical triangulation devices: precision is high in the orientation of walls visible from the ground where reference points may be spaced far apart (group 1), and low in the rooms located in the upper stories of the palace where the spacing is tight (group 2). If tape or rope had been used for triangulation, the smaller distances between reference points on the platforms would have resulted in more precise measurements than on the ground.

The low precision in group 3 results from the inclusion of the interior parts of massive walls, in which, as a rule, the bricks are much less carefully aligned than in zones closer to the wall face (cf. TH4: Plan 5; Waefler TH4).

3.5.3. Estimation of the Modern Component in Angular Errors

The potential relevance of the modern component in the errors determined in § 3.5.1. was repeatedly mentioned in the course of this text. This component is itself a mixture of unquantifiable field measurement errors and positional as well as angular errors introduced into the plans during the documentation process (§ 2.2.).

The angular and distance errors determined in § 3.5.1. are of a type that excludes any kind of measurement device except optical alignment instruments for long distance triangulation (§ 3.5.2.).

Comparison with other sites: There are very few instances where the type of measurement device used by the builders of an archaeological monument can be determined with any certainty, and therefore the angular precision achievable with optical devices in antiquity is difficult to estimate. One such instance, however, is the Giza pyramids, conclusively proven by Spence (2000) to be astronomically aligned due North by using the simultaneous transit of two circumpolar stars, which, of course, implies the use of optical alignment devices by the original builders. Spence i.a. used high-precision measurements of the orientation of the eastern and western sides of the pyramids of Khufu and Khafre and the bent pyramid of Snofru taken with a meridian-seeking theodolite (Dorner 1981). The angular error in these measurements is ± 0.2 arcminutes, i.e. 0.003deg . The 1σ -deviation between the eastern and western sides of these three pyramids is ± 3.017 arcminutes, i.e. 0.050deg . This - trustworthy - value is extremely low compared to the error determined in the outer walls of the Central Palace. Even if an angular precision lower by a factor of ten is assumed for the Maittanian builders, this still leaves two thirds of the error unexplained. In other words: the modern component of the angular precision $\text{sd}(\text{group 1}) = \pm 1.46\text{deg}$ is at least twice as important as the actual error exhibited by the excavated remains.

3.5.4. Architectural Units

Importance of quantified errors: Architectural units are commonly determined in two steps: first, arbitrary distance ratios are extracted from ground plans or - worse - from 'random-insight-reconstructions' of the geometrical principles underlying ground-plans (§ 3.4.1.). For reasons not usually made explicit, the hypothetical units are then expressed as multiples of a standard brick size or arbitrary units known from texts; a recent worst-case example of such clumsy arbitrariness being Allinger-Csollich (1997). This procedure is absurd both on the conceptual level and on the level of metrics because it ignores the impact of errors accumulating both in the translation of an original plan into an actual building and in the reverse translation of modern field measurements into the modern plan available for reconstruction (§ 3.4.1.). To my knowledge, the separate components of this type of combined error have never been analysed quantitatively for any archaeological monument before. The example of Tall al-Hamidiya shows that on the conceptual level an approximate ratio of 2:5 (108.3m : 41.0m) extracted from a modern plan may, viewed through the lens of error analysis, translate into a much less trivial ratio of 67:26. The geometrical framework necessitated by this second ratio cannot be established by traditional means. On the level of metrics, the established distance error $\varepsilon = 1.54\%$ in the modern plans leads to a variation of ± 4 standard bricks (0.365m side length including joints) per

100m, excluding brick size as a possible unit used by the ancient builders for all but relatively short distances.

Architectural units at Tall al-Hamidiya: The grid unit u apparently is the only architectural unit used in the basic layout of the palace. The assumption of a square grid system actually being used matches the independent evidence for triangulation as the only means employed for determining long distances at Tall al-Hamidiya because any angle encoded in the plan by its grid components in x and y can easily be translated into any given reference system set up previously in the construction area. A basically identical modern technique frequently employed before the advent of total stations was the tangent-encoding of angles in combination with conversion-tables within orthogonal reference grids.

At the dimensions of the Central Palace the square grid system in conjunction with field triangulation are the only plausible tools for precisely orienting long straight wall lines, and, thus, for transforming the discrete corner points in the plan into field coordinates. However, their usefulness both for the planning and building of smaller architectural elements like regularly spaced niches or other façade decorations is very limited for two reasons:

a) Once the main wall lines are established in the field, it is easier and much faster to use tape measurements along these lines than to triangulate the position of each small element separately. The additive distance error specific to tape measurements can be compensated between discrete triangulated points by measuring from both directions and averaging the two measurements obtained for each target point.

b) While brick size is irrelevant when building walls over long distances, it is a plausible unit for small architectural elements because the production of custom-made bricks for each element in order to fit the exact metrics of a non-conforming unit system would be uneconomical and impractical. Also, and perhaps more importantly, during the actual construction of walls the simple counting of bricks is less error prone than calculating their number from distances.

This reasoning is corroborated in Tall al-Hamidiya by the spacing of the half-pillars along the façade of the southern ascent structure in 36/35-37 and 39/27-29, the only preserved decorative elements on outer walls (the spacing and width of the niches in 38/33-36 and 37/40-42 indicated in TH4: Plan 2 is purely conjectural): the distance between half-pillars is exactly 6 bricks and each protrusion carrying a half-pillar is itself 3 bricks wide.

In the plans of 1999 brick size is uniformly represented as 0.34m, except where deviations were considered relevant at the time of drawing. The mean brick size can therefore not be calculated. However, as stated in § 2.2 the number of bricks within large excavated brick layers is correctly represented in the plans as are the bricks in the vicinity of layer boundaries. From an arbitrary sample of such patches, the mean side length of the square formed by a brick and the joints on two of its adjacent sides was determined to be $0.365\text{m} \pm 0.005$ (1σ). While the mean is not affected by the normalization of individual brick orientations within these patches, the true spread is certainly wider.

The scaling factor between $u=1.615\text{m}$ and the rough estimate of brick size 0.365m is 4.4. Since a unit below the size of a brick, i.e. the smallest building element, is meaningless, the two are mutually independent units. *ninda* (ell), a building unit widely attested in ancient Near Eastern texts, fits the bill somewhat better at 0.50+ m, i.e. ca. $1/3$ of u . However, there is no evidence whatsoever of it being used in the Central Palace.

The 28 half-pillars preserved in 36/35-37 and 39/27-29 are spaced at $2.17\text{m} \pm 0.11$ from each other (measured center-to-center). If expressed in u , the best-fit is $1.34 u$, i.e. 3 decorations equal $4u$. The protrusions carrying the half-pillars are themselves exactly half as wide as the total distance, i.e. $0.67 u$. Both ratios $4/3u$ and $2/3u$ are impractical for calculating distances compared to the simple sequence of 2×3 bricks for each segment of the decoration.

Hence, the ground-plan of the Central Palace contains evidence for two mutually independent architectural units. The less obvious of the two was used in the design of the palace's basic layout and as a basis for determining major wall lines in the construction area. It has a metric equivalent of $u=1.615\text{m}$. The second architectural unit is the brick. It does not have a metric equivalent but was apparently used for positioning small building elements over short distances without measurement by the simple counting of elements.

4. EXPERIMENTAL RECONSTRUCTIONS OF THE CENTRAL PALACE AT TALL AL-HAMIDIYA

4.1. The CPSR-Reconstruction of 1999

4.1.1. Problems of Implementation

A universal computational framework for algorithmic complexity calculations was developed only in 1996 (Chaitin 1996). When CPSR was theoretically conceived in 1999 hardly any practical applications based on algorithmic complexity had yet been published outside of information science proper concerned with noise/signal optimisation and algorithm optimisation (Li and Vitany 1999). Although the spectrum of applications has since been widening rapidly (Hemaspaandra and Ogihara 2002, Rogers 2002), CPSR still stands out as a comparatively exotic idea and has no precedents on which the early attempts at predicting architectural structures discussed in this section might have built. Before specialized mathematicians joined the project in 2001 (§ 1.4.), a full implementation of the concept was therefore not feasible, and the experiments reported here consequently rely on a number of simplifying assumptions. Although inelegant and unsophisticated, they have nevertheless allowed a preliminary assessment of the method's potential by testing its predictions in the field, and have led to a more thorough understanding of some of the intricacies of the basic mathematical problems to be solved in the future (Blattner, Bieri, Gerber, *in preparation*).

4.1.2. Data

Five types of data recorded between 1984 and 1999 were distinguished (Fig. 36 and fig. 2; cf. also Gerber 2000b):

Type A: Excavated brick structures and quantified surface observations in the form of (x,y,z)-coordinates of all measured elevations, these data define the minimal spatial extension of the reconstruction.

Type B: Angles of the mean brick orientation in each square; where two or more clusters of differing brick orientation could be distinguished in the same square, each was assigned a relative angle. This information also served as a post-hoc control: predicted wall surfaces must have the same orientation as the bricks in the area they delimit.

Type C: Known averaged floor elevations were recorded as sets of (x,y,z)-coordinates, these coordinates define relative minimum/maximum spatial extensions for each level.

Type D: Known facades, defined by their endpoints (x1,y1) and (x2,y2), constitute the fragmentary ground-plan y. Pillars, niches and other decorative elements were ignored.

Type E: The maximum space to be filled by the reconstruction was arbitrarily defined as the 350msl elevation line.

4.1.2. A Simple Model

Let $s(\cdot)$, as defined in § 3.4., be constant, so that $s(y)=s(x')$. Reconstructions $x(\cdot)$ meeting this criterion define a class B within the infinite number of possible reconstructions A that contain y. Thus, $B \subset A$.

Simplifications: In order to bypass computationally difficult complexity calculations and exhaustive searches necessary to determine elements of B, the first set of predictions was restricted to a small class $E \subset B$ of reconstructions that would necessarily preserve the original signature $s(y)$ and that could be generated by hand:

$x' \in E$ if

a) $x(\cdot)$ consists only of ω -elements present in y , and if the number of repetitions in $x(\cdot)$ of the total amount of identical ω -elements in y is equal for all types of ω -elements. The reconstructions with the smallest repetition factor define a class $C \subset B \subset A$.

b) $x(\cdot)$, represented by a set of polygons that may not intersect with the relevant parts of y (i.e. *Type D* data), is among those reconstructions in C that require the smallest number of different polygons. The remaining $x(\cdot)$ define a class $D \subset C \subset B \subset A$. In cases where y allows solutions that consist of two sets of the original ψ -elements, D necessarily consists of these solutions.

c) DNF, or the variant defined by Eq. 4, is constant, so that $DNF(y) = DNF(x[.])$, where, in y , 'area' is the sum of all areas delimited by straight lines from the endpoints of the known outermost walls of each known level in y to each $x(\cdot)$'s relative mass centre, and 'perimeter' is the total length of the said outermost walls. The remaining $x(\cdot)$ define a class $E \subset D \subset C \subset B \subset A$.

Expected results: Obviously, these simplifications severely limit the potential power of CPSR and very likely exclude many interesting solutions present in B : only the basic structure of the Palace, i.e. its outer walls, is taken into account by (c), and overhangs were considered impossible because (b) implies that wall material either present in the original data or predicted in $x(\cdot)$ excludes unbuilt spaces below its known or predicted elevation. Additionally, by applying (a) and (b) highly symmetric reconstructions $x(\cdot)$ were artificially favoured.

However, in cases where B contains a high number of $x(\cdot)$, Occam's razor would have to be applied in order to determine a sub-class F of likely candidates for x' : within the framework outlined in § 3.4. this might only be achieved by including in the signature the length, i.e. complexity, of that part of the $x(\cdot)$ -algorithm that encodes the Turing machine. In the case discussed sub (b), F would necessarily be restricted to solutions that consist of two sets of the original ψ -elements, i.e. those with the least complex Turing machine. Therefore, if such solutions are at all possible for a given y , then $F=D$. From this it follows that if such a solution can be found by trial-and-error, then the classes A , B and C may be ignored from the start, making exhaustive searches and difficult complexity calculations unnecessary.

While convenient, this also points to a serious flaw in the original encoding scheme that results from the separation of ψ -elements and a Turing machine (§ 3.4) insofar as it automatically favours heavily symmetric solutions. At Tall al-Hamidiya this was of no consequence initially, because reconstructions satisfying the requirements (a) and (b) consisting of 2 sets of ψ -elements were found by trial-and-error with comparatively little effort, and although it was already clear at that time that the model's bias towards symmetrical reconstructions was an artefact of the encoding scheme, it was decided that the predictions should be tested in the field anyway, because a fairly high degree of symmetry had already been observed in the Maittanean structures excavated earlier. For other places and periods, this bias might be inappropriate and the results obtained misleading; currently, therefore, CR as defined in § 3.4., has been substituted by encoding methods that do not rely on the separation of Turing machines and operations (Blattner, Bieri, Gerber, *in preparation*; § 3.4.2. and 3.5.).

Inclusion of a shape index: All reconstructions in D found by trial and error were - by definition (twice the same set of ψ -elements) - variants of each other. In 1999, a simple brand of Occam's razor was chosen for determining the most promising candidates for x' in D , namely those that used the available space optimally, in other words, those that had the shortest overall length if measured along the outermost walls. Requirement (c) was inserted post-hoc as a less arbitrary alternative, and in order to provide an objective means of comparing rivaling hypothetical reconstructions in D : if $DNF(y) \cong DNF(x[.])$ then $x(\cdot)$ has the same type of shape as y because it exhibits the same overall elongatedness, i.e. ruggedness as y , or - in other words - the same degree of deviation from a geometrical primitive like, for instance, a circle.

4.1.3. The Hypothetical Reconstruction x'_{1999}

Figs.36 (main window) shows the two reconstructions x' of the Central Palace's basic layout that met the simplified model's requirements best. The resemblance to two sets of tangrams thrown together is no coincidence; the search process can indeed be seen as a search for tangram pieces constructed exclusively from the ψ -elements in y and fitting in three dimensions such that no piece includes coordinates of more than one floor level. In tangram terms, the favoured reconstructions are the solutions with the smallest amount of different piece types (9) and the smallest number of pieces of each type (2).

Effects of archaeological interpretation on the reconstruction: A problematic consequence of the simplification is immediately apparent: the long structure extending to the south can only be included if it is given no z-dimension, because it extends over several floor levels (indicated by transparency). By its construction, it belongs to the 383.5msl floor level. It is repeated in the east on the next lower level at 377.5msl (transparent yellow). In order to make sense of these two incomplete predictions, a brief look at the squares 34-40/25-38 is necessary: The corresponding excavated structure is delimited to the East and West by two facades partly excavated in the years before 1999 over a distance of 140m. It was hypothesised by Wäfler to be a monumental flight of stairs and appears as such in the post-hoc reconstruction of 1998. If this assumption is correct, its northern end must have connected to the 383.5msl floor level, because a tilted plane connecting to the 372.4msl or 377.5msl levels conflicts with the measured elevations at several points regardless of its tilting angle. The minimal total length of the protrusion was calculated by Wäfler in 1999 under the condition that it is a stair rather than a ramp. This prediction was tested and confirmed by excavation in 2000 (Wäfler TH4).

The interpretation as a flight of stairs was assumed to be correct in the CPSR reconstruction 1999. This eliminated the need to disregard the z-dimension of the two predicted extrusions from the main body of the palace: If both are treated as ascent structures with the same inclination, however, the eastern one's surface (A) cuts through two areas (B and C) differing in brick orientation which violates the requirement that a wall face correspond in orientation to the bricks in the adjacent area. The reconstruction must therefore be adapted by rubber-sheeting the eastern ascent structure where it touches the 372.40msl floor level, i.e. the 366.6msl roof level. In 1999 the variant pointing south-eastwards (yellow) was chosen arbitrarily as x'_{1999} .

Comparison with the present tall topography and determination of target structures: The shape of the reconstructed ground-plan x'_{1999} is unusual to say the least. However, it fits the tall's topography remarkably well. The two entities have a similar distribution of their main masses, and many of the larger wadis cut into the tall where the model predicted the most prominent corners of the palace. Hence, despite the theoretical reservations regarding the crudely simplified model, its predictions were considered a promising hypothesis to be tested in the campaign of 2000. The selection criterion was simple. It was decided to dig where the most unexpected architectural structures should, according to x'_{1999} , be found close to the present surface.

4.1.4. Field Test 2000: Excavation Results

(Wäfler et al. 2000, Gerber 2000b, Wäfler TH4). Erosion has long cut away the northern limits of the palace making the predictions concerning its extension in this direction difficult to test. Easily testable predictions existed for three key areas indicated by unbroken red circles in fig. 36:

In the east, massive brick structures conforming in position, elevation and wall orientation to the predicted second monumental ascent structure were found. Contrary to x'_{1999} , however, it appeared to point NE-wards. In the west the predicted odd-angled retaining walls could only be partly recovered due to erosion below the level of the foundations at many points. The brick direction was found to change where expected, but since only the lowest brick layers were preserved this information only

securely confirmed the presence of massive retaining walls in this area, not their precise orientation. The western corner of the southern façade was of interest because at this point the post-hoc reconstruction 1999 and the 1999 CPSR-reconstruction could conceivably be tested at the same time. The results were inconclusive because the walls in this area were not preserved to the required height.

4.1.5. Assessment

The 1999 CPSR-reconstruction and Wäfler's post-hoc reconstruction of 1999 (TH4: Rekonstruktion 1999) were based on exactly the same data. The differences are obvious: the older reconstruction was an attempt at determining the minimal extent of the terraces known in 1998 in the context of the excavated structures. The walls known in the vicinity of 45/50 were not included because the drastic change in brick orientation necessary if the structure was to be incorporated into the main building was considered improbable. This shows how counter-intuitive the first model predictions were and demonstrates their independence of prior expectations.

Despite reservations concerning the encoding method presented in § 3.4, the first set of predictions tested in the field in 2000 was astonishingly successful. While the confirmed minimal length of the southern ascent structure is independent of the CPSR predictions, the excavations in the two test areas in the eastern and western part of the main mound conclusively confirmed the presence of a second large structure at the predicted height and orientation in the East as well as the presence and approximate orientation of the predicted outer walls in the West.

In retrospect, the inclusion into the model of subjective interpretations at a level of detail not supported by the data was a mistake (§ 0.2.3.). By assuming that the southern extension of the palace is an ascent structure - an assumption I still believe to be reasonable - an untestable element was introduced into the post-hoc reconstructions that resulted in the interpretation of the predicted structures in the East and West of the mound as further monumental stairs - a solution, it must be stressed, of almost hypnotic aesthetic appeal.

The field test 2000 proved CPSR to be an effective tool for predictions that could not conceivably have been achieved with traditional reconstruction methods. Its positional accuracy can, however, not be established with any certainty because the excavation data employed for input had, at the time, not yet undergone a critical error assessment (§ 3.4.1. and 3.5.). Such an estimate is impossible post-hoc because the data used in 1999 cannot be replicated from the published plans in TH4 (§ 0.2.3. and 2.2.) and this first CPSR experiment is no longer replicable one-to-one. This, however, is a drawback of the data acquisition and post-processing methods, not of CPSR itself.

4.2. The PSDR-Reconstruction 2002

4.2.1. Predictions 2000-2002

Following the first field test, the excavation strategy for the main body of the Central Palace during the campaign 2001 was based largely on subjective refinements of the initial CPSR-predictions but also on preliminary results obtained by topographic PSDR analysis (§§ 0.2.4. and 3.2.-3.3.). In this section, the unmixed results obtained exclusively by topographic analysis in the PSDR-framework (§§ 3.2. and 3.3.) are briefly summarized. In § 4.2.2.2. a synthetic reconstruction based on these predictions is presented and compared to the parts of the Central Palace excavated until 2002. In contrast to the CPSR- reconstruction of 1999, which was based on previous excavation results and, hence, was prone to the propagation of potential errors of interpretation present in the data, the new reconstruction depends only on topographic survey data (§ 2.1.). In other words: using the methods set forth in § 3.1.-3.3. it could have been done already in 1984, before the inception of excavations. It corresponds to level 3 in the envisioned PSDR-strategy (§ .0.2.1.).

4.2.2. Results

4.2.2.1. Synopsis of Predicted Architectural Features

For the areas referred to in this section see fig. 37, for the reconstruction see fig. 38.

A. Basic Changes in Shape (§ 3.2.)

Date: late 2001 - mid-2002

Block 8

No indication of non-uniform planning within block , i.e. of buildings from different periods or of contemporary buildings that were planned independently.

		Attributes
Shape 1:	>379msl (min. vertical extension)	
Change:	379-373msl (cf. <i>wall orientations</i>)	
Shape 2:	373-370msl (min. vertical extension)	at least 1 concave corner more than shape 1
Change:	370-367msl	

Block 9+

Shape 3:	<367msl (min. vertical extension)	upper northern parts similar to shape 1?
----------	-----------------------------------	--

B. Plateaus/Floor levels (§ 3.3.3.1.)

Date: early 2000 - early 2001

Block 8 (and northern parts of 9+)

Regular intervals of 5m indicate a single building.

North:	≥382msl	≥377msl	≥372msl	≥367msl	<359msl
Northwest:	≥381msl	--	<376msl	--	--
East:	≥381msl	--	<376msl	--	--

'≥': turning points connecting A-A-segments; local contour segments define max. horizontal extension.

'<': turning points connecting A-C-segments; local contour segments define min. horizontal extension.

-- : no indicators, possibly present

C. Wall Orientations and Order Symmetry (§ 3.3.3.2. and 3.3.4.2.)

Date: Symmetry mid-2000; orientations: early 2000 - late 2001

Block 8 (and northern parts of 9+)

Basic changes in wall directions only at 376-373msl (cf. Basic Changes in Shape).

	Sector:	1	2	3	4	5	6	7	
≥ 376msl		2	1	2	2	2	3	2	[group]
≤ 373msl		2	1	1	2	1	3	3	[group]

group 1: 61/151deg

group 2: 85/176deg

group 3: 47/137deg

4.2.2.2. The Reconstruction 2002: Synthesis of Predictions based on Topography

Fig. 38 is a synthesis of the results summarized in § 4.2.2.1. This full reconstruction, x'_{2002} , is based exclusively on the analysis of topographic data as they were available in 1984. It is independent of any excavation results as well as of the CPSR-reconstruction 1999 (§ 4.1.). The general resemblance of the two reconstructions - from the horizontally stepped structure in the eastern part of the northern flank, to the beak-shaped extrusion in the east and the orientation and structure of the western part - is all the more striking. In contrast to the CPSR-reconstruction, where the position of the walls themselves was predicted precisely (though not necessarily accurately!), x'_{2002} consists of predictions on the local orientation and maximum extension of the original walls and the minimum elevation of platforms/floor levels. It contains no information on their precise position; the latter may, however, be estimated roughly (§ 3.3.2.2.): within A-shaped slope segments the deviation between the observed horizontal position of a topographic indicator (i.e. the maximum extension of the original architectural element) and its original position is expected to be very slight. In flattened C-segments at the base of a mound it must be presumed to be much more important. Once tested by excavation a small number of quantified deviations may be used to calibrate the predictions, and thus to compensate for slope gradient-dependent differences in the accuracy of the predictions.

Sector 1 (North): The horizontally stepped structure in this part of the building was already apparent in the determination of areas of high linearity (cf. fig. 22B). There is no indication of wall orientations

other than group 2. The maxima of individual walls oriented generally E-W at the same elevation were therefore connected by walls at right angles where the relevant contours intersect with the areas of high linearity. The position of N-S pointing walls is therefore a maximum in the eastern direction. In the northern direction the original wall positions may be assumed to coincide approximately with the predictions due to the relatively steep slope. The walls indicated by broken lines belong to block 9 and are not predicted by the topographic indicators examined here; they merely represent possibilities. Their elevation was extrapolated from the series of turning points at regular intervals of 5m.

Sectors 2, 3 and 4: The generally steep slopes in all three sectors leave little room for deviations between predicted maxima and original positions. Original wall positions may be assumed to coincide closely with the indicated lines provided the predicted wall orientation is correct.

Sector 5: The prediction of a group 1 orientation of the walls in the lower segment of this sector is subjectively problematic; a group 2 orientation would seem fit the topographic situation in the adjacent parts of block 9 better (§ 3.3.3.2.). The southward extension of the walls in this lower segment is a result of the very flat C-slope at the border to sector 6; the original walls must therefore be assumed to lie much closer to the southern maximum of the 377msl-level even if the orientation is correct.

Sector 6: Because of the flat C-slope extending eastwards below 376msl, the original positions of the predicted walls must be assumed to lie closer to the maximum of the 377msl-level even if the predicted wall orientation is correct.

Sector 7: Due to the initially steep slope, the 382 and 377msl levels may be assumed to be positioned with fair accuracy. The original position of the NW-SE pointing wall faces in the flatter part of the slope may be found slightly further South. Orientation has comparatively little weight because the distances are short.

4.2.3. Comparison with Excavations -2002

Excavated areas are referred to by the numbers indicated in fig. 39. Because the excavation data up to 1999 are lost, plans 3, 4 and 5 (TH4) had to be used for comparison. Their errors are necessarily more important than those established for the plans of 1999 in § 3.5 (§ 0.2.3.). Assuming a relatively low accuracy of the plans distance deviations were measured to the nearest metre, and angular deviations to the nearest degree.

Sector 1, area A: The predicted orientation deviates from the mean orientation of known wall faces by 2deg. The line of maximum extension of the ≥ 382 msl floor level correctly includes the room 41-42/50 at 384.30msl and crosses the room in 44/50 at 377.50msl. The indicated maximum deviates from the true minimum defined by the southern wall of the room by 3m; if the angle is adjusted (red lines), this distance is reduced to 1m.

Sector 2, area B: The small block of bricks in 28/48 has an average brick orientation that deviates from the predicted wall orientation by 15deg. Its elevation (355.90msl) and its location ca. 2m from the maximum extension of the predicted wall line at ≥ 357 are in accordance with the prediction. The angular deviation is irrelevant in this case because the excavated structure lies right behind the point where the tangent touches the contour. A corrected angle would not influence the prediction in this area.

Sector 3, area C: There are no contradictions between the structures excavated in C and the predicted wall lines. If the small wall segment in 33/44 (362.20msl) is indeed a fragment of a wall face, it would conform to the maximum extension of the predicted 372msl floor level if the orientation was adjusted to the one found in 28/48 (red lines).

Sector 4, areas D, E, F, G: As in sector 1, the predicted orientation is off by 2deg. The predicted maximum wall line is too short by -2m (E). D(357.90msl), F(363.20msl) and G(367.90msl) do not contradict the prediction.

Sector 5, areas G, H: In the lower segment the predicted orientation is wrong. The walls found in this area belong to group 2, not to group 1. The maximum southward extension of the 372 and 367msl floor levels would be correct (H) if the angles were adjusted (red lines). There are no contradictory elevations in the excavated areas of the sectors upper segment.

Sector 6, areas I, J: The predicted orientation deviates from the mean angles measured in I and J by 1deg. The maximum extension of the 372msl floor level is 5m in excess of the measured wall line in I as indicated on the plan of 1999 (fig. 28). The lowest elevation measured in I is 1m below elevations; in J elevations are in accordance with the prediction.

Sector 7, areas K, L: The extrapolated wall line K is correctly included in the predicted maximum extension of the 372msl floor level. If the extrapolation is correct, the true position is 8m behind the predicted maximum. The very small segment of a wall face L is -2m from the predicted maximum extension of the 377msl floor level; its orientation is off by 2deg from the prediction. If the angle is adjusted (red lines) this distance is reduced to 1m.

4.2.4. Assessment

The predicted angles for groups 2 and 3 are very close to the wall orientations in TH4: plans 3, 4 and 5 at 2 and 1 deg respectively. Group 3 is grossly off target by 15deg, but was correctly identified as a separate group. Angles in the former groups were extracted exclusively from tangents to gullies whereas in the latter they were determined exclusively by the tangents to the A-slope of the north-western face of the mound. Results obtained by the GT-method (§ 3.3.3.2.) applied to slopes that are heavily eroded by a river cutting into the base should therefore be used with caution. However, this drawback may be easily compensated by excavating in the vicinity of both points of contact between the tangent and the contour of interest. Even if the predicted orientation is grossly off-target, the probability of finding a wall at one of these points is high, and once the true orientation is known, the distance error of the predictions is in the 1m-range in relatively steep slopes (cf. red lines in areas A, C, L); in areas within a C-segment close to the base of a slope the deviation between the predicted maximum and the true wall positions is around 5m (cf. area I).

Only in sector 5 is the reconstruction incorrect. The wall orientation predicted by the order symmetry within block 8 is wrong; also the reconstruction does not identify the southern ascent structure at all. Both miss-identifications may be artefacts of restricting the analysis to block 8 since most of the known parts of the monumental flight of stairs belong to block 9.

On the whole, considering that only topographic data were used, the distance and angular errors are extremely small, and the overall shape and organisation of those parts of the Central Palace that belong exclusively to block 8 are predicted with a very high degree of accuracy. I therefore consider topographic PSDR-analysis, even in the crude form proposed here, a more than even match for both traditional excavation strategies and traditional methods of reconstruction: a glance at the latest - overly elaborate - post-hoc reconstruction in TH4: Plan 2 shows that the differences to the purely topographic PSDR-reconstruction in the eastern and western parts of the mound are very slight on the low level of detail supported by the - in parts inaccurately represented - excavation data. Since the relevant aspects of the basic structure of the western and eastern parts of the Central Palace as far as they are known today were predicted with good accuracy by purely topography-based PSDR, its predictions concerning the northern part of the palace may - until further testing - be assumed to be essentially correct.

5. DISCUSSION

5.1. Hits and Misses

The aim of this work as defined in the introduction (§ 0.2.1.) was to validate the general idea of PSDR by presenting one PSDR-strategy in some detail. This strategy was to be limited in scope to the detection of tall potentially harbouring monumental architecture (level 1) and to the identification (level 2) and reconstruction of these monumental buildings on the basis of the traces they have left in the topography of the chosen sites alone (level 3). Interesting buildings were to be singled out for excavation and mathematical methods were to be developed that would allow the extraction of characteristic regularities from their topographical traces and, at later stages, from preliminary excavation results. These regularities were to be processed in a predictive mathematical reconstruction model employed in alternation with targeted small-scale excavations feeding back test results into the model. Reconstructions were to be entirely data-driven and to be resistant to the influence of subjective interpretation (level 4). The expectation was a significantly higher overall gain in non-redundant information relative to the investments in time and effort than achievable on the basis of traditional excavation and/or prospection strategies.

Level 1; Detection of sites on the scale of landscapes: At this level the aims were clearly missed. Although a general theoretical framework for detection algorithms based on fractality signatures of urban tall in large-area scans of VHR remote imagery was presented (§ 3.2.), an implementation is currently beyond my possibilities. Its worth therefore remains to be tested.

The progressive fractalisation of eroding mudbrick structures was argued to lead to an increase in random noise hiding the original low-fractality/high-artificiality signature of buildings. In an image of appropriate resolution, the expected medium to low-fractality/medium to high-artificiality signature of the remains of the target buildings within a site should therefore stand out clearly at scales around 0.01-0.10km and be bordered at the upper end by signatures typical of natural topographic surfaces or agricultural areas depending on the land use in the surroundings. Remote imagery at the necessary resolutions is currently becoming commercially available, and prices are dropping to levels that will soon allow a large scale test of the proposed type of algorithm. I consider the odds to be in favour of positive results because similar algorithms have been successfully employed in military reconnaissance for the detection of camouflaged artificial structures since the 1970ies. To my knowledge, comparable civil applications have so far been restricted to experiments by the SETI community in the search for extraterrestrial artefacts on Mars. While this does not necessarily lend credence to fractality-based methods, it does not lessen their potential either.

Level 2; Identification of monumental structures and individual buildings: Using a very simple shape index based on the area/perimeter ratio of individual contours extracted from the DEM, blocks of contours defined by saddle-shaped watersheds were examined for changes in shape at 1m-intervals (§ 3.2). As far as the distribution of monumental buildings on the tall is known, these buildings do indeed correspond to separate blocks (cf. TH4: Abb. 1): Block 13 includes the known parts of the Southwest Palace and block 12 corresponds to the hypothetical Eastern Building. The main body of the Central Palace is contained in Block 8 while the southern protrusion of the monumental flight of stairs is encompassed by block 9. There are no overlaps between buildings. For block 8, the shape index indicated the presence of at least two platforms defined by different shapes. The predicted elevations for these two building elements are in accordance with predictions obtained by independent methods discussed sub *level 3* below.

The shape indexing and segmentation methods employed successfully allowed a segmentation of the complex topography of the mound that corresponded roughly to the known distribution of individual monumental buildings. It did, however, not identify the southern ascent structure as belonging to the main body of the Central Palace.

Despite the crudeness of the methods the aims at this level were achieved to a satisfactory degree. The development of more appropriate shape indices is ongoing, and employing more sophisticated segmentation techniques, the southern ascent structure is likely to be attributable correctly to the Central Palace.

Level 3; Determination of basic structure of individual buildings: Block 8, known to correspond to the main body of the Central Palace, was singled out for further analysis. Based on simple models for the collapse and subsequent erosion of complex mudbrick buildings and simple probabilistic considerations, topographic indicators for specific architectural elements were defined and their detectability over time assessed theoretically (§ 3.3.), namely the elevation of turning points between specific types of slope segments as indicators of original floor levels intersecting with the tall surface, and tangents to two points of local concavities in the contours extending over several contours, i.e. gullies and wadis. These tangents were separated in two types assumed to correspond to original orientations of straight wall faces and to large concave corners respectively.

Applied to the parts of the DEM corresponding to block 8, three groups of homogenous original wall orientations were identified and positioned on the mound surface. The analysis of a total of 20 slope profiles on the western, northern and eastern faces of the mound indicated floor levels at regular intervals of 5m in the north (extending into block 9) and individual floor levels at corresponding elevations in the west and east. The combined results of the two methods led to a segmentation of block 8 into 7 sectors consisting of two segments each, defined by homogenous wall orientations. Two such segments could not be attributed to one of the three groups.

In § 3.5. rotational symmetric behaviour in the order of sectors and segments was identified by autocorrelating the sequence of predicted elements. The missing data for the two elements that lacked a group attribution were then replaced by the solution providing the best fit with the original autocorrelation signature.

The results of the individual methods of topographic analysis were merged into the full level 3 PSDR-reconstruction presented in § 4.2. Since this reconstruction is totally independent of any excavation results it could have been generated from a DEM already in 1984. It can therefore be compared to the later excavation results and other types of reconstruction without running the risk of circularity or the miss-attribution of specific result to specific methods. A comparison with the excavation results available in 2002 (inaccurately represented by TH4: Plans 3, 4 and 5) showed a high degree of accuracy on the level of detail of the predictions. Two of three groups of wall orientations were identified to the nearest 2deg. The third group was off-target by 15deg, but was correctly positioned on the mound. The maximum extensions of individual floor levels were accurate to the nearest 1-2m for groups 2 and 3. The reconstruction is grossly wrong only in one of 14 sector elements, where, in reality, the southern ascent connects to the main body of the palace. It is unclear whether or not the systematic inclusion of block 9 would have led to a correct prediction in this area.

Judging by the limited evidence from Tall al-Hamidiya, the effectiveness of the level 3 methods measured by knowledge gain/investment is immense by any standards because they allow reliable reconstructions prior to excavations or geophysical prospection.

Level 4; Iterative reconstruction of buildings on the basis of excavation results: At level 4, CPSR was proposed as a means to rapidly increase the level of reliably known detail (§§ 3.4.). Its full implementation has proved too difficult for me to undertake on my own. In 1999, therefore, I only devised a simple CPSR-model that could be handled using pen and paper and a PC. Its results were tested in the field in 2000 (§ 4.1.). The reconstruction appeared to be fairly accurate as far as could be assessed by the walls found on the basis of its predictions.

Interestingly, the CPSR reconstruction of 1999 and the PSDR-reconstruction of 2002 agree closely in many relevant points. Both models were only used on a single set of data each, namely the plans of 1999 and the topo survey data of 1984. In the envisioned PSDR-framework (§ 0.2.1.) CPSR was intended to be used iteratively after each field test. The close agreement at iteration one between the

two methodically independent models processing completely different types of data may point to an even higher effectiveness of CPSR than anticipated in 2000 (Gerber 2001). Basing much of the excavation strategies in 2000 and 2002 on predictions generated by the two models has led to an increase in knowledge about the Central Palace that would, I believe, not have been possible by using any other methods.

In retrospect the effectiveness of CPSR is surprising because excavation data was processed uncritically and supplemented by reasonable but untestable assumptions on the nature of the southern protrusion of the palace (§ 4.1.3.). In § 3.5. the potential weight of modern errors introduced at various levels of measurement, interpretation and CAD post-processing was established, and, thus, the importance of thoroughly documented error estimates. Because the data used in 1999 cannot be replicated anymore (§ 0.2.3. and 2.2.) the effect of incorporating error estimates into the model cannot be assessed.

Even though, therefore, CPSR cannot be considered properly tested - not even in the crude preliminary form of the 1999 model - I believe the theoretical concept to be valid on its own: Bannai and Miyano (1999) intelligently view science as the art of data compression and consequently define a good discovery as one that considerably compresses information. In contrast to the widespread but necessarily subjective notions of 'architectural style' implicit in most architectural typologies, $C_R(x)$, $|p_o(x)|$ and $p_o(x)$ objectively and completely capture architectural identity as far as it is reflected in partially known ground-plans. In principle, there is no information loss whatsoever, and the degree of compression is by definition maximal for the information contained in the known remains of a building.

Provided the excavation results used for input are reliably documented and of good quality and that a thorough error estimation is undertaken in advance, CPSR data on a large number of buildings might in the future allow comprehensive quantitative intra- as well as inter-site comparisons while effectively eliminating subjective bias. Employing mathematical cladistics such comparisons might result in reliable models of long term architectural evolution in a mechanistic explanatory framework comparable to the one of biological evolution. This would be interesting mainly because mechanisms and criteria of inheritance and innovation underlying cultural change could be examined from the perspective of ecological fitness and selection instead of continuing to waste time, money and brains on pondering arbitrary, stylistic typologies. Similarly, large amounts of CPSR data might pave the way for meaningful synchronistic comparisons of architecture in large geographical areas using techniques of multivariate proximity analysis.

By-products/Additional Results: in § 3.5. evidence for the use of square grid constructions by the builders of the Central Palace was presented. By determining the maximum square size necessary to match discrete points in the architectural remains known in 1999 with grid nodes, an architectural unit distance $u=1.615\text{m}$ inherent in the Central Palace was established using a simple resampling strategy. The type of distance error determined in the course of this procedure is compatible only with the use of optical triangulation devices during the construction of the palace. A comparison with high-precision measurements of the parallelity of the eastern and western sides of Egyptian monuments conclusively proven to have been aligned astronomically, i.e. necessarily with optical instruments, additionally allowed a rough estimate of the modern component of the errors determined in the plans of 1999. This component is at least twice as important as the errors accumulated at all stages between the planning and construction of the Central Palace.

5.2. Conclusion

The aims formulated at the beginning of this text have only been partly achieved. It is hoped that the results nevertheless demonstrate the potential and effectiveness of PSDR as a concept. The methods set forth are simple - some to the extent of being simplistic - and the degree of their implementation is low. Improvements are obviously possible at every level of the envisioned strategy. Judging by the results, however, they do their job very well. In fact, where site reconstruction and excavation strategies for large buildings are concerned the methods proposed here beat every other approach known to me in terms of effectiveness, reliability and scientific validity - even in their current, crudely implemented form.

Many of the problems encountered in the course of this research are directly linked to the means of data acquisition and the methods of documentation at Tall al-Hamidiya. The raw data extractable from excavation reports cannot be taken at face value, and error estimates - if they are at all possible - include a modern component of unknown and potentially overwhelming weight. The future of CPSR or other data-driven methods processing excavation results therefore critically depends on the introduction of new acquisition technologies like VHR 3D-Laser scanners yielding raw data resistant to post-hoc manipulations on the basis of subjective interpretations.

These constraints do not apply to the topography-based methods proposed at level 3. The predictions generated by topo-survey data from Tall al-Hamidiya were highly accurate. It is, however questionable, if they would work effectively if smaller buildings were to be detected and reconstructed using the same type of survey data. The low local measurement densities achieved by traditional topo-surveying may well set the limit of detectability at an uncomfortably high level. Here as well, the use of VHR-data acquired by Laser scanning or close-range photogrammetry is imperative in the future.

Because tests were conducted exclusively at Tall al-Hamidiya, the universality of the individual theoretical concepts remains to be investigated; the good fit between CPSR and topography-based predictions obtained by processing very different and mutually independent data sets may be seen as a preliminary indication of a satisfactory degree of general applicability.

At the level of targeted site detection much additional research has to be done. While I consider the theoretical approach outlined herein to have a certain potential, its implementation - whether successful or not - also depends on the availability and quality of VHR data.

The general lack of replicable methods plaguing Near Eastern archaeology will not be solved by PSDR or any other scientific approach as long as tallies are viewed as objects of prestige instead of scientific inquiry. As a personal gain I may at least claim to understand the still mysterious Tall al-Hamidiya a little better due to PSDR. In the words of my childhood mentor:

"I think my sight's improving. Before I could only see a dark blur, now I can see a light blur."

(Han Solo, in: Star Wars - The Return of the Jedi, 1983)

6. REFERENCES

6.1 Abbreviations

- APACK 2001: APACK analysis software. Version 2.15., by D. Mladenoff and B. DeZonia.
(<http://landscape.forest.wisc.edu/Projects/APACK/apack.html>)
- CHILD 2002: Dynamic 3D Computer Simulation of Erosion, Deposition, and Landscape Evolution.
(<http://platte.mit.edu/~child>)
- CORONA 2002: CORONA satellite photography, U.S. Geological Survey.
(<http://edcwww.cr.usgs.gov/glis/hyper/guide/disp>)
- CYRAX/CYCLONE 2002: CyraX 2500 3D Laser scanner and Cyclone software. Version 4.0., Cyra Technologies/Leica Geosystems. (<http://www.cyra.com>)
- GRASS 2002: Geographic Resources Analysis and Support System. Version 5.0, September 2002.
(<http://www3.baylor.edu/~grass>)
- IKONOS 2002: IKONOS VHR satellite imagery, SpaceImaging, Inc.
(<http://www.spaceimaging.com/products/ikonos/index.htm>)
- IQSUN 2002: iQsun continuous wave 3D Laser scanning system. (<http://www.iqsun.com>)
- LASERGEN 2002: LaserGen point cloud handling and visualisation software, BitWyse Solutions, Inc.
(<http://www.bitwyse.com/Products/PointCloud/ModelCreator/body.htm>)
- RIEGL 2002: Riegl Laser imaging scanners. (<http://www.riegl.com>)
- PARAFORM 2002: Paraform point cloud processing and visualisation software. Version 2.0.
(<http://www.paraform.com>)
- QUANTAPOINT 2002: Quantapoint high-precision 3D Laser measurement and imaging.
(<http://www.quantapoint.com>)
- QUICKGRID 2001: QuickGrid DEM generator. Version 4.5, November 2001, by J. Coulthard.
(<http://www.perspectiveedge.com>)
- RUSLE 2002: Revised Universal Soil Loss Equation project. Version 1.06b, USDA-Agricultural Research Service (ARS).
(<http://www.sedlab.olemiss.edu/rusle/>)
- SYSTAT 2002: Systat statistical analysis software. Version. 10.2., Systat, Inc.
(<http://www.systat.com>)
- TH1: Eichler et al. 1985.
- TH2: Eichler et al 1990.
- TH3: Wäfler 2001.
- TH4: Wäfler, *forthcoming*

6.2 Literature

Arikawa, S. and Furukawa, K. (eds.) 1999. *Discovery Science, Proceedings of the Second International Conference DS '99, Tokyo, Japan, December 1999*. Springer: New York

Abrahams, A.D. (ed.) 1986. *Hillslope processes*. Allen & Unwin: Boston.

Allinger-Csollich, W. 1997. Die Heiligtümer auf der Ziqqurrat von Babylon. Online paper. (<http://info.uibk.ac.at/c/c6/c616/vor-97.html>)

Anderson, D.C., Lee, K. (eds) 2001. *Proceedings of the 6th ACM Symposium on Solid Modelling and Applications, Ann Arbor, Michigan, June 4 – 8, 2001*. ACM Press: New York. (<http://portal.acm.org/toc.cfm?id=376957&coll=portal&dl=ACM&type=proceeding&CFID=6550231&CFTOKEN=26946863>)

Ankerst, M., Kastenmüller, G., Kriegel, H.P., Seidl, T. 1999. 3D Shape Histograms for Similarity Search and Classification in Spatial Databases. *Proceedings of the International Symposium on Large Spatial Databases (SSD) 1999 (LNCS 1651)*: 207-226.

Armstrong, A.C. 1976. A three-dimensional simulation of slope form. *Zeitschrift für Geomorphologie, Supplementband 25*: 20-28.

Bailey, D.W., Andreescu, R., Mills, S., Trick, S. (eds.) 2001. *Southern Romania Archaeological Project. Second Preliminary Report* (Cardiff Studies in Archaeology). Online publication. (<http://www.cf.ac.uk/srap/Srapmain.html>)

Bannai, H. and Miyano, S. 1999. A Definition of Discovery in Terms of Generalized Descriptive Complexity. *In: Arikawa and Furukawa 1999*: 316-318.

Barnsley, M. F. 1988. *Fractals everywhere. The First Course in Deterministic Fractal Geometry*. Academic Press: Boston.

Barnsley, M.F., Demko, S. 1985. Iterated Function Systems and the global construction of fractals. *The Proceedings of the Royal Society of London A399*: 243-275.

Baxter, M.J., Beardah, C.C., Wright, R.V.S. 1997. Some archaeological examples of kernel density estimates. *Journal of Archaeological Science 24*: 347-354.

Beardah, C.C., Baxter, M.J. 1996. The Archaeological use of Kernel Density Estimates. *Internet Archaeology 1* (http://intarch.ac.uk/journal/issue1/beardah_index.html).

Bell, M. and Boardman, J. (eds.) 1992. *Past and present soil erosion: archaeological and geographical perspectives*. Oxbow Books: Oxford.

Bernardini, F., Mittleman, J., Rushmeier, H., Silva, C., Taubin, G. 1999. The Ball-Pivoting Algorithm for Surface Reconstruction. *IEEE Transactions on Visualization and Computer Graphics 5.4*: 349-359

Besl, E. 1998. 3-D range imaging sensors. *Technical Report GMR-6090*, General Motors Research Lab., Warren, MI.

Bettis, E.A., Mandel, R.D. 2001. The effects of temporal and spatial pattern of Holocene erosion and alluviation on the archaeological record of the central and eastern Great Plains, U.S.A. *Geoarchaeology 17*: 141-154.

- Bigün, J. 1988. Recognition of local symmetries in gray value images by harmonic functions. *Proceedings of the 9th IEEE International Conference on Pattern Recognition, Rome, November 1988*. IEEE Computer Society Press: Los Alamitos: 345-347.
- Bindlish, R., Barros, A.P. 1996. Aggregation of digital terrain data using a modified fractal interpolation scheme. *Computers & Geosciences* **22**: 907-917.
- Bishop, Ch.M., Frey, B.J. (eds.) 2003. *AI & Statistics 2003. Proceedings of the Ninth International Workshop on Artificial Intelligence and Statistics, January 3-6, 2003, Key West, Florida*. Preprints available online.
(<http://research.microsoft.com/conferences/aistats2003/proceedings/papers.htm>)
- Blaschke, Th., Lang, S., Lorup, E., Strobl, J., Zeil, P. 2000. Object-Oriented Image Processing in an Integrated GIS/Remote Sensing Environment and Perspectives for Environmental Applications. In: Cremers and Greve (eds.) 2000: 555-570.
(http://enviroinfo.isep.at/UI%20200/Blaschke_et_al_engl200700.el.hsp.pdf)
- Braidwood, L.S., Braidwood, R.J., Howe, B., Reed, Ch.A., and Watson, P.J. (eds.) 1983. *Prehistoric Archeology Along the Zagros Flanks* (The University of Chicago Oriental Institute Publications 105). University of Chicago Press: Chicago.
- Brethour, J.M. 2001. Transient 3-D Model for Lifting, Transporting, and Depositing Solid Material. *Proceedings of the 2001 International Symposium on Environmental Hydraulics, Dec. 5-8, 2001, Tempe, AZ*. Online publication.
(<http://www.flow3d.com/pdfs/paper2.pdf>).
- Brothwell, D.R., Pollard, A.M. (eds.) 2001. *Handbook of Archaeological Sciences*. John Wiley and Sons: Chichester.
- Brown, Ch. 2000. Terminology and Procedures for Evaluation of Surface Textures using Fractal Geometry. Preprint.
(<http://www.wpi.edu/Academics/Depts/ME/MFE/SurfMet/asmeb46.pdf>)
- Burenhult, G. (ed.) 2001. *Proceedings of the 28th CAA conference held at Visby, Gotland, Sweden, 25-29 April 2001* (BAR International Series 1016). Archaeopress: Oxford.
- Campana, S. 2002. Ikonos-2 multispectral satellite imagery to the study of archaeological landscapes: An integrated multi-sensor approach in combination with “traditional” methods. Preprint.
(<http://arceologiamedievale.unisi.it/NewPages/Testi/campana03.rtf>)
- Carlotto, M.J. 1988. Digital imagery analysis of unusual Martian surface features. *Applied Optics* **27**: 1926-1933.
- Carlotto, M.J. 1993. Digital image analysis of possible extraterrestrial artifacts on Mars. *Digital Signal Processing* **3**: 139-144.
- Carlotto, M.J., Stein, M.C. 1990. A Method for searching for artificial objects on planetary surfaces. *Journal of the British Interplanetary Society* **43**: 209-216.
- Chaitin, G.J. 1995/1996. A New Version of Algorithmic Information Theory. *Complexity* **1/4**: 55-59.
- Chen, C.H. (ed.) 1999. *Information Processing for Remote Sensing*. World Scientific: New Jersey.

- Christopherson, G.L. and Guertin, D.P. 1995. Soil Erosion, Agricultural Intensification, and Iron Age Settlement in the Region of Tall al-'Umayri, Jordan. Paper presented at the Annual Meeting of the American Schools of Oriental Research, Philadelphia, November, 1995. (online publication) (http://www.casa.arizona.edu/MPP/Um_erosion/erosion_pap.html)
- Clarke, K.C. 1987. Scale-based simulation of terrain. *Proceedings of the 8th International Symposium on Computer-Assisted Cartography, Baltimore, MD*: 680-688.
- Conyers, L.B., Cameron, C.M. 1998. Ground-penetrating Radar techniques and three-dimensional computer mapping in the American southwest. *Journal of Field Archaeology* **25**: 417-430.
- Crater, H.B. 2002. Review of "Symmetry and Geometry of the Face on Mars Revealed" by Mark Carlotto. *New Frontiers in Science* **1.1**: b. Online publication. (<http://www.newfrontiersinscience.com/Members/v01n01/b/NFS0101b.shtml>)
- Cremers, A.B., Greve, K. (eds.) 2000. *Computer Science for Environmental Protection '00. Environmental Information for Planning, Politics and the Public* (Umweltinformatik aktuell, Band 26). Metropolis: Marburg. (<http://enviroinfo.isep.at/Umweltinformatik2000.htm>)
- Davidson, D.A., Shackley, M.L. (eds.) 1976. *Geoarchaeology*. Duckworth: London.
- Delougaz, P. 1940. *The Temple Oval at Khafajah* (The University of Chicago Oriental Institute Publications 53). University of Chicago Press: Chicago.
- Delougaz, P., Hill, H.D., Lloyd, S. 1967. *Private houses and graves in the Diyala region* (The University of Chicago Oriental Institute Publications 88). University of Chicago Press: Chicago.
- Dorner, J. 1981. Die Absteckung und astronomische Orientierung ägyptischer Pyramiden. PhD thesis, University of Innsbruck (cited in Spence 2000).
- Eichler, S., Haas, V., Steudler, D., Wäfler, M., Warburton, D. 1985. *Tall al-Hamidiya 1. Vorbericht 1984* (OBO Series Archaeologica). Presses Universitaires de Fribourg: Fribourg/Göttingen.
- Eichler, S., D., Wäfler, M., Warburton, D. (eds.) 1990. *Tall al-Hamidiya 2. Symposium 'Recent Excavations in the Upper Khabur Region', Berne, December 9-11, 1986, and Vorbericht 1985-1987*. (OBO Series Archaeologica). Presses Universitaires de Fribourg: Fribourg/Göttingen.
- Evans, K.G., Loch, R.J., Aspinall, T.O., Bell, L.C. 1992. Spoil erosion prediction - How far have we advanced? *Proceedings of 3rd Large Open Pit Conference, August 1992, Mackay*: 201-206.
- Esteban, C. Belmonte, J.A. (eds.) 2000. *Astronomy and Cultural Diversity. Proceedings of the Oxford VI Conference on Archaeoastronomy & SEAC 99*. Museo della Ciencia y il Cosmos: Santa Cruz.
- Favis-Mortlock, D., Boardman, J., Parsons, T., Lascelles, B. 1998. Emergence and erosion: a model for rill initiation and development. *Proceedings of the 3rd International Conference on GeoComputation, Bristol, 17 - 19 September 1998*. Online publication. (<http://divcom.otago.ac.nz/SIRC/webpages/Conferences/GeoComp/GeoComp98/geocomp98.htm>)
- Gaspar, P. and Menz, G. 1999. Landschaftsmaße zur Bestimmung der räumlichen Strukturen in klassifizierten Satellitenbildern. *Publikationen der Deutschen Gesellschaft für Photogrammetrie und Fernerkundung* **7**: 333-340.
- Gerber, M. 2000a. A Common Source for the Late Babylonian Chronicles Dealing with the 8th and 7th Centuries. *Journal of the American Oriental Society* **120**: 553-569.

- Gerber, M. 2000b. Report on the first CPSR-field test 1999/2000 (Complexity-based Predictive Site Reconstruction). Technical Report, Institute of Ancient Near Eastern Archaeology and Languages, University of Berne.
- Gerber, M. 2000c. The Babylonian Civil Calendar 731-626 B.C. Evidence for Pre-'Metonic' Periodic Intercalation Patterns. *In: Esteban and Belmonte 2000*: 244-248.
- Gerber, M. 2001. Predictive Site Reconstruction based on Algorithmic Complexity: CR-Signatures of Partly Destroyed Mudbrick Buildings. Technical Report, Institute of Ancient Near Eastern Archaeology and Languages, University of Berne.
- Gerber, M. 2002. 3D long range Laser scanning. *Unipress* **115**: 31.
- Goodchild, M.F., Mark, D.M. 1987. The fractal nature of geographic phenomena. *Annals of the Association of American Geographers* **77**: 265-278.
- Gray, A.G., Moore, A. 2002. *Nonparametric Density Estimation: Toward Computational Tractability*, Preprint (submitted).
- Gray, A.G., Moore, A. 2003. Rapid Evaluation of Multiple Density Models. *In: Bishop and Frey 2003*. Preprint online.
(<http://research.microsoft.com/conferences/aistats2003/proceedings/180.pdf>) .
- Gurzadyan, V.G. 1999. Kolmogorov Complexity, Cosmic Microwave Background Maps and the Curvature of the Universe. *Europhysics Letters* **46**: 114-117.
(<http://xxx.sissa.it/abs/astro-ph/9902133>)
- Haff, P.K. 2001. Waterbots. Online publication.
(http://www.duke.edu/~7Ehaff/geomorph_abs/waterbot%20paper/waterbot%20paper.pdf)
- Haita, C. 2001. Soils and sediments: report for the 2000 field season. *In: Bailey et al. 2000*: 81-98.
- Hall, P., Kang, K.-H. 2002. Bandwidth choice in non-parametric classification. Abstract:
(<http://www.math.ucsd.edu/~politis/contributed.html>)
- Harmon, R.S., Doe, W.W. (eds.) 2001. *Landscape Erosion and Evolution Modeling*. Kluwer: Dordrecht.
- Heinrich, E. 1982. *Tempel und Heiligtümer im Alten Mesopotamien. Typologie, Morphologie und Geschichte* (Denkmäler Antiker Architektur 14). Deutsches Archäologisches Institut: Berlin.
- Heinrich, E. 1984. *Paläste im Alten Mesopotamien* (Denkmäler Antiker Architektur 15). Deutsches Archäologisches Institut: Berlin.
- Hemaspaandra, L. A., Ogihara, M. 2002. *The Complexity Theory Companion* (Series: Texts in Theoretical Computer Science). Springer: New York.
- Heyden, A. (ed.) 2002. *Computer Vision ECCV* (Lecture Notes in Computer Science 2351). Springer: Berlin.
- Hoffmann, V. 2002. Messbilder. Ein Laserscanner im Dienste der Bauforschung. *Unipress* **115**: 27-30.
- Hugus, M.K., Mark, D.M. 1985. Digital simulation of erosion: A model based on geomorphic processes. *Proceedings of the Annual Pittsburgh Conference on Modeling and Simulation* **16**: 305-309.

- Istanbulluoglu, E., Tarboton, D.G., Pack, R.T. 2002. A probabilistic approach for channel initiation. Forthcoming in *Water Resources Research*.
- Istanbulluoglu, E., Tarboton, D.G., Pack, R.T. 2003. A Sediment Transport Model for Incising Gullies On Steep Topography. Online paper.
(http://moose.cee.usu.edu/dtarb/Erkan_agufall_01.ppt)
- Jaeger, H.M., Nagel, S.R. 1992. Physics of the Granular State. *Science* **255**: 1523.
- Kazhdan, M., Chazelle, B., Dobkin, D., Finkelstein, A., Funkhouser, T. A Reflective Symmetry Descriptor. *In: Heyden 2002*: 642–656.
- Kearns, M.J., Vazirani, U.V. 1994. *Introduction to Computational Learning Theory*. MIT Press: Boston.
- Kienholz, H., Erismann, T., Fiebiger, G., Mani, P. 1993. Naturgefahren: Prozesse, Kartographische Darstellung und Maßnahmen. *Tagungsbericht zum 48. Deutschen Geographentag, Basel*: 293 - 312.
- Kirkby, M.J. 1971. Hillslope process-response models based on the continuity equation. *Institute of British Geographers Special Publications* **3**: 15-30
- Kirkby, M.J. 1986. A two-dimensional simulation model for slope and stream evolution. *In: Abrahams 1986*: 203-222.
- Kirkby, M.J. 1990. The landscape viewed through models. *Zeitschrift fur Geomorphologie, Supplementband* **79**: 63-81.
- Kirkby, A., Kirkby, M.J. 1976. Geomorphic processes and the surface survey of archaeological sites in semi-arid areas. *In: Davidson and Shackley 1976*: 229-253.
- Koch, H.v. 1906. Une méthode géométrique élémentaire pour l'étude de certaines questions de la théorie des courbes planes. *Acta Mathematica*. **30**: 145-174.
- Krummel, J.R., Gardner, R.H., Sugihara, G., O'Neill, R.V., Colemann, P.R. 1987. Landscape patterns in a distributed environment. *Oikos* **48**: 321-324.
- Kube, P., Pentland, A. 1988. On the imaging of fractal surfaces. *IEEE Transactions on Pattern Analysis and Machine Intelligence* **10**: 704-707.
- Langer, D., Mettenleiter, M., Härtl, F., Fröhlich, C. 2000. Imaging Laser Scanners for 3-D Modeling and Surveying Applications. *Proceedings of the 2000 IEEE International Conference on Robotics & Automation*: 116-121.
- Lapointe, R., Mercier, D. 2000. Laser scanning applied to archaeological heritage. *Innovision Internal Report*.
(<http://www.innovision3D.com>)
- Laurini, R., Thompsen, D. 1992. *Fundamentals of Geographic Information Systems* (The A.P.I.C. Series, 37). Academic Press: London.
- Leou, J., Tsai, W. 1987. Automatic rotational symmetry determination for shape analysis. *Pattern Recognition* **20**: 571–582
- Li, M., Vitáni, P. 1997. *An introduction to Kolmogorov Complexity and its applications*. Second edition. Springer: New York.

- Loehle, C. 1990. Home range: a fractal approach. *Landscape Ecology* **1**: 39-52.
- Lovejoy, S. 1982. Area-perimeter relation for rain and cloud areas. *Science* **216**: 185-187.
- Makse, H.A., Havlin, S., Stanley, H.E. 1995. Modelling Urban Growth Patterns. *Nature* **377**: 608-612.
- Mandelbrot, B.B. 1967. How long is the coast of Britain? Statistical self-similarity and fractional dimension. *Science* **156**: 636-638.
- Mandelbrot, B.B., 1977: *Fractals : form, chance and dimension*. Freeman: San Francisco
- Mandelbrot, B.B. 1982. *The fractal geometry of nature*. Freeman: San Francisco.
- Mandelbrot, B.B. and Van Ness, J. 1968. Fractional Brownian motions, fractional noises and applications. *SIAM Review* **10**: 422-437.
- Mark, D.M. 1984. Automated detection of drainage networks from digital elevation models. *Cartographica* **21**: 168-178.
- Mark, D.M., Aronson, P.B. 1984. Scale-dependent fractal dimensions of topographic surfaces: An empirical investigation, with applications in geomorphology and computer mapping. *Mathematical Geology* **16**: 671-683.
- Marola, G. 1989. On the detection of the axes of symmetry of symmetric and almost symmetric planar objects. *IEEE Transactions on Pattern Analysis and Machine Intelligence* **11**: 104-108.
- Martin, Y. 2000. Modelling hillslope evolution: linear and nonlinear transport relations. *Geomorphology* **34**: 1-21.
- Martin, Y., Church, M. 1997. Diffusion in landscape development models: on the nature of basic transport relations. *Earth Surface Processes and Landforms* **22**: 273-279.
- Matthews, W., French, C.A.I., Lawrence, T., Cutler, D.F., Jones, M.K. 1997. Microstratigraphic traces of site formation processes and human activities. *World Archaeology* **29**: 281-308.
- McFarlane, W.W., Pederson, J.L., Petersen, P.A. 2002. Testing the limits of photogrammetry to monitor erosion of archaeological sites in Grand Canyon. Abstract. (http://gsa.confex.com/gsa/2002AM/finalprogram/session_3008.htm)
- McGarigal, K., Marks, B.G. 1995. FRAGSTATS: spatial pattern analysis program for quantifying landscape structure. *USDA Forest Service General Technical Report PNW-351*. U.S. Department of Agriculture, Forest Service, Pacific Northwest Research Station, Portland.
- McGunnigle, G., Chantler, M.J. 2001. Evaluating Kube and Pentland's fractal imaging model. *IEEE Transactions on Image Processing* **10**: 534-542.
- Michael Bessey, K. 2002. *Structure and Dynamics in an Urban Landscape: Toward a Multi-Scaled View*. Technical report. Graduate School of Design, Harvard University, Cambridge, MA.
- Milne, B.T. 1988. Measuring the fractal geometry of landscapes. *Applied Mathematics and Computation* **27**: 67-79.
- Mills, B.I., Langbein, F.C., Marshall, A.D., Martin, R.R. 2001. Approximate Symmetry Detection for Reverse Engineering. In: Anderson and Lee (2001): 241-248. (<http://cyl.cs.cf.ac.uk/research/BoRG/SM01-009.pdf>)

- Mitasova, H., Hofierka, J., Zlocha, M., Iverson, R.L. 1996. Modeling topographic potential for erosion and deposition using GIS. *International Journal of Geographical Information Science* **10**: 629-641.
- Mitsumoto, H., Tamura, S., Okazaki, K., Kajimi, N., Fukui, Y. 1992. Reconstruction using mirror images based on a plane symmetry recovery method. *IEEE Transactions on Pattern Analysis and Machine Intelligence* **14**: 941-946.
- Möller, L.E., Kuhlmann, K.R., Marshall, R., Towner, M.C. 2002. The Snoopy Angle of Repose Experiment. Calibration of an instrument to determine the angle of repose of Martian dust. *Proceedings of the 33rd Lunar and Planetary Science Conference, NASA Johnson Space Center, Houston, Texas, 11-15 March 2002*. (online publication) (<http://www.lpi.usra.edu/meetings/lpsc2002/pdf/2015.pdf>)
- Nance, J.D. 1983. Regional sampling in archaeological survey. The statistical perspective. *Advances in Archaeological Method and Theory* **6**: 289-356.
- Oates, D., Oates, J., McDonald, H. 1998. Excavations at Tell Brak - Vol. 1: The Mitanni and Old Babylonian periods. McDonald Institute for Archaeological Research: Cambridge.
- Ockman, J. (ed.) 1993. *Architecture culture 1943-1968. A documentary anthology*. Columbia Books: New York.
- O'Neill, R.V., Krummel, J.R., Gardner, R.H., Sugihara, G., Jackson, B., DeAngelis, D.L., Milne, B.T., Turner, M.G., Zygmunt, B., Christensen, S.W., Dale, V.H., Graham, R.L. 1988. Indices of landscape pattern. *Landscape Ecology* **2**: 63-69.
- Pavlidis, L., Fraser, C.S., Ogleby, C. 2001. The application of high-resolution satellite imagery for the detection of ancient Minoan features on Crete. *In: Burenhult 2001*: 393-400.
- Pelletier, J.D. 2002. *Why is topography fractal?* Preprint. (<http://www.gps.caltech.edu/~jon/topography.ps>)
- Petersen, P.A., Pederson, J.L., McFarlane, W.W. 2002. Gully erosion of archaeological sites in Grand Canyon - photogrammetry and GIS used in geomorphic studies. Abstract. (http://gsa.confex.com/gsa/2002AM/finalprogram/session_3008.htm)
- Pierce, J. R. 1980. *An Introduction to Information Theory: Symbols, Signals and Noise*. Dover Publications: New York.
- Rami, M. 1997. Landschaftsstrukturmaße und Satellitenfernerkundung. Entwicklung des Programms METRICS und seine Anwendung auf Landsat und NOAA-Szenen aus dem Bereich Schwarzwald/Oberrhein. *Unpublished thesis*, Institute of Geography, University of Bonn. (cited in Gasper and Menz 1999)
- Riitters, K.H., O'Neill, R.V., Hunsaker, C.T., Wickham, J.D., Yankee, D.H., Timmins, S.P., Jones, K.B., Jackson, B.L. 1995. A factor analysis of landscape pattern and structure metrics. *Landscape Ecology* **10**: 23-39.
- Ritter, D.F., Kochel, R.C., and Miller, J.R. 1995. *Process Geomorphology*. C. Brown Publishers: Dubuque.
- Rogers, J. (ed.) 2002. *Complexity Abstracts 2002. Vol XII*. Abstract booklet for the 2002 IEEE Conference on Computational Complexity, Montreal. Online publication. (<http://facweb.cs.depaul.edu/jrogers/complexity/Abstracts/2002.pdf>)

- Ross, G., Levine, M.D. 1993. Extracting geometric primitives. *CVGIP: Image Understanding* **58**: 1-22.
- Russ, J. 1994. *Fractal surfaces*. Plenum Press: New York.
- Safar, F., Mustafa, M.A., Lloyd, S. 1981. *Eridu*. Organization of Antiquities and Heritage: Baghdad.
- Safdie, M. 1984. Collective Significance. *Harvard Architecture Review* **4**: 87-97.
- Sawyer, T. 2002. Lasers go into overdrive, pushed by technology gains. *Engineering News Report* (16 September 2002): 54-56.
- Schmid, J.G. 1980. *Die Madrasa des Kalifen al-Mustansir und der sog. Palast in der Zitadele in Baghdad* (Baghdader Forschungen 3). Philipp von Zabern: Mainz.
- Schmid, J.G. 1995. *Der Tempelturm Etemenanki in Babylon* (Baghdader Forschungen 17). Philipp von Zabern: Mainz.
- Schweitzer, F. (ed.) 1997. *Self-organization of complex structures: From individual to collective dynamics*. Gordon and Breach: London.
- Sheather, S.J., Jones, M.C. 1991. A reliable data-based bandwidth selection method for kernel density estimation. *Journal of the Royal Statistical Society* **B**: 683-690.
- Shennan, S. 1997. *Quantifying Archaeology*. Edinburgh University Press: Edinburgh.
- Shiner, J.S. 1997. Self-organisation, entropy and order in growing systems. *In: Schweitzer 1997*: 21-36.
- Silverman, B.W. 1986. *Density estimation for statistics and data analysis* (Monographs on Statistics and Applied Probability 26). Chapman and Hall: London
- Spence, K. 2000. Ancient Egyptian chronology and the astronomical orientation of pyramids. *Nature* **408**: 320-324.
- Stein, M.C. 1987. Fractal image models and object detection. *Society of Photo-optical Instrumentation Engineers* **845**: 293-300.
- Stuedler, D. 1985. Eine archäologische Vermessung in Syrien. *Mensuration, Photogrammétrie, Génie rural* **8/85**: 259-262.
- Sugihara, G. and May, R.M. 1990. Applications of fractals in ecology. *TREE* **3**: 76-86.
- Tetik, S., Wymann, D. 1997. Shape Indexing. Unpublished term paper in image analysis, supervised by H. Bunke und X. Jiang, Institute of Computer Science and Applied Mathematics, University of Berne.
(To be made available as a technical report soon; <http://www.iam.unibe.ch>)
- Trigger, B. 1990. Monumental architecture: A thermodynamic explanation of symbolic behaviour. *World Archaeology* **22**: 119-132.
- Tucker, G.E., Gasparini, N.M., Lancaster, S.T., Bras, R.L. 1997. An integrated hillslope and channel evolution model as an investigation and prediction tool. *Technical report DACA88-95-R-0020*, Dept. of Civil Engineering, MIT, Cambridge, MA.

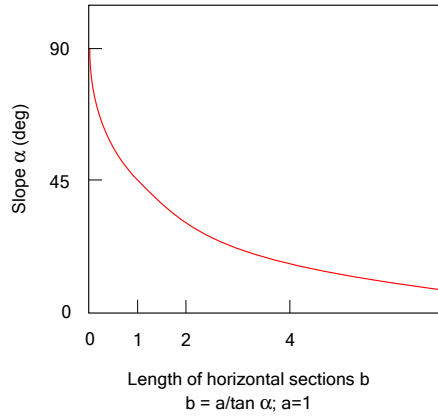
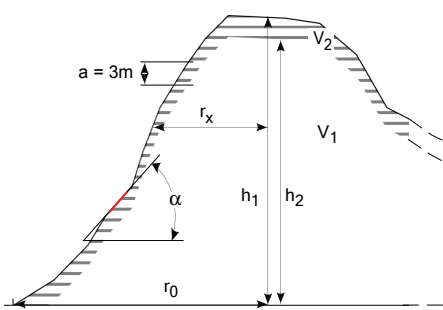
- Tucker, G.E., Lancaster, S.T., Gasparini, N.M., Bras, R.L. 2001. The Channel-Hillslope Integrated Landscape Development (CHILD) Model. *In: Harmon and Doe 2001*: 349-388.
- Turcotte, D. 1997. *Fractals and Chaos in Geology and Geophysics*. Cambridge University Press: Cambridge, New York.
- Turner, M.G., Gardner, R.H. (eds.) 1991. *Quantitative methods in landscape ecology*. Springer: New York.
- Wäfler, M. 2001. *Zur historischen Geographie von Idamaras zur Zeit der Archive von Mari und Shubat-enlil/Shehna. Mit Beiträgen von Jimmy Brignoni und Henning Paul* (OBO Series Archaeologica). Presses Universitaires de Fribourg: Fribourg/Göttingen.
- Wäfler, M., Hanhart, C. 1999. Tall al-Hamidiya. Final Report 1999. *Chroniques des Fouilles en Syrie 1999*.
- Wäfler, M., Gerber, M., Hanhart, C. 2000. Tall al-Hamidiya. Final Report 2000. *Chroniques des Fouilles en Syrie 2000*.
- Wäfler, M., Gerber, M., Kälin, O. 2001. Tall al-Hamidiya. Final Report 2001. *Chroniques des Fouilles en Syrie 2001*.
- Wainwright, J. 1992. Assessing the impact of erosion on semi-arid archaeological sites. *In: Bell and Boardman 1992*: 227-241.
- Wainwright, J. 1994. Erosion of archaeological sites: Results and implications of a site simulation model. *Geoarchaeology* **9**: 173-201.
- Washburn, D., Crowe, D. 1988. *Symmetries of Culture: Theory and Practice of Plane Pattern Analysis*. University of Washington Press: Washington, D.C.
- Weidlich, W. 1997. From fast to slow processes in the evolution of urban and regional settlement structures. *In: Schweitzer 1997*: 475-488.
- Westcott, K. and Brandon, R. 1999. *Practical applications of GIS in archaeology - A Predictive Modelling Toolkit*. Taylor and Francis: New York.
- West, D.B. 2001. *Introduction to Graph Theory*. Second edition. Prentice Hall: USA.
- Weyl, H. 1989. *Symmetry*. Princeton University Press: Princeton.
- Wheatley, D., Gillings, M. 2002. *Spatial technology and archaeology. The archaeological applications of GIS*. Taylor and Francis: London.
- Wilkinson, T. 2001. Surface collection techniques in field archaeology: theory and practice. *In: Brothwell and Pollard 2001*: 529-541.
- Young, A. 1961. Characteristic and limiting slope angles. *Zeitschrift für Geomorphologie* **5**: 126-131.
- Zabrodsky, H., Peleg, S., Avnir, D. 1995. Symmetry as a continuous feature. *IEEE Transactions on Pattern Analysis and Machine Intelligence* **17**: 1154-1166.
- Zhang, W., Montgomery, D.R. 1994: Digital elevation model grid size, landscape representation, and hydrologic simulations. *Water Resources Research* **30**: 1019-1028.

Fig. 1: Penetration Depth of Surface Sensors vs. Mound Volume

A: Dependence of b on local slope α

$a_{\max} = 3\text{m}$ (GPR)

— Length of horizontal sections (b) at uniform penetration depth (a)



B: Percentage of mound volume covered by sensor

Semi-ellipsoid mound ($h_1 \ll r_0$)

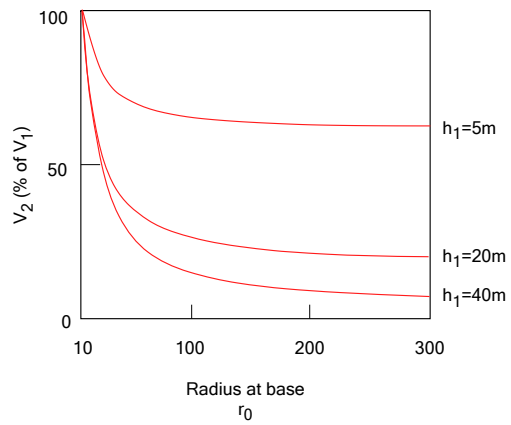
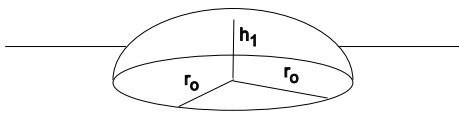


Fig. 2: Tall al-Hamidiya

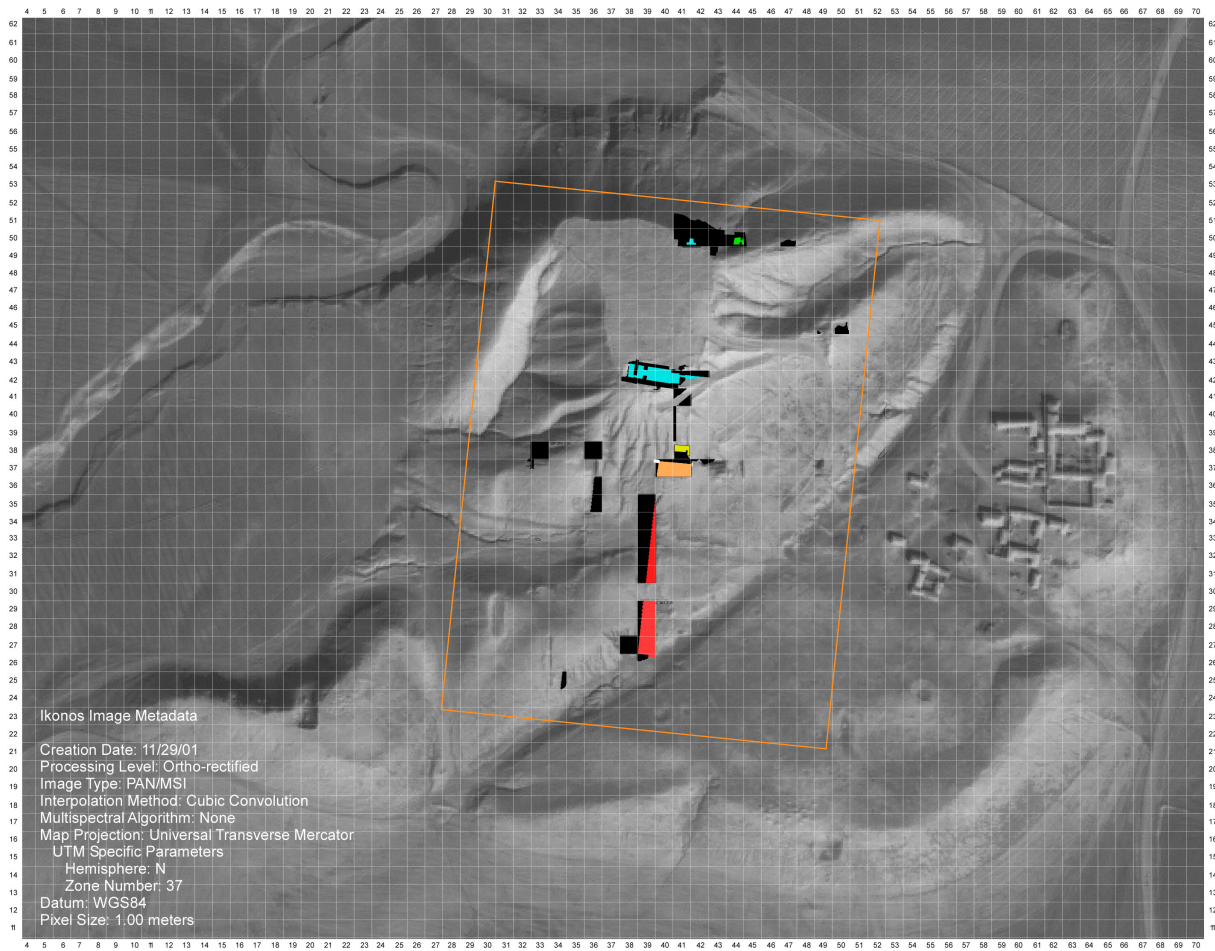
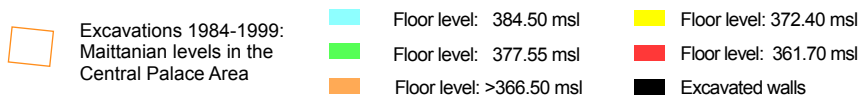
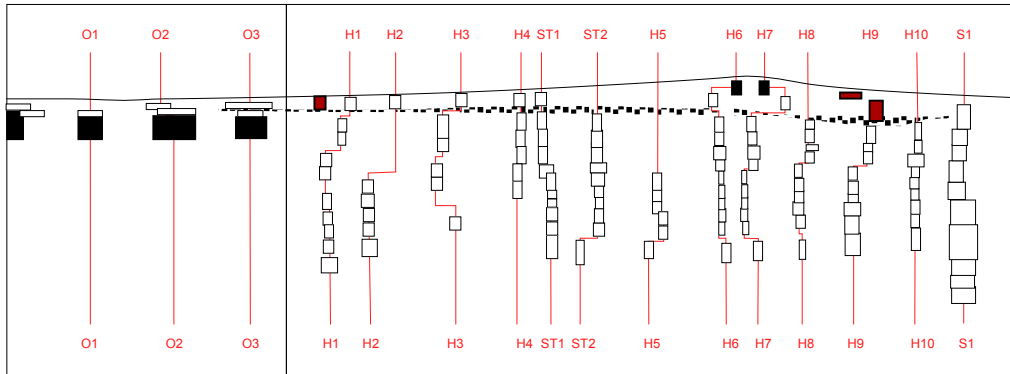


Fig. 3: Schematic Sections Khafajah

■ Isolated
— Sequence



Section 8; 12-12'
(OIP 53: Plate VIII)

Cross section through Houses (H), Small Temple (ST) and Sin Temple (S)
(OIP 53: Plate XII)

Fig. 4: Expected Cross-over Scales in the Presence of Eroded Monumental Buildings

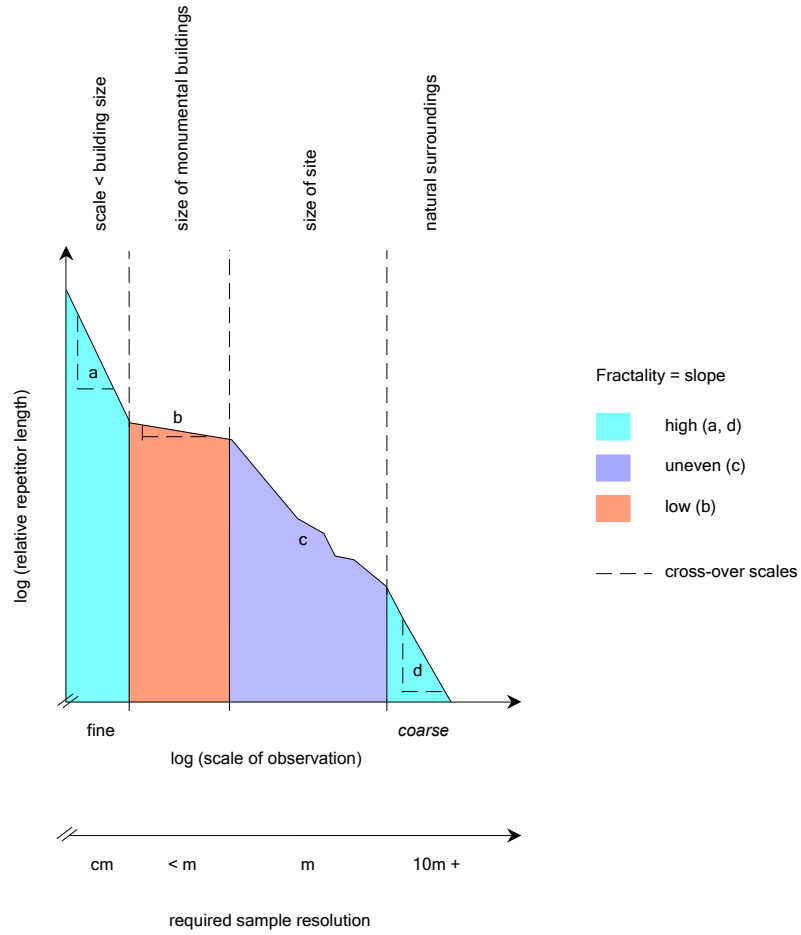
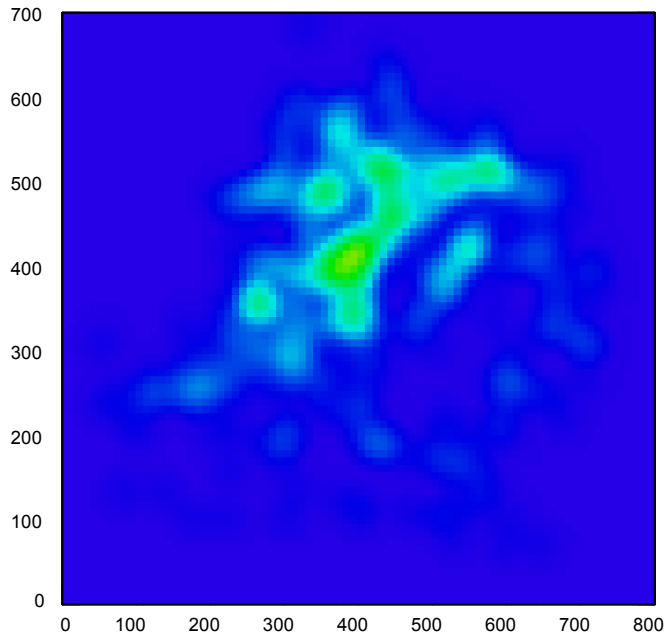
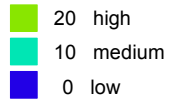


Fig. 5: Local Measurement Density

A: Kernel density; $t=0.25$



B: Survey Data 1984

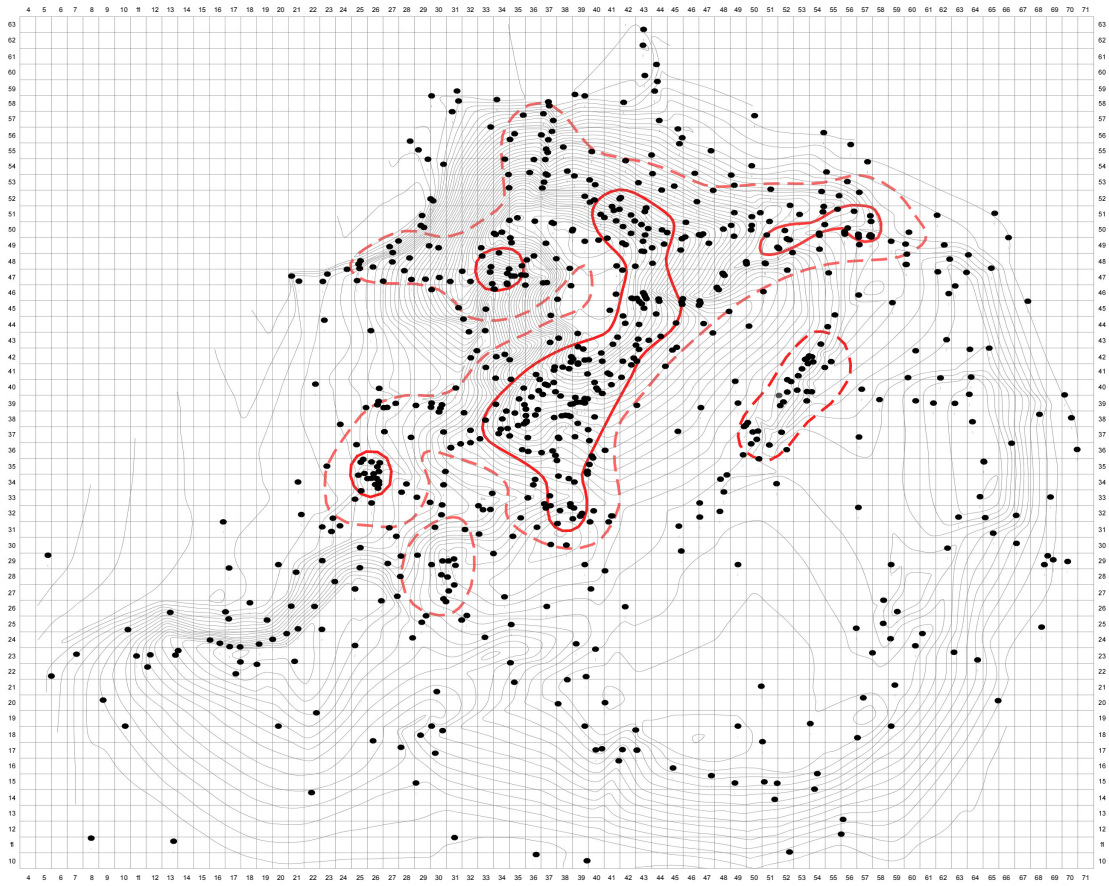



Fig. 6: The von Koch Curve

N: Number of linear segments

r: scaling factor

$d = \log N / \log (1/r)$

 Repetitor pattern: $N = 4$, $r = 1/3$

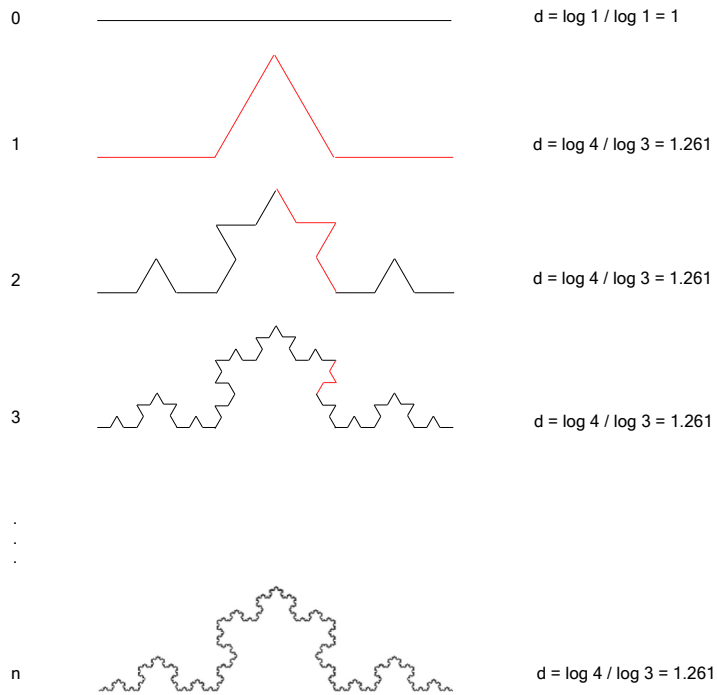
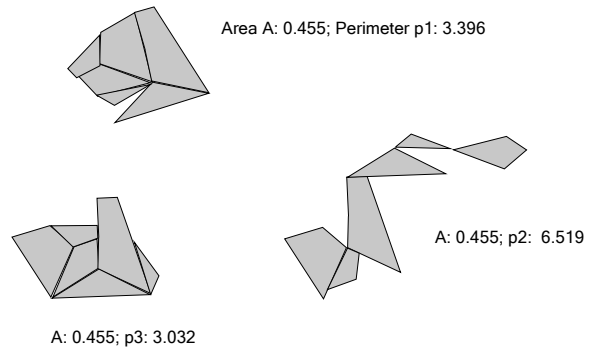


Fig.7: Scale-independent Shape Indexing



$$B = \text{SQR}(A)/p$$

B(1) = 0.198:
B(2) = 0.069
B(3) = 0.223

Fig. 8: Hierarchical Structuring of Talls by Merged Contours (Watersheds)

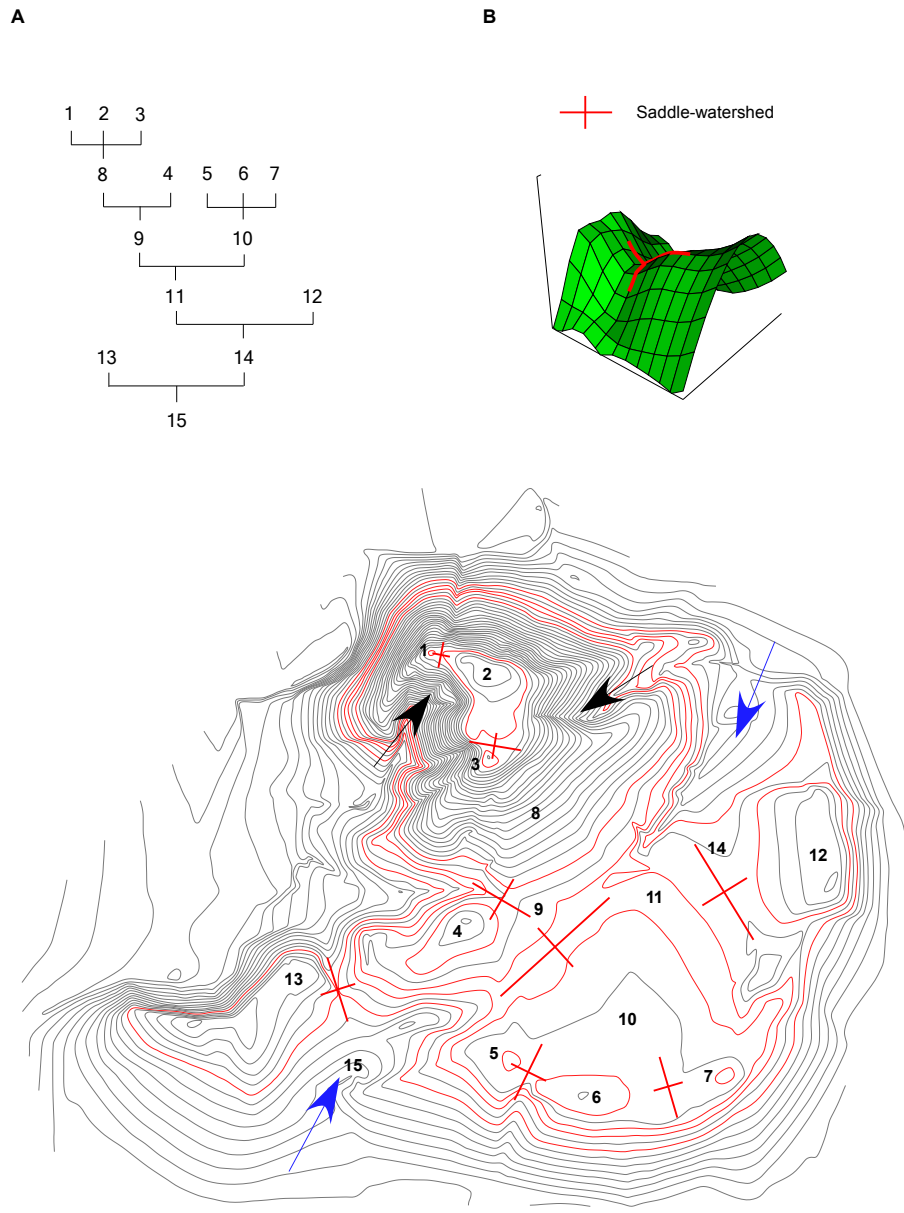
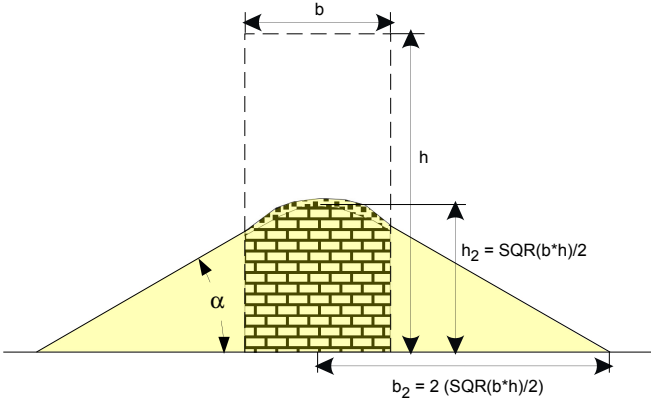


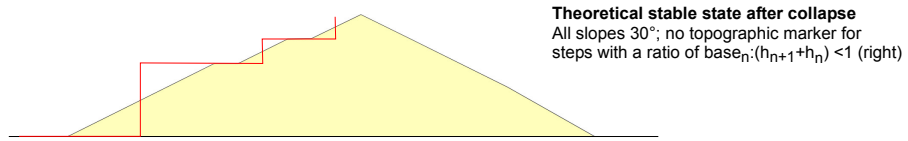
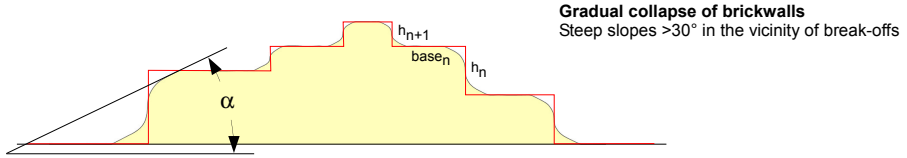
Fig. 10: Wall Collapse



α = angle of repose: ca. 30°

Fig. 11: Collapse of Complex Mudbrick Structures

A: Ignoring stability threshold



B: Taking account of stability threshold

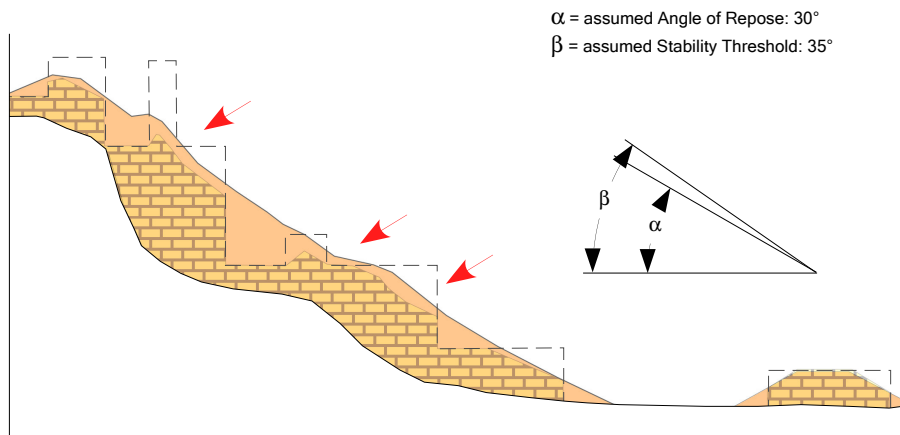


Fig. 12: Slope Development

A. Simple Initial Shape

D = constant (Diffusivity)

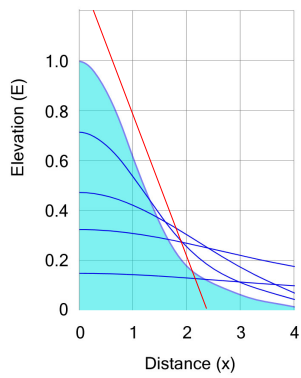
t = {0, 1..n}

$$E = \{A/\text{SQR}(4\pi Dt)\} \text{EXP}\{-x^2/4Dt\}$$

A: Cross-sectional area

S: Rate of transport

Initial Shape (t=0)



B. Complex Initial Shape

D = constant (Diffusivity); $C \infty x, I \infty t$

$$E_{(C,I)} = E_{(C,I-1)} + \Delta E$$

$$\Delta E = -(D \cdot \Delta t / \Delta x^2) \{ (E_{(C,I-1)} - E_{(C-1,I-1)}) + (E_{(C,I-1)} - E_{(C+1,I-1)}) \}$$

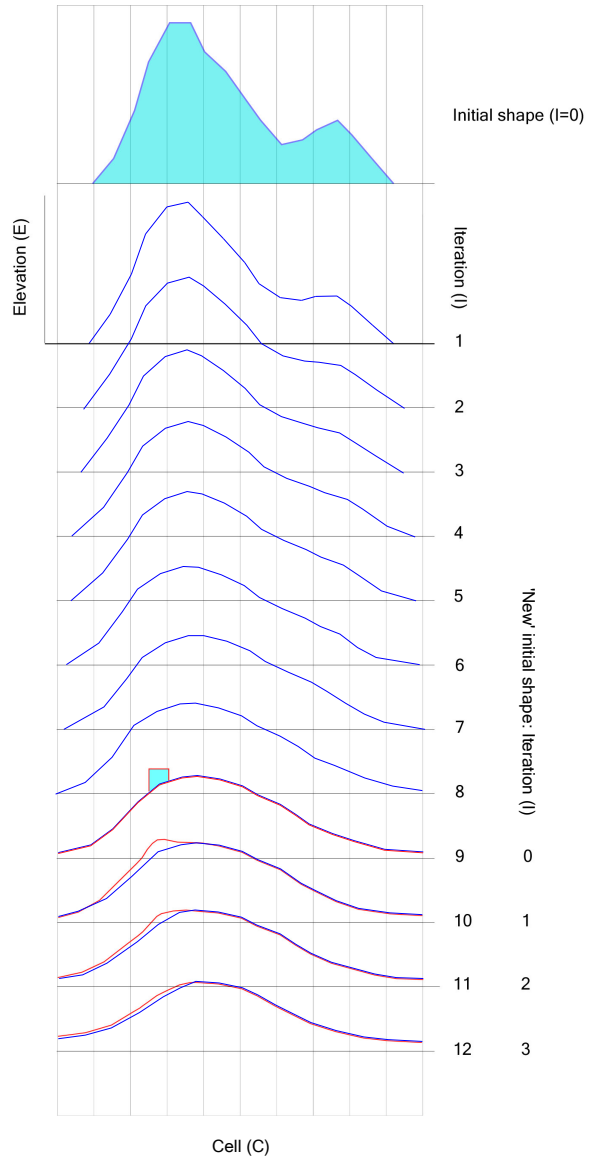
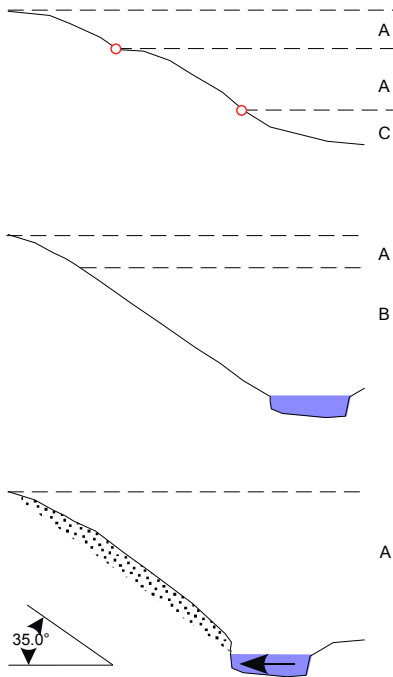


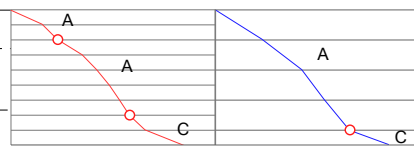
Fig. 13: Slope Profile Segments



A: Encoding Slope Profile Attributes



B: Detecting Slope Profile Attributes



C: Selective Decimation

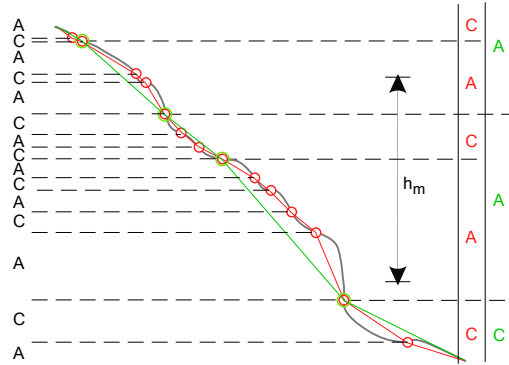
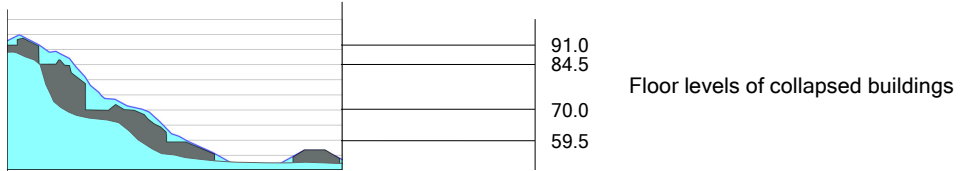


Fig. 14: Detectability and Horizontal Movement of Slope Attributes over Time

Initial State: Post-Collapse Shape



Progressive erosion of mound Attributes Detectable turning points in slope

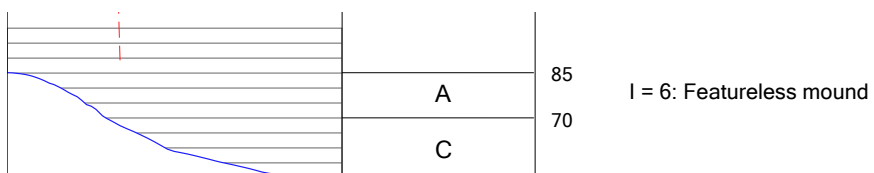
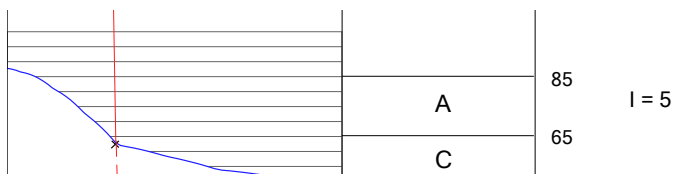
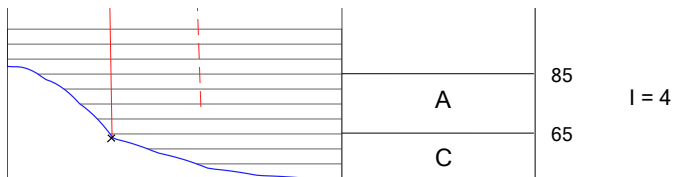
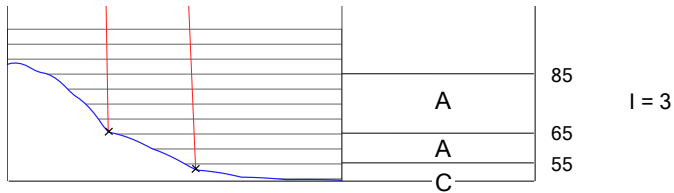
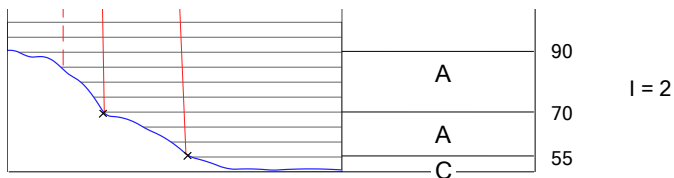
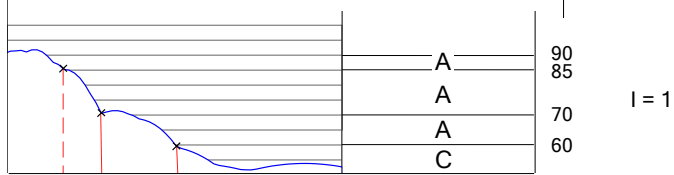


Fig. 15: Elevation Change of Slope Profile Attributes over Time

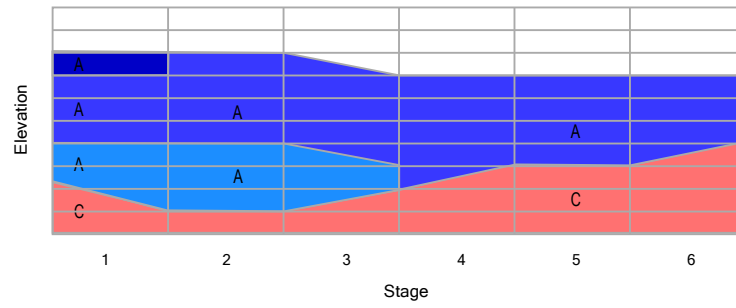
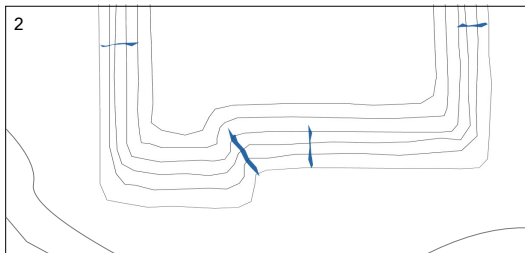
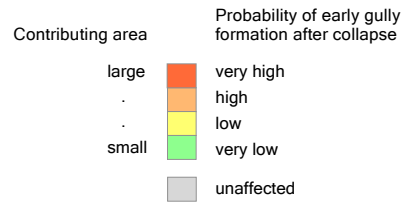
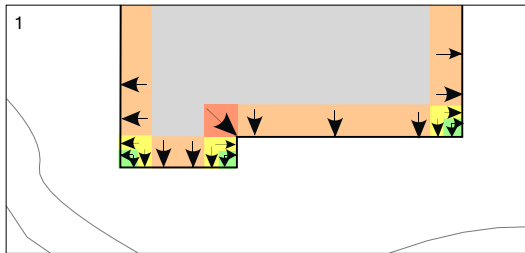
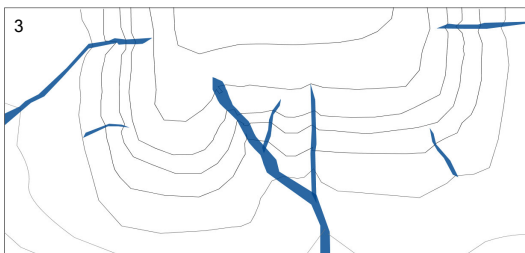


Fig. 16: Gully Formation

A



Collapsed building: Linearity and parallelity preserved. Primary gullies form on concave and straight contour segments



Formation of secondary gullies in randomly formed small local concavities

B

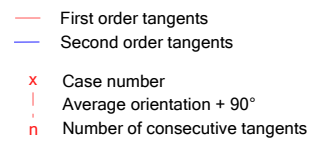
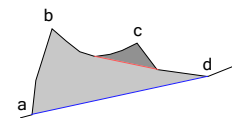
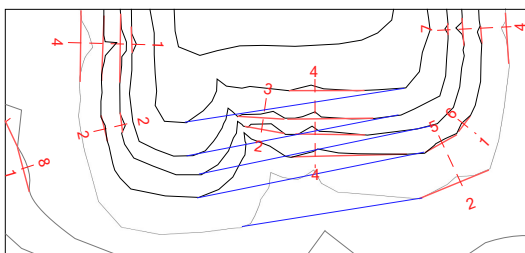


Fig. 17: Secondary Channels in Lateral Walls of Primary Channels

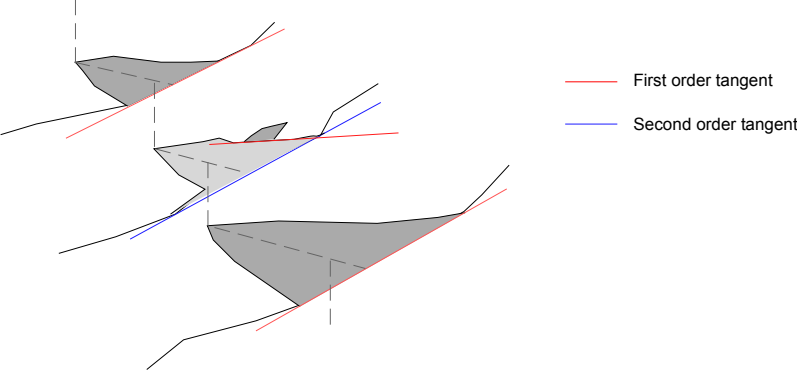
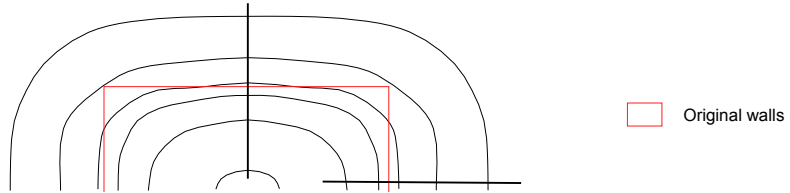
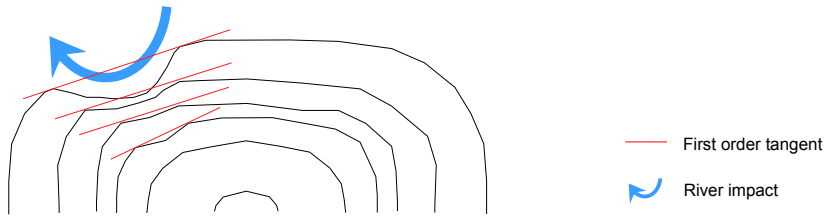


Fig. 18: Incisions by Rivers

A: No impact



B: Impact at Edge



C: Impact near Center

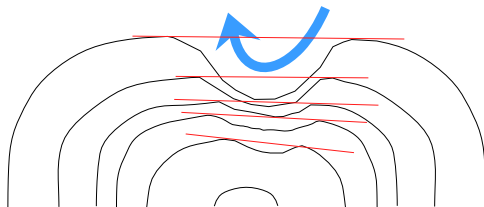
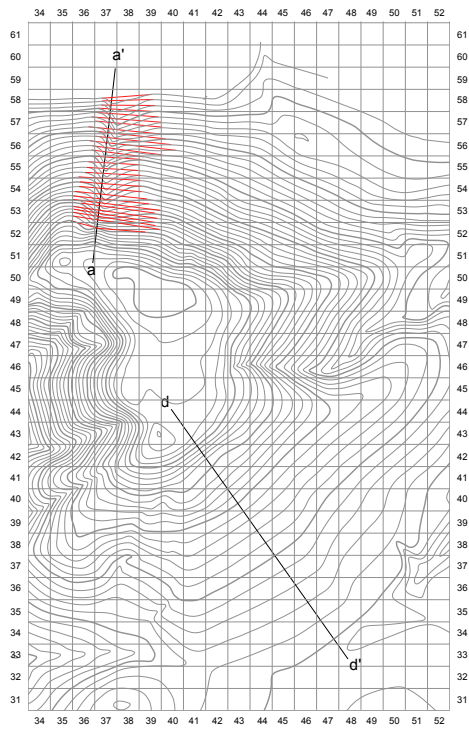
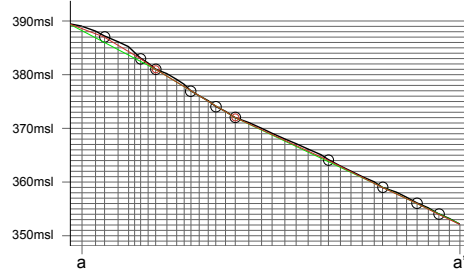


Fig. 19A: Sample Sections a-a', d-d'



Slope a-a' (North)

Measured: 1st order tangents



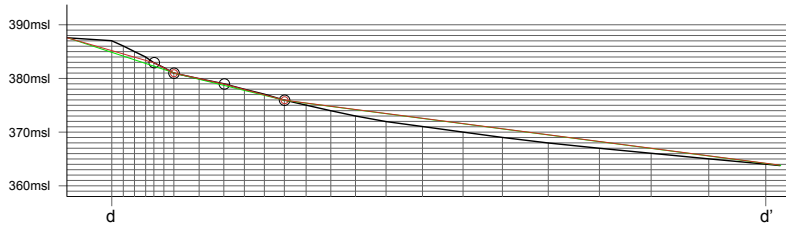
Original curve:	A	A	A	A	A	A	A	A	A	A
decimated:	A		A		A				A	
	381msl				372msl					

- Original curve with turning points; extracted from topographical map
- Level 1 decimation (curve defined by ○) and remaining turning points
- Level 2 decimation (curve defined by ○)

1st order tangents

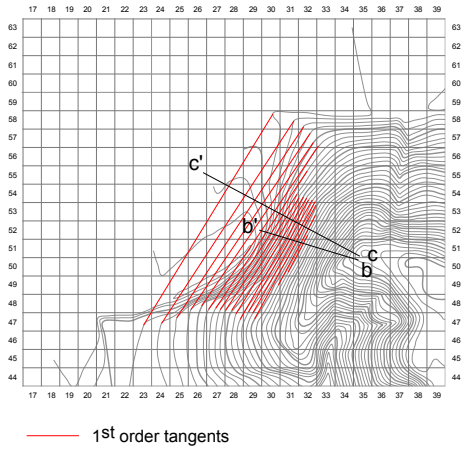
Slope d-d' (Southeast)

Measured: contours



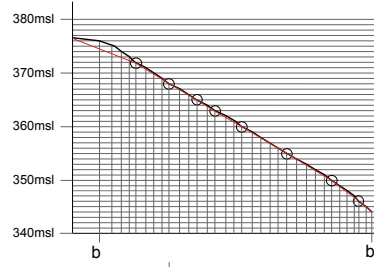
Original curve:	A	A	B	A	C
decimated:	A		A		C
	381msl			376msl	

Fig. 19B: Sample Slopes b-b', c-c'



Slope b-b' (West)

Measured: contours



Original curve:

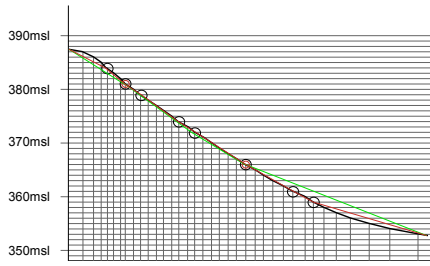
A	A	A	A	A	A	A	A	A
---	---	---	---	---	---	---	---	---

decimated:

A								
---	--	--	--	--	--	--	--	--

Slope c-c' (West)

Measured: 1st order tangents on contours



Original curve:

A	A	A	A	A	A	B	A	C
---	---	---	---	---	---	---	---	---

decimated:

A	A				C			
---	---	--	--	--	---	--	--	--

381msl 376msl

Fig. 20: SN-Profiles 350-500

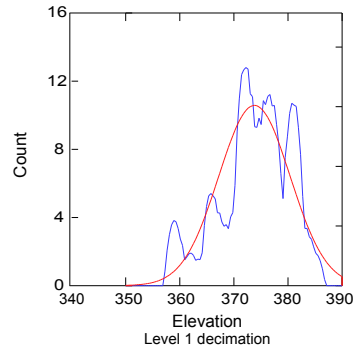
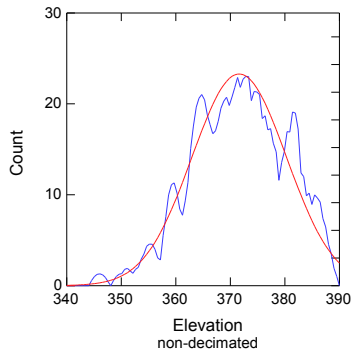
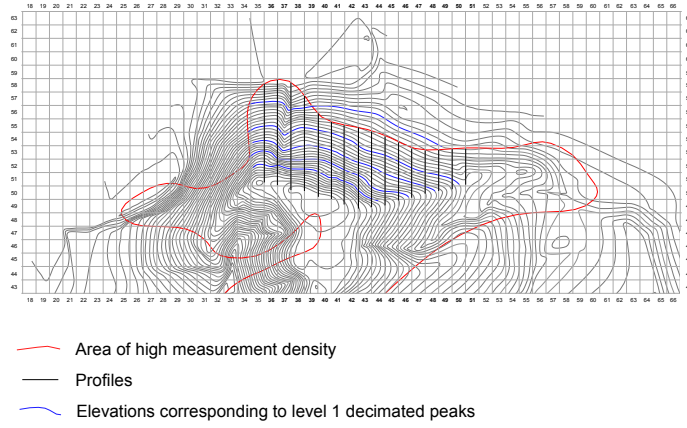
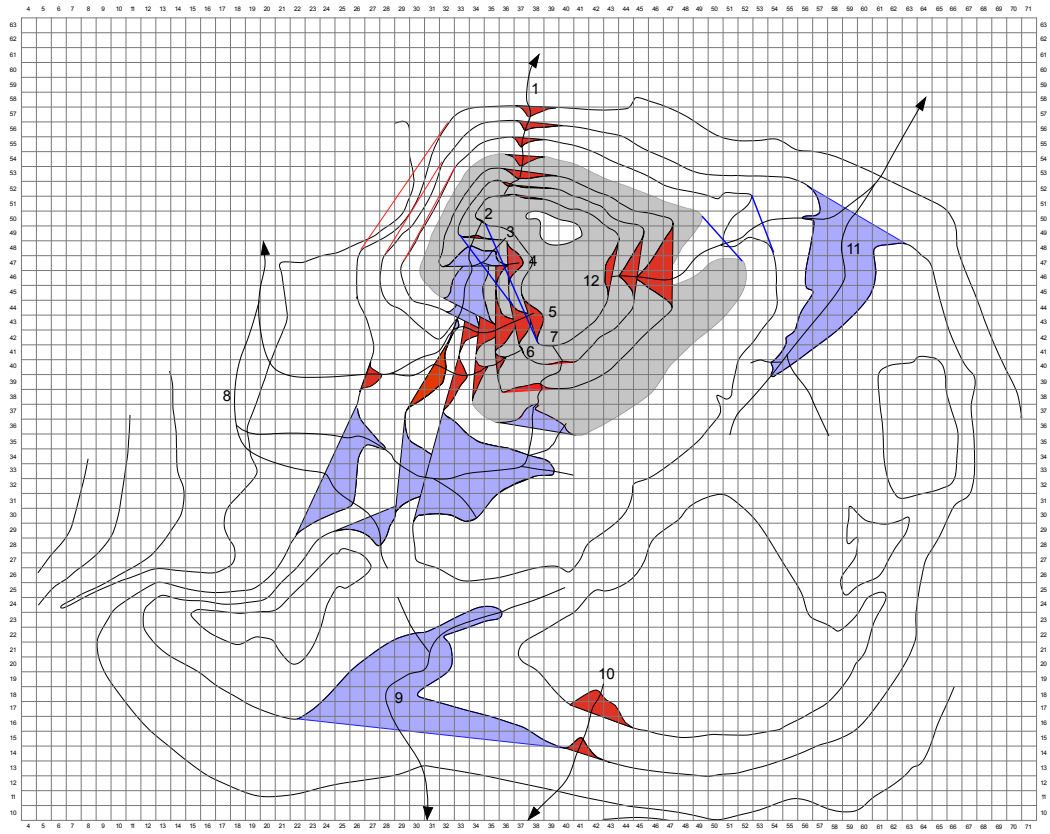


Fig. 21: 'Gully Termination'



Equidistance = 5m





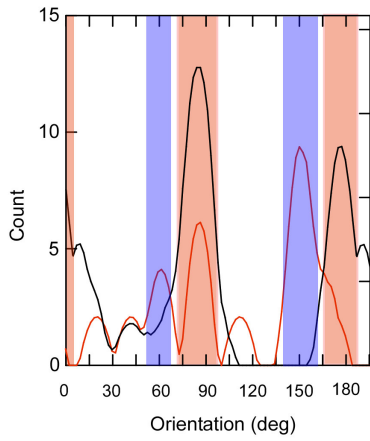
-  Drainage channel network
-  Block 8
-  1st order tangents
-  2nd order tangents; **bold** = original concavities/corners

Fig. 22: Extracted Orientations

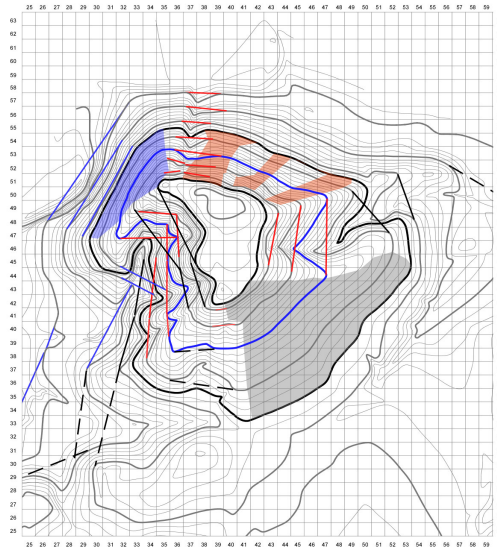
A: Kernel Density Plot, $t=0.15$
1st and 2nd order tangents
at channel and river incisions



Kernel curves: — Block 8
— Rest of window

Paired local density maxima:
■ $61^\circ/151^\circ$
■ $85^\circ/176^\circ$

B: Local Wall Orientation



👁 Block 8

Tangents at gully incisions: — group 1: $61^\circ/151^\circ \pm 7$
— group 2: $85^\circ/178^\circ \pm 7$
— no group (— - excluded)

Within areas of high linearity: ■ corresponds to group 1
■ corresponds to group 2
■ no group (mean of contours: 46.5°)

Fig. 23: Determination of Areas of High Linearity (Block 8)

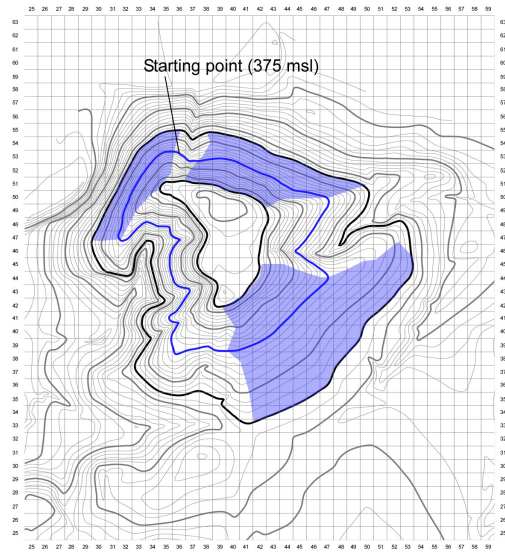
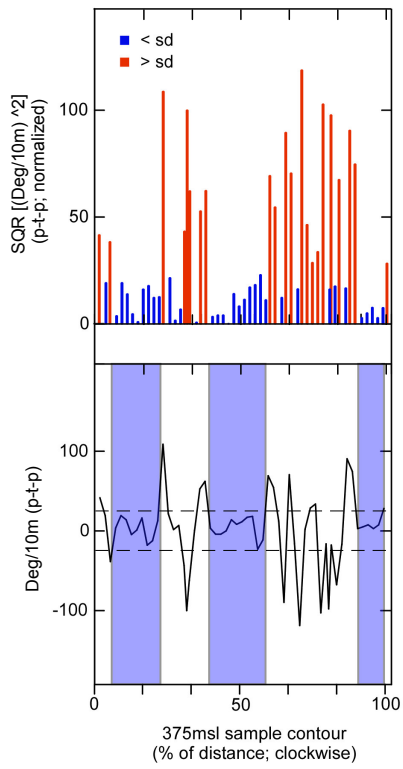


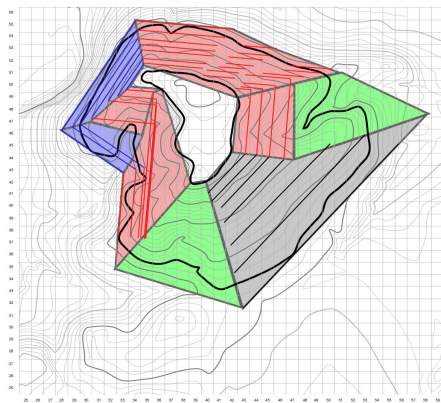
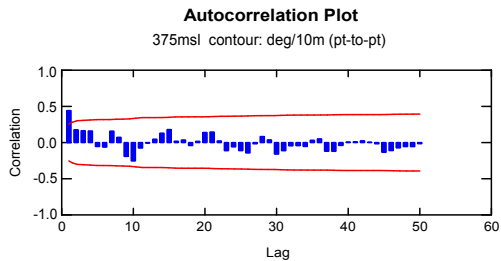
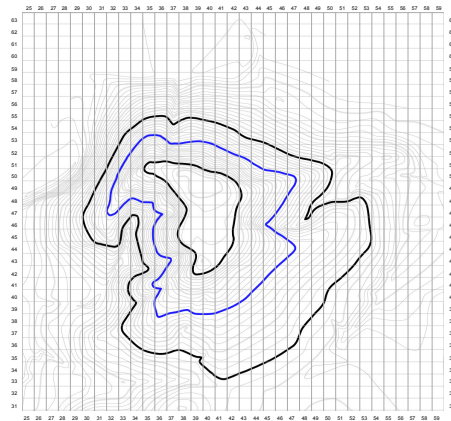
Fig. 24: Wall Orientations



⊙ Block 8

Fig. 25: Symmetry Detection by Autocorrelation

A: Distance-dependent encoding



Autocorrelation Plot

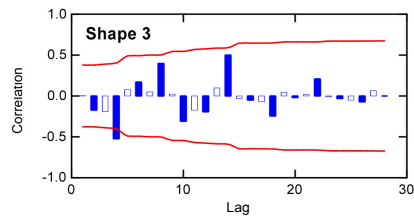
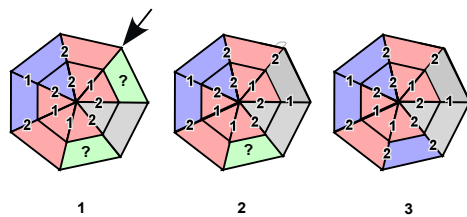
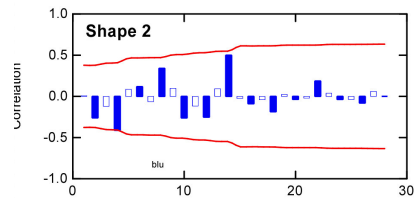
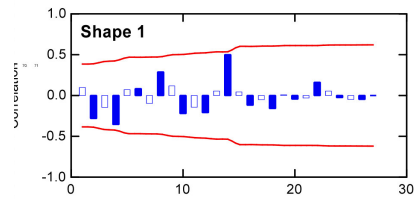


Fig. 26: Wall Orientations Predicted by Rotational Order Symmetry (Non-isometric)

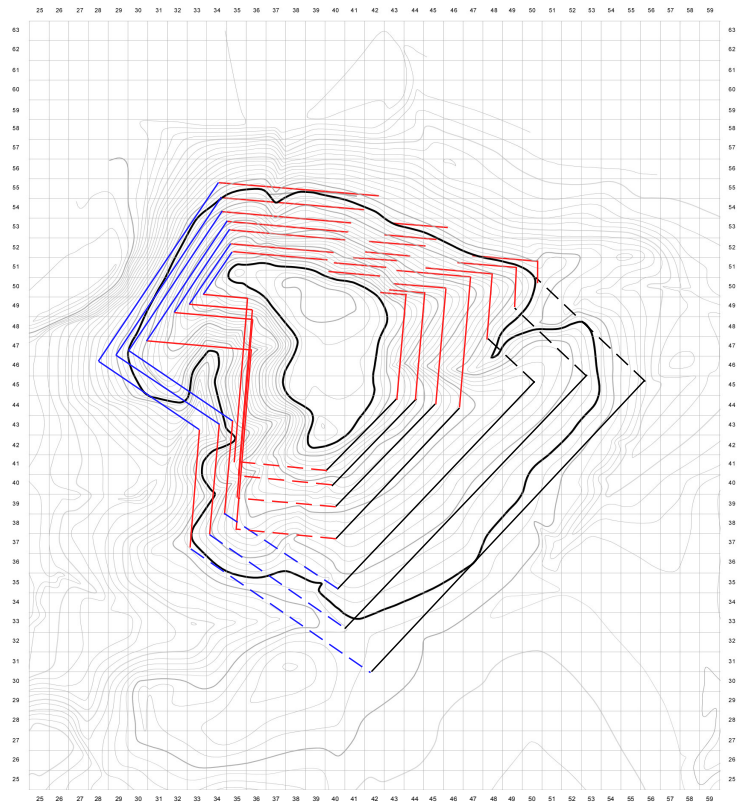
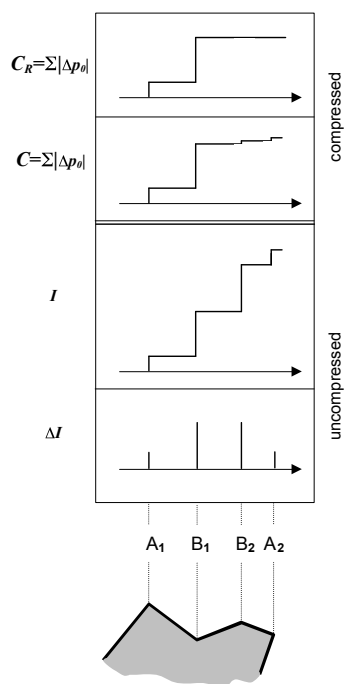


Fig. 27: Different Cumulative Effects of of New vs. Redundant Information



Cumulative effects of new (A1, B1) vs. redundant (A2, B2) information (I) on C and C_R .

Fig. 28: Tall al-Hamidiya, Squares 40-43/37, 41/38
(Gerber 2000b)

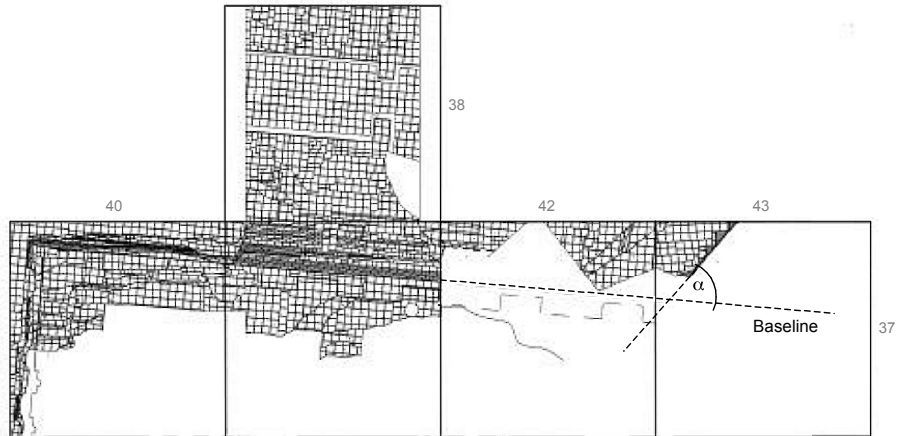


Fig. 30: Constructors of Solution B Redundant in y

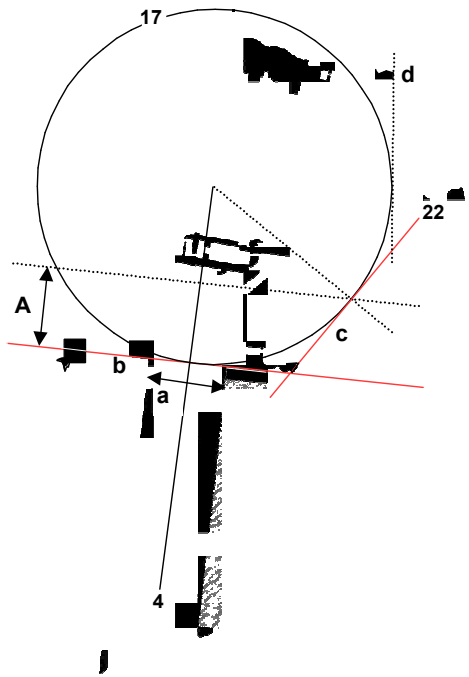


Fig. 31: Square Grid Angles

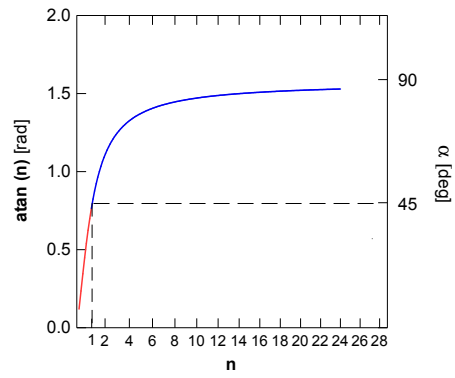
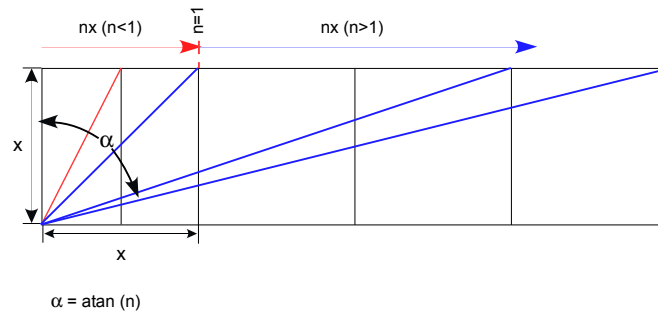


Fig. 32: Wall Orientations extracted from Plans -1999

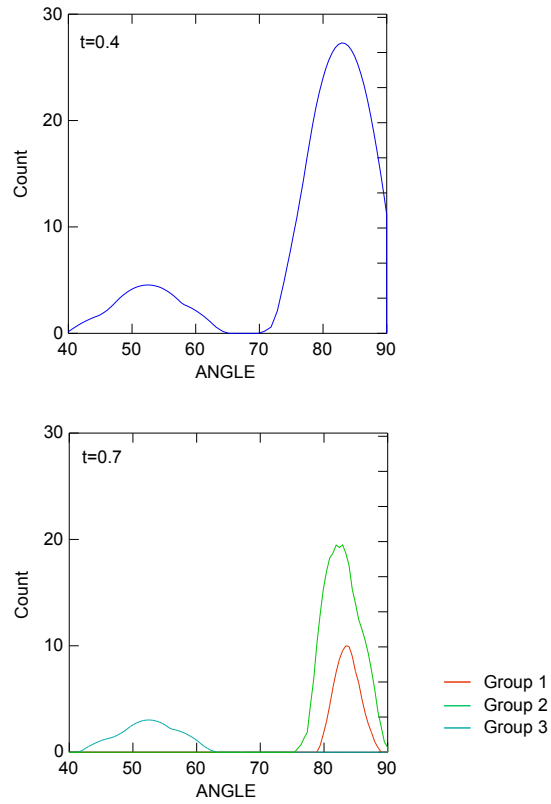
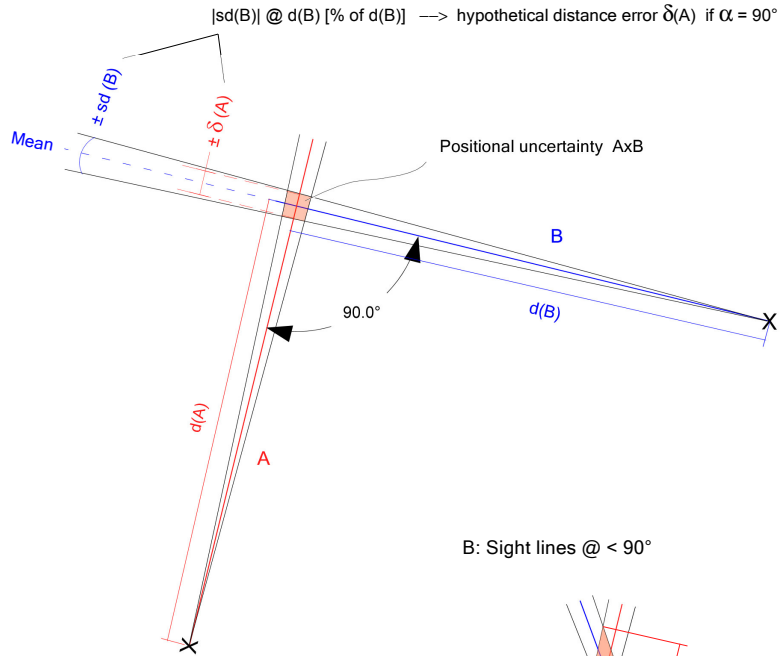


Fig. 33: Positional Uncertainty; 2 reference points

A: Sight lines @ -90°



B: Sight lines @ $< 90^\circ$

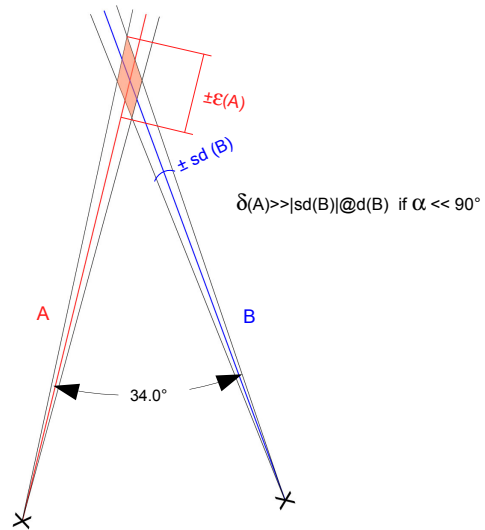


Fig. 34: Distances between Discrete Points

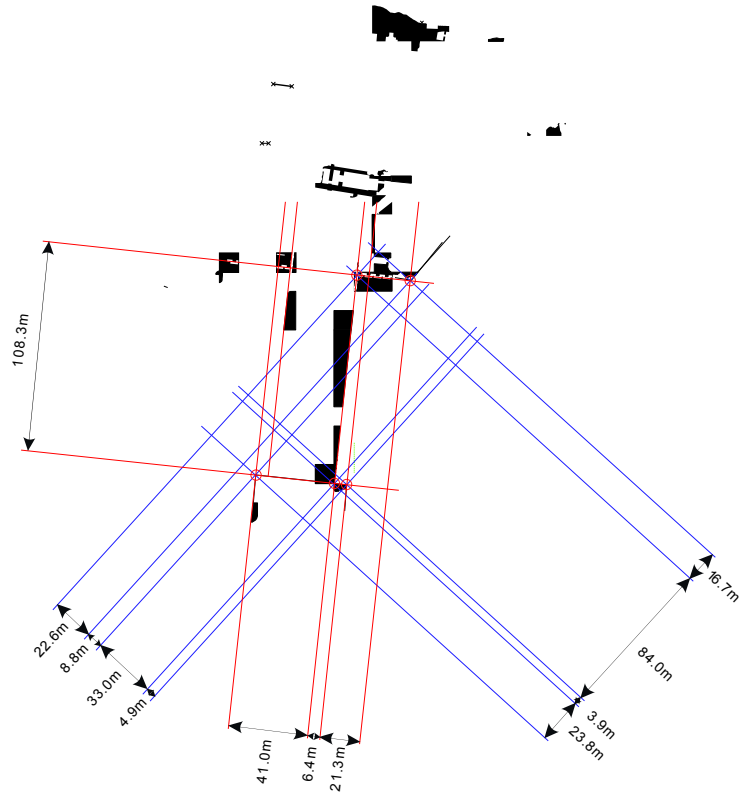


Fig. 35: Resampled Distances d , d'

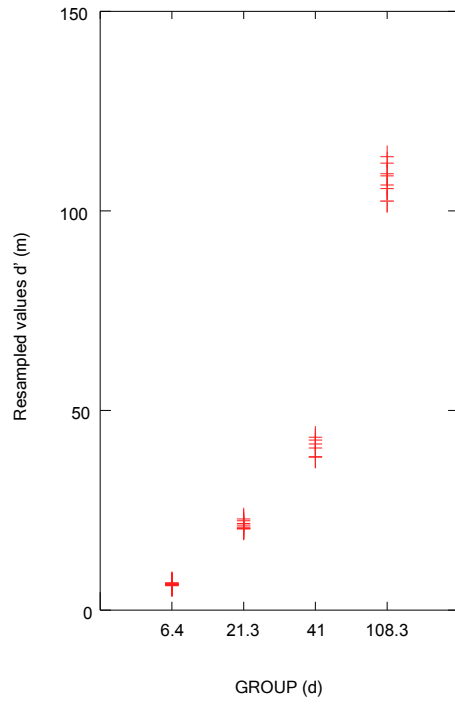
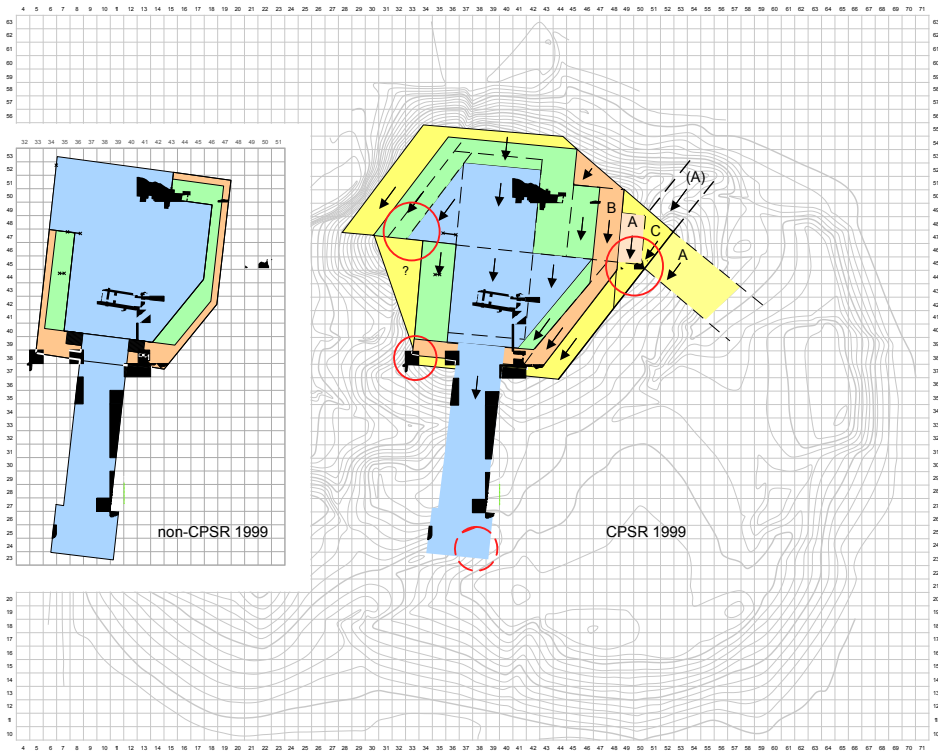
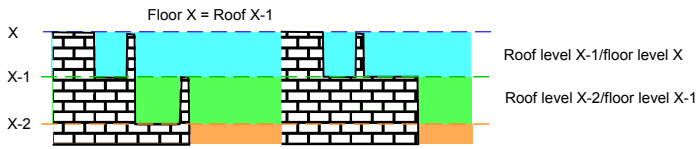


Fig. 36: The 1999 CPSR-Reconstruction



Colour coding:

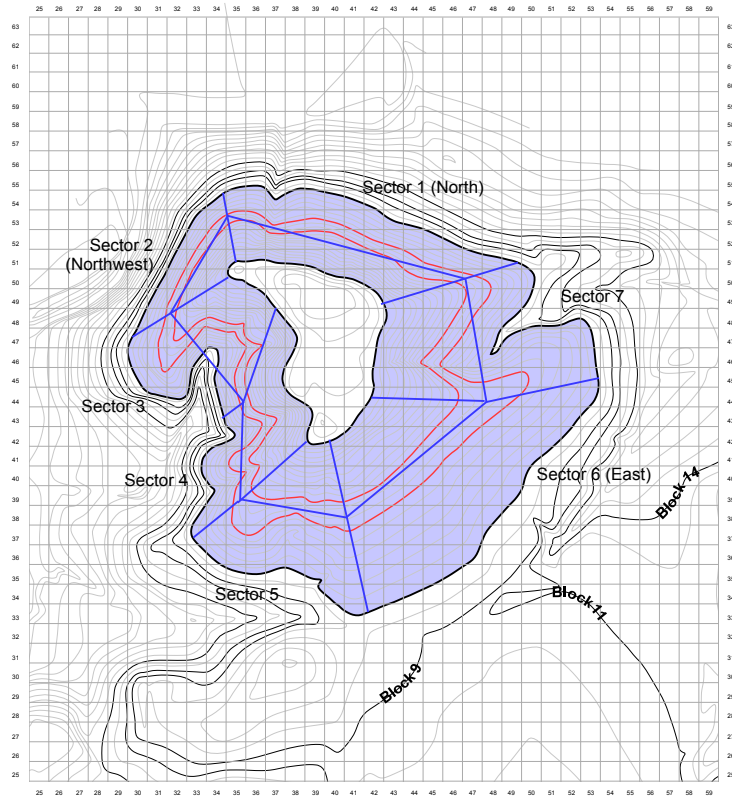


- | | |
|---------------------------------------|--|
| Roof/floor level: 384.50 / 390? msl | Roof/floor level: >366.50 / 372.40 msl |
| Roof/floor level: 377.55 / 384.50 msl | Roof/floor level: 361.70 / 366.50 msl |
| Roof/floor level: 372.40 / 377.55 msl | y : Excavated walls |

CPSR-field test 2000

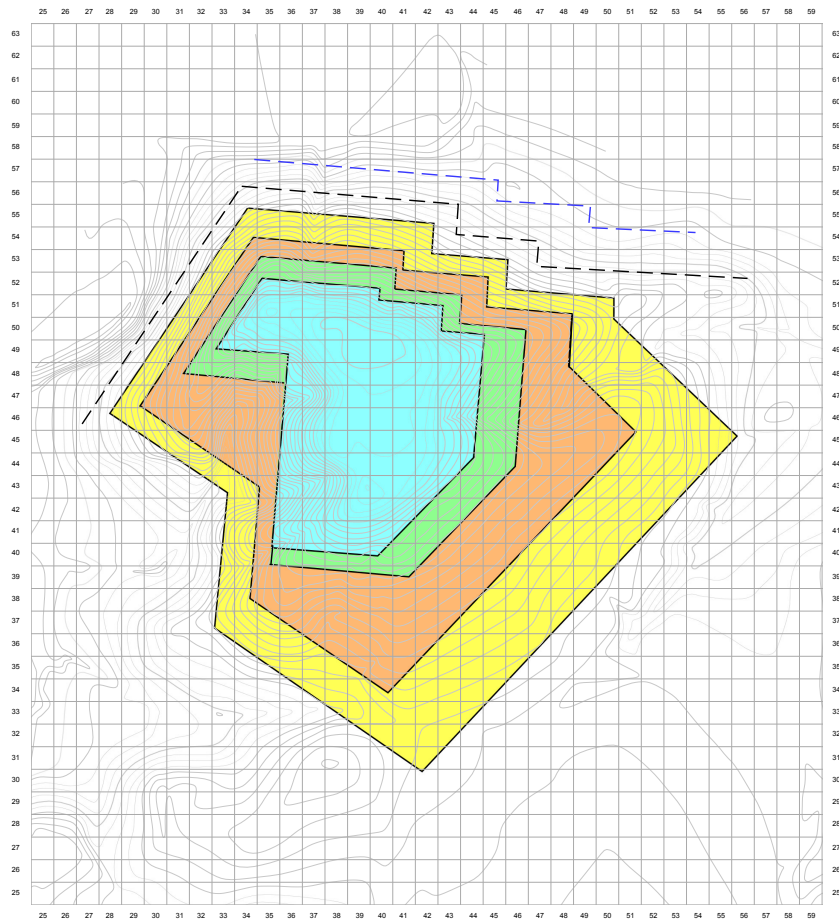
Test of Wäfler's non-CPSR prediction on the length of the southern ascent structure

Fig. 37: Areas Referred to in § 4.2



-  Block 8
-  376-373msl

Fig. 38: PSDR-Reconstruction 2002 (excluding CPSR)



- | | |
|--|--|
| ■ Floor/roof level: $\geq 382/387$ msl | ■ Floor/roof level: $\geq 367/372$ msl |
| ■ Floor/roof level: $\geq 377/382$ msl | - - Floor/roof level: $\geq 362/367$ msl? |
| ■ Floor/roof level: $\geq 372/377$ msl | - - Floor/roof level: $\geq 357/362$ msl? |
| Maximum extension of levels | |

Fig. 39: Comparison with Excavation Results -2002

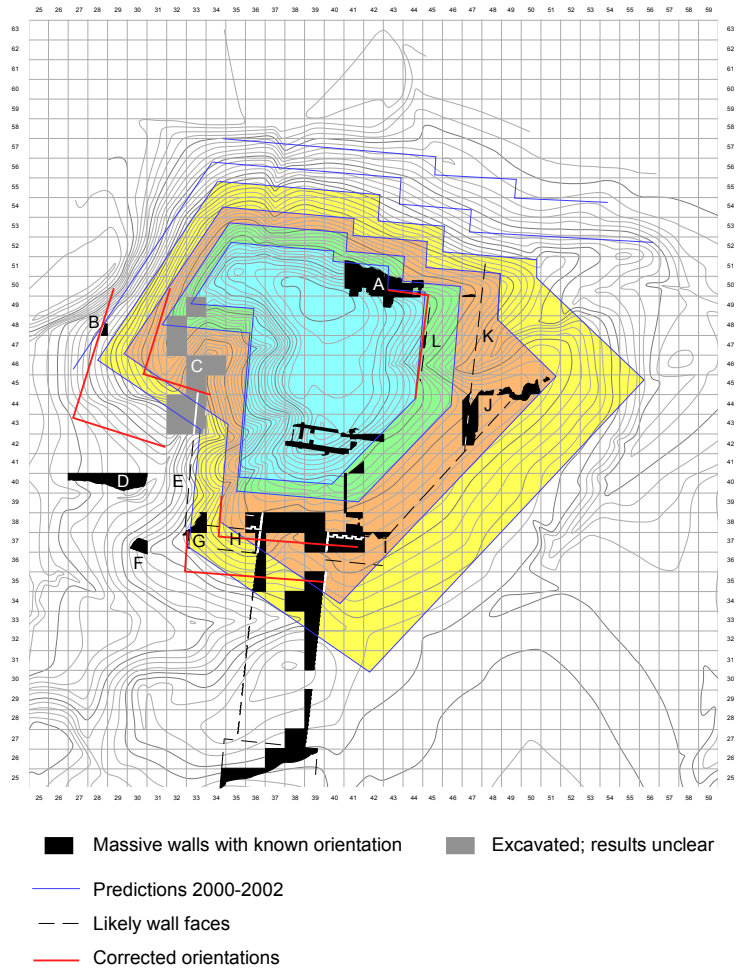


Table 2

This file (pp. 1-11) contains the original toposurvey data from Tall al-Hamidiya 1984. It may be ordered from the author in printed (pp. 23) or electronic form.

Data courtesy of D. Steudler, Melbourne (cf. Acknowledgements)

Data Structure:

Point number	Break	Northing [m]	Easting [m]	Elevation [m]	Break
1204	0	377.94	312.47	369.07	
1205	17	317.70	458.91	373.18	17
1034	17	300.00	400.00	357.14	17
1207	17	325.59	681.26	350.74	17
1380	0	351.18	962.52	344.34	
1553	0	376.77	243.78	337.94	
1726	18	402.36	525.04	331.54	18
1899	18	427.95	806.30	325.14	18

Table 2

This file (pp. 1-11) contains the original toposurvey data from Tall al-Hamidiya 1984. It may be ordered from the author in printed (pp. 23) or electronic form.

Data courtesy of D. Steudler, Melbourne (cf. Acknowledgements)

Data Structure:

Point number	Break	Northing [m]	Easting [m]	Elevation [m]	Break
1204	0	377.94	312.47	369.07	
1205	17	317.70	458.91	373.18	17
1034	17	300.00	400.00	357.14	17
1207	17	325.59	681.26	350.74	17
1380	0	351.18	962.52	344.34	
1553	0	376.77	243.78	337.94	
1726	18	402.36	525.04	331.54	18
1899	18	427.95	806.30	325.14	18